UNCLASSIFIED//~~FOR OFFICIAL USE ONLY~~

Space Assembly

Contact: Gordon Long [redacted] (b)(6)

March 2020

JSR-19-2J

[redacted] (b)(3)

JASON
The MITRE Corporation
7515 Colshire Drive
McLean, Virginia 22102-7508
[redacted] (b)(6)

UNCLASSIFIED//~~FOR OFFICIAL USE ONLY~~

Approved for Release: 2021/04/27 C05132459

Contents

Approved for Release: 2021/04/27 C05132459

1 (U) EXECUTIVE SUMMARY: SPACE ASSEMBLY

(U) The launch of spacecraft and of hardware to space is currently limited in terms of size, mass, strength, and affordability by rocket design. Furthermore, operation in space is limited by technological obsolescence, component damage or failure, fuel consumption, and Earth-manufactured materials. To achieve effective, agile, resilient, and technologically advanced operations in space, there is a need to develop new capabilities for deploying space structures and for maintaining, repairing, improving, and even recycling such structures, while also protecting human safety. *In-Space Assembly and Manufacturing (iSAM)* appears to have potential for enabling these advances within the [redacted] [redacted] in robotics, autonomy, and additive manufacturing that, combined with lower-cost launch, make iSAM increasingly attractive and feasible.

(U) JASON was asked to study the benefits of iSAM that are likely realizable [redacted] considering how iSAM might enable the deployment and operation of a large-scale aperture [redacted] and discussing the current state of the art in component technologies and technological challenges to realizing the potential of iSAM. (b)(3)

(U//~~FOUO~~) The study was informed by briefings in January 2019, discussing in-space manufacturing and on-orbit assembly and servicing, followed by two days of briefings in June 2019 on topics including design of large ground-based telescopes and novel means of realizing large apertures in space. JASON also visited researchers working in the area of iSAM at JPL, and held remote conversations with others at Caltech, JPL, and the University of Arizona. [redacted] served as the points of contact for this study. Sherry Olson of MITRE was instrumental in facilitating the briefings. (b)(3)

(U) Several in-depth studies have analyzed iSAM, space missions for which the benefits of iSAM would be potentially significant, and readiness of component iSAM technologies. Two studies of note are:

1. *On-Orbit Manufacturing and Assembly of Spacecraft*, completed in Jan. 2017, written by researchers at the IDA Science and Technology Policy Institute [8]. This study concluded, "We find that many missions could benefit from on-orbit manufacturing and assembly including astronomy, Earth observation, space exploration, telecommunications, and national security."

2. A NASA-chartered In-Space Assembled Telescope Study (iSATS), a 14-month effort that concluded in July 2019; the effort involved 72 participants from 14 private companies, 2 government agencies, 5 universities, and 6 NASA centers [56]. The objective of the iSATS study was to determine "When is it worth assembling space telescopes in space rather than building them on the Earth and deploying them autonomously from single launch vehicles?" Moreover, the iSATS study provided a detailed reference concept for iSAM telescopes with apertures of four sizes from 5 to 20 m, designed for non-cryogenic operation at UV, visible, and near-IR wavelengths.

(U/~~FOUO~~) These foregoing studies do not necessarily target the benefits of iSAM that will be of greatest use to [redacted] but call attention to the fact that key technologies necessary for enabling iSAM are, at present, only partially developed. While extensive analyses have been carried out in developing component iSAM technologies, JASON's assessment is that full realization of iSAM potential can only be achieved by addressing the systems-level challenges. JASON believes that [redacted] is well-positioned to advance iSAM readiness by spearheading a proof-of-concept deployment that could [redacted] (b)(3) experiments. Such a program can leverage ongoing iSAM activities to realize the [redacted]

(U) The Astronomy Community has contributed a great deal to setting forth motivations and designs for iSAM, since such technologies can enable the deployment of larger-diameter telescopes. However, the implications and enabled applications of iSAM can be much broader and far-ranging than the "simple" realization of larger-size telescopes. Accordingly, JASON also explored some *imagineering ideas* of important structures and capabilities that iSAM could enable in the future. The integrative imagineering concepts discussed, include the following:

1. The report discusses possible architectures for a [redacted] RF array in space, with a frequency range of 50 MHz - 20 GHz, that is modeled on the planned, Earth-based *Square Kilometer Array (SKA)*. Key enabling technologies for both Earth-based and Space-based large RF arrays relate to the efficient production of appropriately-scale antennas, as well as the ability to carry out high-speed signal processing, communications, computation and electronic storage. Such technologies are currently being driven by commercial applications. (b)(3)

2. The report discusses the components of the Earth-based *Extremely Large Telescope (ELT)*, a 39.3 m telescope operating in visible and near-infrared wavelengths, that is still under development. The ELT can provide guidelines and constraints for the degree of precision and metrics of operation needed for a space-based version of the ELT.

The *imagineering concepts* described above hold great promise for more agile, resilient and technologically advanced operations in space. However, their successful realization depends on the prior demonstration and validation of a reliable, scalable and cost-effective baseline iSAM technology.

(U) The following are the principal findings and recommendations of this study. Additional findings and recommendations are found in the body of the report.

1. (U) **Finding**: Several recent, extensive studies have identified key advantages of iSAM for future-generation space structures. Some studies have provided detailed guidelines for the design, assembly methodology, and technological challenges involved. iSAM appears to be at a "tipping point" for implementation and demonstration.

   (U) **Recommendation**: JASON recommends that [ ] leverages the detailed analyses, designs, and technological assessments of these studies to help shape an iSAM roadmap for [ ] needs and opportunities. (b)(3)

2. (U) **Finding**: Although many key capabilities for iSAM are in place, successful demonstration of iSAM will require a systems-level integration of technologies ranging from design and assembly of components to implementation and test in space. Without leadership in developing and demonstrating these enabling technologies, capabilities potentially enabled by iSAM will remain unrealized in the coming decades.

   (U) **Recommendation**: JASON recommends that [ ] moves forward in designing, launching, and building a proof-of-concept iSAM structure, utilizing modular components that provide a clear pathway to scale-up to larger structures. In this way, technology challenges can be addressed and overcome within the context of a well-defined, integrated iSAM architecture. (b)(3)

3. (U) **Finding**: There is a wide range of innovative, emerging technologies that may be of great future benefit in enabling iSAM to produce technologically advanced, agile and resilient structures. Such innovation stems from a broad community of academic and industrial researchers, as well as from government labs.

   (U) **Recommendation**: In developing iSAM projects and presence, [ ] can benefit from partnerships with the community that is currently carrying iSAM forward. JASON recommends that [ ] seek out such partnerships and active engagements. (b)(3)

2 (U) INTRODUCTION TO THE STUDY

2.1 (U) Sponsorship and Scope of the Study

(U//~~FOUO~~) The launch of spacecraft and of hardware to space is currently limited in terms of size, mass, strength, and affordability by rocket design. Furthermore, operation in space is limited by technological obsolescence, component damage or failure, fuel consumption, and Earth-manufactured materials. Cognizant of these limitations, [redacted] requested that JASON study the benefits of *In-Space Assembly and Manufacturing (iSAM)* that might be realized within a time frame that would help to drive forward [redacted] of effective, agile, resilient, and technologically advanced operations in space. (b)(3)

(U//~~FOUO~~) [redacted] served as the points of contact for this study. Sherry Olson of MITRE was instrumental in facilitating the briefings.

2.2 (U) Briefers

(U) The study was informed by briefings in January 2019, discussing in-space manufacturing and on-orbit assembly and servicing, followed by two days of briefings in June 2019 on topics including design of large ground-based telescopes and novel means of realizing large apertures in space. JASON also visited researchers working in the area of iSAM at JPL (Dave Redding and Keith Coste), and held remote conversations with others at Caltech (Sergio Pelligrino), JPL (Nick Siegler), and the University of Arizona (Roger Angel and his colleagues).

(U) A listing of the briefers appears in the Table below:

Name	Organization
Roger Angel	University of Arizona
[redacted]	(b)(3)
Bill Doggett	NASA
Roberta Ewart [1]	Air Force
[redacted]	
Justin Kugler [3]	Made in Space
Al Tadros [4]	SSL
Chris Walker	University of Arizona

2.3 (U) Framework of the Study

(U) JASON was encouraged to be broadly *imagineering* within the constraints of the study, seeking new and necessary component technologies to realize iSAM. To provide a focus and integrative platform for technical discussions, JASON considered *large aperture systems* to be deployed in space: these constitute the *Point Designs for Large Apertures* that comprise Section 6.

2.4 (U) Organization of the Report

(U) The report is organized in the following way:

1. The report begins with an introduction to the ideas and definitions of *In-Space Assembly (iSAM)*, their historical context and present-day opportunities (Section 3).

2. The section on *Architectures and Building Blocks for iSAM* necessarily can only briefly touch upon some of the candidate building blocks that

comprise space structures, and the inherent challenges for in-space assembly. Since the Point Designs relate to large area, space-assembled apertures, the discussions in Section 4 focus on the qualities of those apertures, the control of the surfaces and resulting signal to noise.

3. The section on *Technological Consideration* (Section 5) addresses important underlying themes such as *Thermal Issues* and also introduces new technological solutions that may be applicable for iSAM.

4. [redacted] (b)(3)

5. (U) After the concluding remarks, Appendix I provides a *Space Assembly Case Study* with a detailed narrative of the Large Deployable Reflector (LDR). Section 8 also offers important insights into "lessons learned" from the LDR experience.

This Page Intentionally Left Blank

3 (U) SPACE ASSEMBLY: THE BACKGROUND

3.1 (U) Motivation

(U) Spacecraft have historically been manufactured and assembled on the ground, then integrated with launch vehicles for delivery into orbit. The construction of the International Space Station (ISS) represents the successful realization of in-space assembly and manufacturing techniques. Thus, at one level *in-Space Assembly and Manufacturing, (iSAM)* is not a new concept. However, the past several decades have been marked by increased experience in launches into space, rendezous and proximity operations, cargo delivery and robotic assemby of space components. There has been a multitude of technological advances in the component materials, electronics and sensors comprising components for space. These collective advances may hold important implications for the broader vision for iSAM:

- The deployment of structures in space whose size and capabilities are not constrained by the size, shape and other limitations of launch vehicle fairings.
- The ability to inspect and repair spacecraft on-orbit, extending the lifetime and capabilities of those structures.
- The ability to maintain technological vitality through addition of state-of-the-art sensors, electronics and other components.

(U) Is this vision now a timely one, is this the right time to move forward with compelling demonstrations of iSAM? If so, what are the inspiring applications, the technological lacunae, and the way forward? These are the questions that the [redacted] asked JASON to consider. (b)(3)

3.2 (U) The Demands for Ever-larger Aperture Size

(U) One application that would benefit from iSAM relates to the assembly and deployment of larger, space-based imaging apertures, where the size of the aperture is far larger than could be accommodated in a single launch vehicle. The ability of larger imaging apertures to provide lower-noise (higher photon collection), higher-spatial resolution images has provided strong incentive for the Astronomy community to aspire to construct telescopes with ever-increasing diameters, as shown in Figure 1.

Because extensive analyses and designs have been developed by the Astronomy community, this report will build upon that body of knowledge. However, JASON realizes that the implications and benefits of iSAM can extend to applications much broader than enhanced imaging for Astronomy alone. In fact, the early ideas of a *Large Deployable Reflector*, described in Section 8, related to a bold vision for enhanced communications technologies. The broader applications will be reflected in the Point Designs discussed in Section 6, particularly in the two candidate designs for [redacted] (b)(3) operating at GEO.

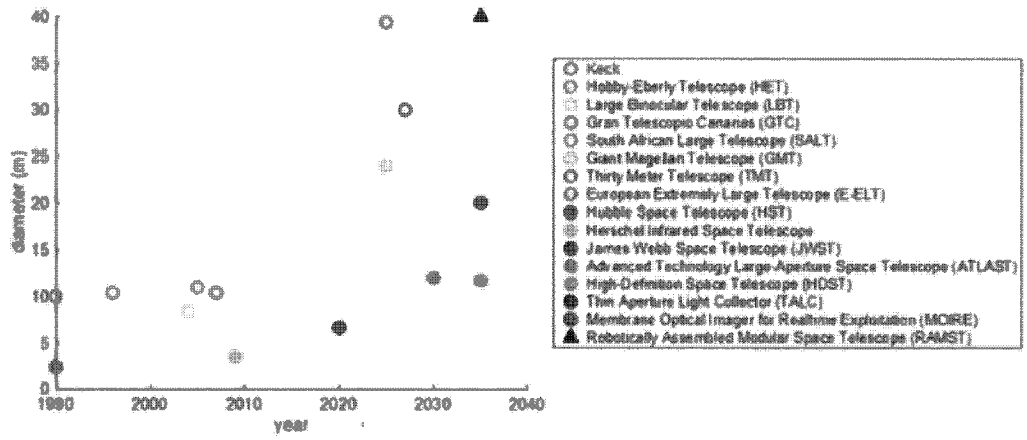

Figure 1: (U) Trends in telescope diameter (from Huybers).

(U) Table 1 provides some detail on recent and planned Earth-based and Space-spaced telescopes. As telescope diameters increase, segmented, rather than monolithic mirrors facilitate telescope construction. Such segmented mirrors are the natural building blocks of a *modular* telescope architecture, which in turn provides an important platform for an in-space assembled structure.

(U) As early as 1977, Robert Powell and Albert Hibbs put forth the vision of a large aperture deployed in space, in their paper entitled *An Entree for Large Space Antennas*, postulating a 10m, and subsequently a 20m diameter aperture [67]. The ideas in that paper formed the genesis of *the Large Deployable Reflector (LDR)* concept, a concept that was sporadically pursued and refined during the 1980s and 1990s. LDR concepts included the use of modular (rather than monolithic) mirror segments formed of light-weight beryllium or ultra-low-expansion (ULE) glass, ultimately producing a 15-30 m aperture that would require multiple launches for all components, and also require in-space assembly. Thus, the concept of using in-space assembly for large telescopes has a long history, yet at present the largest planned telescope apertures (20m, 40 m) are Earth-based, while space-based telescopes are limited to 6.5m apertures (the James Webb Space Telescope), with 15m diameter space-based telescopes only under study at the moment.

(U) Further details of the LDR concept and its history are provided in Appendix I, Section 8. The LDR experience can provide useful insights on what comprised past limitations to realization of iSAM to better assess current capabilities in addressing those limitations.

3.3 (U) What is New in Space Assembly?

(U) Over the past decades there has been a plethora of reports, designs and studies related to iSAM; the in-Space Assembled Telescope Study website provides an excellent archive of many of these studies [74]. As an example, the NASA OpTIIX project [66] developed concept designs for the robotic

Table 1: (U) Past and ongoing efforts in large-aperture telescopes.

#	Name, Earth-based	Size.	First light	Ref.
1.	Large Binocular Telescope (LBT)	8.4m monolithic x2	2004	[31]
2.	Keck	10m segmented x2	1990, 1996	[60]
3.	Hobby-Eberly Telescope (HET)	10.4m segmented	1996	[40]
4.	Gran Telescopio Canarias (GTC)	10.4m segmented	2007	[4]
5.	South African Large Telescope (SALT)	11m segmented	2005	[76]
6.	Giant Magellan Telescope (GMT)	24m segmented	2025	[37]
7.	Thirty Meter Telescope (TMT)	30m segmented	2027	[59]
8.	European Extremely Large Telescope (E-ELT)	39.4m segmented	2025	[52]
9.	Overwhelmingly Large Telescope (OWL)	100m segmented	cancelled	[17]
#	**Name, Space-based**	**Size.**	**First light**	**Ref.**
1.	Hubble Space Telescope (HST)	2.4m monolithic	1990	[23]
2.	Herschel Infrared Space Telescope	3.5m monolithic	2009	[63]
3.	James Webb Space Telescope (JWST)	6.6m segmented	2020	[25]
4.	Advanced Technology Large-Aperture Space Telescope (ATLAST)	8-16m segmented	2025-2035	[65]
5.	High-Definition Space Telescope (HDST)	11.7m segmented	2030s	[16]
6.	Thin Aperture Light Collector (TALC)	20m segmented	unknown	[20]
7.	—	30m segmented	unknown	[69]
8.	Membrane Optical Imager for Realtime Exploitation (MOIRE)	20m membrane	unknown	[18]
9.	Robotically Assembled Modular Space Telescope (RAMST)	100m segmented	unknown	[42]

assembly of a 1.5m telescope on the ISS. The new paradigm that was to be demonstrated in OpTIIX was the construction of *a modularized, actively controlled, segmented, scaleable* telescope by robotically assembling components in space and autonomously phasing it up to diffraction-limited performance. OpTIIX incorporated key features of an in-space assembly approach, which also includes the following:

1. Modularity of components,
2. Multiple launches,
3. Rendezvous and Proximity Operations (RPO),
4. Cargo Delivery Vehicles (CDVs) to deliver components to the structure being assembled,
5. Robotic Assembly,
6. In-space Verification and Validation (V&V).

(U) The NASA-chartered In-Space Assembled Telescope Study (iSATS) recently concluded (July 2019) a 14-month study involving 72 participants from 14 private companies, 2 government agencies and 5 universities, as well as 6 NASA centers [56]. iSATS posed the same question relevant to this study:

> When is it worth assembling space telescopes in space rather than building them on the Earth and deploying them autonomously from single launch vehicles?

(U) Moreover, the iSATS study provided a detailed reference concept for iSAM telescopes operating at UV, visible and near-infrared (NIR) wavelengths, with apertures of four sizes between 5 and 20 m. These reference concepts provided guidelines for identifying the key ISA capabilities and their corresponding *readiness for observatory ISA*. That chart is shown in Figure 2.

#	ISA Key Capabilities	Status	Representative Examples	Readiness for Observatory ISA
1	Modular Elements	Flight Demonstrated	Instruments on HST, instruments installed on ISS	Low
		Active Development	JWST primary mirror segments	
2	Launch Vehicles	Flight Demonstrated	SpaceX Falcon, Falcon Heavy, ULA's Delta IV	High
		Active Development	SLS, Blue Origin, Starship, Vulcan Centaur	
3	RPO	Flight Demonstrated	DARPA Orbital Express, NASA OSIRIS-Rex, Cygnus, Dragon, Crew Dragon, ATV, HTV, Progress, Soyuz	High
4	CDVs	Flight Demonstrated	SpaceX Dragon, Cygnus from Northrop Grumman	High
5a	Space Robotics Hardware	Flight Demonstrated	Several robotic arms on ISS (e.g. Canadarm 2), Orbital Express robotic arm, Mars Rover arms, Shuttle arm	High
		Active Development	NASA Restore-L and DARPA RSGS robotic servicing arms, Canadarm 3, Maxar's Dragonfly arm, Mars 2020 rover	
5b	Space Robotics Software	Flight Demonstrated	Mars Rover Autonomy (e.g. MSL, MER), ISS, Orbital Express	Medium
		Active Development	Mars 2020, Mars Sample Return, NASA Restore-L, DARPA RSGS, NASA Tipping Point Demonstrations	
6	In-space Verification and Validation	Flight Demonstrated	Instruments on HST, instruments installed on ISS	Low
		Active Development	JWST primary mirror segments and wavefront control	

Figure 2: (U) Key capabilities needed for in-space assembly of large telescope observatories. Technology gaps and development needs remain specific to observatory assembly (from [21]).

(U) Figure 2 provides the capabilities that presently have *high readiness* for Observatory ISA, but perhaps of greater importance are those technologies listed as *low-readiness capabilities* and the concomitant technology challenges.

(U) Influenced by a growing commercial presence in the construction and launch of space structures, launch opportunities are becoming more abundant and lower-cost. The commercial space sector has also generated proofs of concept of rapidly-developed and deployed space structures that incorporate state-of-the art electronics and sensor components. Thus, the combination of technology maturation and the pull of the benefits realizable by iSAMs provides a *tipping point* for the particular relevance of iSAM at this point in time.

3.4 (U) Summary

(U) The time is right from both technological promise and applications. Substantial technological challenges remain, however, and this report is structured to address those challenges, as outlined in Section 2.4.

1. (U) **Finding**: Several recent, extensive studies have identified key advantages of iSAM for future-generation space structures. Some studies have provided detailed guidelines for the design, assembly methodology, and technological challenges involved. iSAM appears to be at a "tipping point" for implementation and demonstration.

2. (U) **Finding**: Although many key capabilities for iSAM are in place, successful demonstration of iSAM will require a systems-level integration of technologies ranging from design and assembly of components to implementation and test in space. Without leadership in developing and demonstrating these enabling technologies, capabilities potentially enabled by iSAM will remain unrealized in the coming decades.

4 (U) ARCHITECTURES AND BUILDING BLOCKS FOR iSAM

(U) As noted earlier in this report, the idea of constructing very large telescopes in space is not a new one, and a variety of design architectures have been proposed. In the following narrative, we will incorporate elements of a design proposed by Caltech and the Jet Propulsion Lab simply as an illustration of the use of modular building blocks, issues of design for assembly and challenges in metrology [42]. The point designs described later in this report (Section 6 will also provide some information on necessary assembly tolerances, components and interfaces (e.g. see Section 6.3) but the discussion here is intended to be a more generic introduction to in-Space Assembly.

4.1 (U) Assembly Methodologies

(U) As a preamble to the discussions below, we identify three categories of space assembly methodologies: (1) human labor in space, (2) remote (telepresence) assembly methods, and (3) autonomous robotic methods. The first of these is limited to LEO, with subsequent repositioning of partial or fully completed system elements. The benefits of astronaut adaptability and innovation must be balanced against the increased costs needed for human flight safety. The telepresence approach must contend with latency (especially at GEO) and less adaptability to unforeseen circumstances, but does not require fully autonomous operations. The most technically demanding method involves fully independent robotic assembly operations. Our sense is that, pending verification with laboratory and on-orbit tests, the telepresence method is the likely sweet spot for the assembly of components in space. The iSAM building blocks must complement the Assembly Methodologies employed.

4.2 (U) Large, Segmented Optical Apertures

(U) The development of larger apertures, even operated on Earth, has stimulated approaches in modular, light-weight mirror segments with integrated actuators and sensors that allow fine-tuning the assembly and performance of the complete aperture. Mirror modules that will form the images may take the form of hexagonal units that also incorporate actuators and electronics. These mirror modules are supported by corresponding truss modules, formed of lightweight yet stiff materials (e.g. Ti) whose geometry facilitates compact storage. Grapple points and attachment points integrated onto the truss structures can facilitate robotic handling and assembly. The truss modules are first deployed and attached, and mirror modules are then attached to the underlying truss. Figure 3(a) provides a schematic of the modular components and the assembly process. The figure shows the truss module as being foldable or stowable, requiring the incorporation of hinges that will facilitate folding.

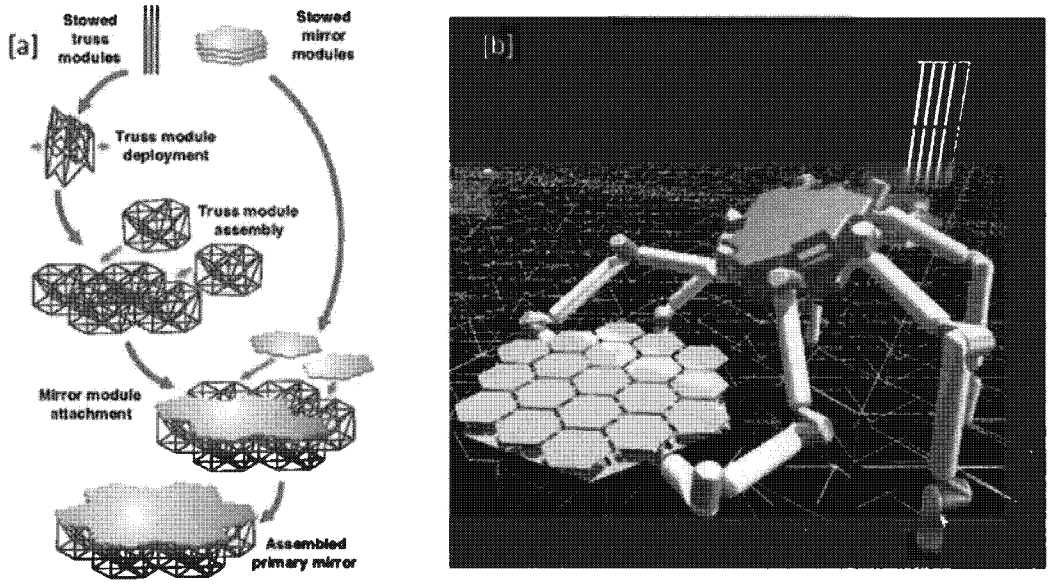

Figure 3: (U) [a] Schematic of primary mirror assembly, from [42], [b] Multi-limbed robot used to assemble mirror and truss components (from [58]).

(U) The robot used to carry out assembly should be designed to match the modular components and the assembly process. For example, the multi-limbed robot shown in Figure 3(b) is able to position and align the modules for assembly, and, as well, travel over the primary mirror truss structure to carry out the assembly. In cases where the robot remains with the space structure, future servicing is naturally incorporated.

(U) For a given modular geometry, there are important additional choices to be made regarding the "packing" or tessellation of the final structure, as shown in Figure 4, that illustrates both "fully filled" and "sparse tessellation". The sparse geometry contains fewer redundant truss members (the red lines in the figure) and allows the robot greater access and maneuvering space. The hexagons in the sparse case are 12.4 % smaller in side length, reducing the effective buckling length. Given a geomtery for the modular building block, and a choice of tessellation to form the fully assembled structure, there may still be critical decisions in how the robotic connections are to be made. Figure 4(e) and (f) illustrate the differences in making the connection of the green hexagon either in the horizontal plane or from the vertical plane. With the horizontal approach, two of the edge connections must be oriented tangentially to the rest of the module structure, while the remaining edge must be oriented radially. The edge connections for the vertical approach are the same, potentially making robotic alignment easier to accomplish.

4.3 (U) Monolithic Shells

(U) The considerations in this section relate to the use of a monolithic shell for the support of mirror segments, rather than supporting trusses. This approach may serve to minimize the thermal distortions described in Section 5.2.2.

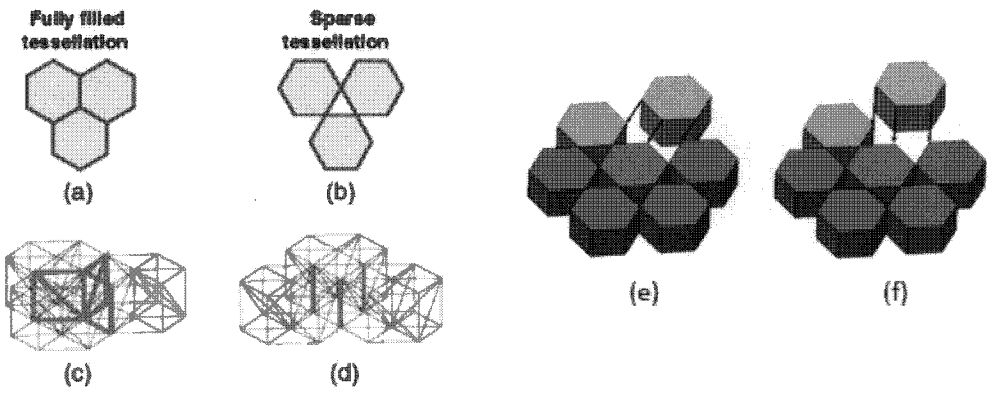

Figure 4: (U) Top views of [a] fully filled and [b] sparse hexagonal tessellation. Hexagonal truss modules arranged in [c] fully filled and [d] sparse tessellations, with redundant members are shown in thickened red lines. From [42]. For sparse tessellation, [e] shows approaching the connection horizontally, while [f] shows approaching the connection vertically (from [32]).

4.3.1 (U) Shell stiffness

(U) *Shells*, defined as having nonzero Gaussian curvature, are much stiffer than thin *plates*, defined as having zero Gaussian curvature, because bending a shell requires stretching its elements. As a result, while differential thermal expansion induces large shape changes in thin plates (the bimetallic strip of a thermostat is a familiar example), it only makes small changes to the shape of a shell, typically $\mathcal{O}(\alpha\Delta T)$. Examples of surfaces with nonzero Gaussian curvature are spheres, paraboloids and hyperboloids. These are used as optical reflectors and hyperboloids are widely employed in architecture, where they are the usual shape supporting cooling towers. Cylinders and cones, as well as flat sheets, have zero Gaussian curvature, and require depth (in the form of supporting trusses) for stiffness.

(U) Materials with low thermal coefficients of expansion are useful for shell structures that will not undergo substantial shape deformation under conditions of thermal variation. Zerodur ® is a lithium-aluminosilicate

glass ceramic, manufactured by Schott AG, that is designed and formulated to exhibit essentially zero thermal expansion over a wide temperature range. This is an extremely useful property for applications involving precision components that will face wide thermal conditions. `https://www.insaco.com/materials/glass-ceramics/zerodur`.

(U) For a material like Zerodur with α as small as 10^{-8}/K, and (with careful sun and Earth shieldiing and heat pipes) $\Delta T \sim 0.1$ K, $\alpha\Delta T \sim 10^{-9}$ may be achievable. Then, for a reflector with diameter $d = 30$ m, the thermal strain of $\alpha\Delta T d \approx 300\,\text{Å}$. Uncorrected $\lambda/20$ stability is not far out of reach for a low f-number reflector, independent of its thickness[5]. The stiffness of a thin curved shell, defined as its spring constant for an applied force, is $\sim Eh$, where E is a modulus and h its thickness; it is as stiff, in proportion to its mass or filling factor, as a filled solid.

(U) The following discussion provides a simple model that allows good working estimates of shell stiffness. We compare the stiffness of a spherical shell of radius R subtending an angle θ, as shown in Fig. 5. We compare the shell to a flat plate covering its aperture.

(U) The stiffness of the flat plate, parametrized by its spring constant in response to a normal force at its center is

$$k_{plate} \sim \frac{Eh^3}{(R\theta)^2}, \tag{4-1}$$

where E is Young's modulus and we roughly approximate the chord length AB by the arc length. The coefficient depends strongly on the boundary conditions at the edge of the plate, but here we are interested in scaling estimates only.

(U) We estimate the stiffness of the shell by imagining a force pressing down on its edge, balanced by an upward force distributed across its surface. These act to flatten the shell. We make the approximation that elements

[5](U) This f-number only describes the shell's geometry for the purpose of mechanical response. Not all its area need be reflectorized and be part of the optical system, that need not be designed for such low f-number.

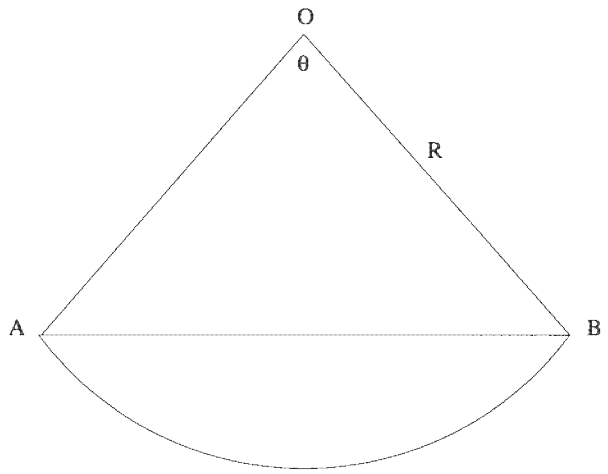

Figure 5: (U) A small f-number reflector (drawn spherical) and a flat plate covering the aperture of the reflector. The $\angle$AOB is denoted θ.

in the shell extending radially from its center do not stretch, but consider stretching of circumferential elements as it flattens and becomes wider and flatter. This can be a good approximation for shallow ($\theta \ll 1$) shells, but, in the spirit of our rough approximations and scaling arguments, apply it to deep shells with $\theta \sim 1$.

(U) As a result of the application of these forces the shell flattens, and its radius R becomes $R + \Delta R$. In our approximation the arc length $A = R\theta$ of the shell does not change, so that to lowest order in small quantities

$$\frac{\Delta\theta}{\theta} = -\frac{\Delta R}{R}. \tag{4-2}$$

The shell's resistance to the applied force comes from the work that must be done on its circumferential elements. The periphery of the shell has a radius

$$r = R\tan\frac{\theta}{2} = R\left(\frac{\theta}{2} + \frac{\theta^3}{24} + \ldots\right). \tag{4-3}$$

After deformation its radius becomes

$$r + \Delta r = (R + \Delta R)\tan\frac{\theta + \Delta\theta}{2}. \tag{4-4}$$

The dimensionless strain

$$\epsilon = \frac{\Delta r}{r} = \frac{\Delta r}{R\theta} = \frac{\theta^2}{8}\frac{\Delta\theta}{\theta} + \frac{\theta^2}{24}\frac{\Delta R}{R} = -\frac{\theta^2}{12}\frac{\Delta R}{R}. \tag{4-5}$$

This occurs in a volume $V \sim \pi r^2 h$ and corresponds to an elastic energy, ignoring factors of order unity,

$$\mathcal{E} = \frac{1}{2} E \epsilon^2 V. \tag{4-6}$$

(U) The vertical displacement corresponding to these strains is $\Delta L \approx \theta \Delta R$. Combining these results, we find an effective vertical spring constant

$$k_{shell} = \frac{2\mathcal{E}}{(\Delta L)^2} \approx \frac{\pi}{144} E h \theta^4. \tag{4-7}$$

Comparing Eqs. 4-1 and 4-7 we find

$$\frac{k_{shell}}{k_{plate}} \sim \frac{\pi}{144} \theta^6 \left(\frac{R}{h}\right)^2. \tag{4-8}$$

For a deep shell $\theta = \mathcal{O}(1)$. For a 1 cm thick reflector with $R = 60$ m (for $f/1$ R is twice the aperture diameter) $(R/h)^2 \approx 3 \times 10^7$. The stiffness of a deep shell may greatly exceed that of a plate (or a shallow shell, because of the factor of θ^6). This stiffness minimizes its deformation under differential thermal expansion as well as other loads.

4.3.2 (U) Fabrication of a monolithic shell

(U) Here we suggest a means of fabricating a monolith in space from segments a few m in size, small enough to fit within a rocket fairing. Such a monolith would resemble a conventional segmented mirror, except that its segments would be fused into a monolith; stiffness and overall structure would be maintained, at least in part, by the stiffness of the monolithic shell rather than by a supporting truss.

(U) Segments of a large complete reflector may be fused together rather than supported on a truss. For example, they may fit together with tongues and grooves. If the contact surfaces are coated with carbon black or similar light-absorbing material, then a lens may focus enough sunlight to heat them to their fusing (more properly, sintering) temperature. The segments would

need to be accurately aligned by a supporting structure during this process, although final alignment could be provided by the actuators used to compensate for differential thermal expansion and other small effects. A segment constrained by fitting into two or more prevously aligned and fused segments would be well, although not to final accuracy, aligned by their tongues and grooves, but alignment of a segment fitting into only one previously aligned segment would be less closely constrained, and require more of the supporting structure in order to be properly aligned.

(U) The surface through which sunlight passes to heat the absorber cannot be reflecting. It might be reflectorized after the segments are fused, or sunlight could be passed through the "back" surface of the reflector that is never reflectorized.

(U) The focussing lens could be small, and robotically moved along the shell surface.

4.3.3 (U) Considerations at optical frequencies

(U) The magnitude of expected thermal distortions of a truss structure is estimated in Sec. 5.2.2. Here we suggest minimizing thermal distortion by eliminating most of the truss, fabricating a monolithic primary mirror in orbit. Zerodur has a coefficient of thermal expansion 10^{-8}/K, about two orders of magnitude less than assumed in Sec. 5.2.2 for truss material, and it is likely even less at the reduced temperature of a shielded structure. That may be small enough to eliminate the need for adaptive figuring at GEO, and reduces the demands on it at LEO.

4.3.4 (U) Considerations at radio frequencies

(U) It is possible to contemplate much larger collecting areas at radio frequencies than for visible or infrared light. The [redacted] is very ambitious, but recall that the Arecibo telescope has a collecting area of nearly (b)(3)

0.1 km^2 and the Chinese FAST (Five-hundred-meter Aperture Spherical Telescope) of about 0.2 km^2. Of course, these are terrestrial, with the advantages of easy supply of components and the availability of human workers to build them in a benign environment. On the other hand, such construction must also deal with terrestrial wind and gravity loads.

(U) The fundamental principle of shell stiffness (Sec. 4.3.1) may be used to good advantage for radio frequency reflectors as well as for visible light reflectors. When applied to a radio frequency reflector the shell can be the supporting truss, rather than the reflective surface itself, with a thickness orders of magnitude greater. This also applies to a truss that supports an optical reflector.

(U) The wavelength of nominal 20 GHz radio waves is about 3×10^4 that of visible light, while the contemplated [redacted] radio reflector is only [redacted] times larger than a contemplated 30 m large space telescope; the relative demands on the figure of the radio reflector are $\sim 10^{-3}$ as severe. (b)(3)

(U) However, the coefficients of thermal expansion of the metals used for a radio frequency reflector, in a supporting truss as well as for the reflecting surface itself, are 1 2 $\times 10^{-5}$/K at room temperature, 1000 2000 greater than that of the best zerodur glass. The problems of dealing with differential heating are then comparable in severity.

4.4 (U) Metallized Balloons as Radio Reflectors

(U) JASON heard briefings from Chris Walker, University of Arizona, on the use of inflatable balloons as putative simple, deployable structures that could provide the framework for space structures (see Figure 6). Balloons have the virtue that it is easy to make very large balloons and that uninflated balloons are very light and readily folded into small volumes. The shapes of balloons are unlikely to be controllable accurately enough to permit their use as diffraction-limited optical reflectors, but they should be considered

as radio frequency (conceivably as short as mm-wave) reflectors, for which the required precision of shape is less and very large sizes are required to obtain high angular resolution. Balloons might be considered for km-scale filled apertures.

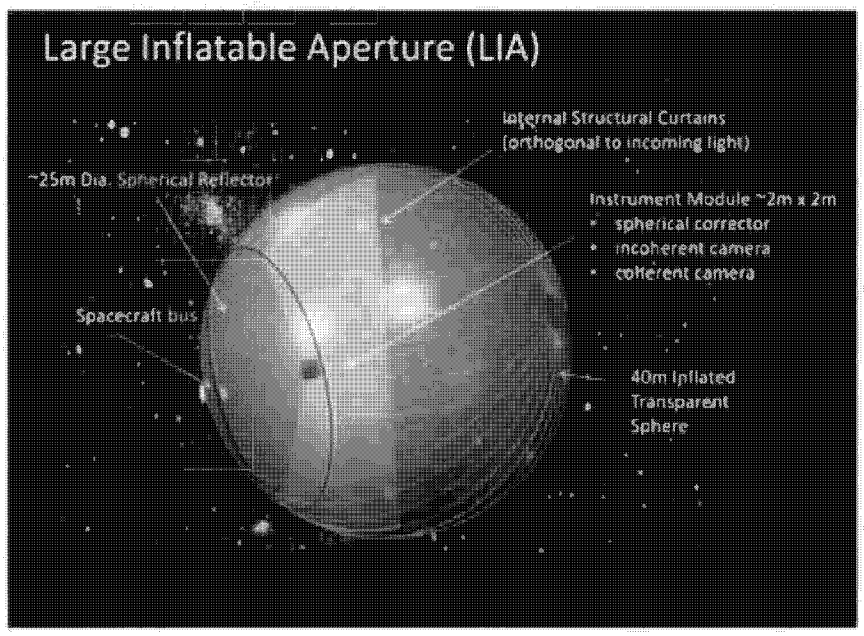

Figure 6: (U) Schematic of a Large Inflatable Aperture (LIA) or balloon-like structure that could serve as the basis of a large spherical reflector for imaging (from C. Walker, briefing to JASON).

4.4.1 (U) Materials for balloons

(U) A natural means of creating a large reflector is to inflate a reflectorized balloon of the desired shape, spherical or paraboloidal. We first distinguish between stretchable (like children's rubber) balloons and nearly unstretchable (typically mylar, although other materials may be used) balloons.

(U) Stretchable elastomeric balloons are unsuitable because their shape depends on their thickness and material properties, that cannot be closely controlled. In addition, because any metallic reflective coating would have elastic constants much greater than those of the elastomer it would delam-

inate and be lost when the balloon contracts from its stretched state, and would fragment, opening up large gaps, when the balloon is inflated.

(U) This problem would be mitigated in "unstretchable" balloons because the mismatch between elastic constants would be less (the elastic constants of most plastics are 10 30 kbar, in contrast to tens of bars for elastomers) and because inflation would only require very low pressure and correspondingly low strain of the plastic. This is evident even in toy aluminized mylar balloons, that do not lose their aluminizing when inflated.

(U) A suitable material for a balloon may be a flashspun nonwoven fabric, made by rapid evaporation of a solvent in which a polymer is dissolved after the solution is sprayed on a mandrel. If the polymer is a high or ultra-high molecular weight polyethylene (HMWPE or UHMWPE) the resulting film may be very stiff and strong. Tyvek, widely used in tear-resistant envelopes and building wraps, is such a commercial product (made from high density polyethylene HDPE), although it is unsuitable for balloons because it is permeable to vapors (necessary for its use in building insulation). Such a material could be made impermeable by application of an impermeable coating, or inclusion of a nonvolatile component dissolved in the spray solvent.

4.4.2 (U) Superpressure balloons

(U) Superpressure balloons (which any space balloon must be!) have been proposed (and to some extent tested) for high altitude scientific ballooning. The tension in the balloon membrane can be expressed as:

$$\sigma = \frac{pR}{2h}, \tag{4-9}$$

where p is the internal pressure, h the skin thickness, and R the radius of curvature. The ratio R/h is very large (perhaps $\gtrsim 10^6$) for superpressure balloons in the upper atmosphere that must maintain constant buoyancy through the diurnal temperature cycle. Atmospheric superpressure balloons have had a lobed structure in which each lobe has a comparatively small

radius of curvature (the shape resembles that of a pumpkin), with the tensile load taken up by high-strength (aramid or UHMWPE) cables between the lobes.

(U) Such a lobed structure is obviously unsuitable for a focusing mirror. However, in space the inflating pressure may be very low (Sec. 4.4.4) and the tensile load carried by the balloon fabric.

4.4.3 (U) Making Balloons

(U) Active and adaptive optics can refine the shape of a reflectorized balloon, but are limited in their range of motion. In addition, they create high-order (high spherical harmonic indices) shape distortions when correcting low-order imperfections. As a result, the uncorrected balloon shape should be as close to the desired final shape as possible.

(U) It is not possible to fabricate thin membranes (balloons) with highly uniform thickness and mechanical properties. The fractional uniformity required of an uncorrected shape is $\approx \lambda/(20R)$; for a 30 m $f/2$ optical reflector (radius of curvature $R = 120$ m) this is this is about 4×10^{-10} while for a 100 m $f/2$ radio (30 GHz) reflector it is about 2.5×10^{-6}. These values are relaxed by orders of magnitude by correction, but still indicate the difficulty of the problem.

(U) A partial solution is to fabricate the reflector's shape accurately without demanding extreme accuracy in its thickness, and minimizing the inflation pressure to minimize the effects of heterogeneity in thickness and mechanical properties. This can be done by spraying or vapor-depositing the balloon material on a stiff and accurately shaped mandrel. The deposited material need not be the ultimate polymer but rather a chemical precursor that can be cured (polymerized) and stiffened by ultraviolet light or a chemical agent; this would permit the use of liquid or high vapor pressure precursors that themselves would not be suitable balloon materials.

(U) The reflectorizing material (typically Al) could be vapor-deposited after the balloon is formed, but while it is still on the mandrel (requiring a concave mandrel). The shape would be correct to the accuracy of the mandrel although the thickness and materials properties would necessarily be significantly (perhaps 10% across the balloon) nonuniform.

4.4.4 (U) Inflation pressures

(U) A balloon fabricated on a mandrel accurately reproduces the shape of the mandrel, that can be tightly (to 1 mil or even more closely) controlled. However, its thickness is difficult to control accurately, particularly if sprayed on, perhaps the only process for making large balloons or their gores segments). As a result, inflation pressure will strain them and distort their shape. The fractional variation in thickness $\Delta h/h$ might be ~ 0.1. This is representative of the variations in thickness of light initiated high explosives, sprayed-on as we suggest for accurate fabrication of balloons, and may be a general feature of such processes[6]. As nominal parameters we will generally take $h = 2.5 \times 10^{-3}$ cm (1 mil) and $\Delta h = 2.5 \times 10^{-4}$ cm (0.1 mil).

(U) The distortion ΔR from a balloon's nominal shape when the balloon is inflated, as a result of stretching of its fabric, may be estimated

$$\Delta R = \frac{R^2}{2h}\frac{\Delta h}{h}\frac{p}{E}, \tag{4-10}$$

where $\Delta h/h$ is the non-uniformity of the balloon skin's thickness and mechanical properties, h is its nominal wall thickness, p is the pressure of the filling gas and E is the Young's modulus of the balloon fabric and R is its nominal radius of curvature.

4.4.4.1 (U) Radiation Pressure. It may not be feasible to shield a km-scale balloon against Solar radiation pressure because of the mass and size

[6](U) Developable surfaces, such as cylinders, may be made very uniform by rolling, but that is not applicable to non-developable surfaces such as spheres and paraboloids.

of the required sunshield, and the difficulty of keeping it extended. Possible solutions include using another reflectorized balloon as the shield or centrifugally stabilizing a flat shield with a mass-loaded periphery. However, here we assume that is not done and estimate the minimum inflation pressure needed to maintain the balloon's shape against Solar radiation pressure.

(U) The radiation pressure on a reflective surface is $2I_\odot/c$, where $I_\odot = 1.4 \times 10^6$ erg/(cm^2 s). This produces a distortion

$$\Delta R = \frac{2I_\odot}{cp} R. \tag{4-11}$$

Equating ΔR from Eqs. 4-10 and 4-11 gives a cross-over, and the minimum pressure required that radiation pressure distortion not dominate distortion produced by imperfect fabrication:

$$p_{rp} = \sqrt{\frac{4I_\odot E}{c} \frac{h}{\Delta h} \frac{h}{R}}. \tag{4-12}$$

Adopting $\frac{h}{\Delta h} = 10$, $\frac{h}{R} = 2.5 \times 10^{-8}$ ($h = 1$ mil and $R = 500$ m) and $E = 20$ kbar yields $p_{rp} = 1.4$ dyne/cm^2.

(U) Taking $p = p_{rp}$, Eqs. 4-10 and 4-12 may be used to find ΔR:

$$\Delta R = \sqrt{\frac{I_\odot}{c} \frac{\Delta h R^3}{h^2 E}} \approx 3.4 \text{ cm}. \tag{4-13}$$

Correction would be required to achieve $\lambda/20$ accuracy even at radio wavelengths, except perhaps at frequencies $\lesssim 5 \times 10^8$ Hz (UHF).

4.4.5 (U) Gravity gradient

(U) The gravity gradient force per unit area of balloon surface can be described as a pressure $GM_E R\rho h/D^3$, where $\rho = 1$ g/cm^3 is the density of the balloon material and M is the mass of the Earth. This produces a distortion

$$\Delta R = \frac{GM_E R^2 \rho h}{D^3 p}. \tag{4-14}$$

As before, we find the cross-over between distortion produced by gravity gradient and that produced by imperfect fabrication by equating the values

of ΔR found from Eqs. 4-10 and 4-14 to find the pressure that minimizes the distortion:

$$p_{gg} = \sqrt{\frac{h^3}{D^3}\frac{2GM_E\rho E}{\Delta h}} \tag{4-15}$$

and

$$\Delta R = \sqrt{\frac{R^4}{D^3}\frac{\Delta h}{h}\frac{GM\rho}{2E}}. \tag{4-16}$$

Taking $p = p_{gg}$ we find

$$p = \begin{cases} 1.7 \text{ dyne/cm}^2 & \text{LEO} \\ 0.12 \text{ dyne/cm}^2 & \text{GEO.} \end{cases} \tag{4-17}$$

Eq. 4-10 or 4-15 yield

$$\Delta R = \begin{cases} 4.3 \text{ cm} & \text{LEO} \\ 0.3 \text{ cm} & \text{GEO.} \end{cases} \tag{4-18}$$

(U) At LEO gravity gradient is slightly more distorting than radiation pressure for the assumed parameters, but at GEO gravity gradient is less distorting. However, in either case correction would be required to achieve $\lambda/20$ accuracy even at radio wavelengths. As discussed in Sec. 4.6, the number of independent actuators required to correct the shape of a balloon is likely prohibitive.

4.5 (U) "Tensegrity"

(U) "Tensegrity" is a term applied to structures that contain a combination of compression and tension members, such as may pertain to the "backbone" structure that supports the mirrors under consideration. Its understanding underlies approaches to forming mirror structures with the appropriate degree of smoothness. This is an ancient technology that has even been described in the Bible: it is used in tents (Numbers 24:5). Their tension members, ropes, are pinned to the ground with pegs or nails (Judges 5:26), themselves held in place by a frictional force that itself results from the compressive stress on the sides of the peg produced when it is driven into the

ground. This is in contrast to structures made of stone in which all stresses must be compressional because stone cannot support significant tension.

(U) Fortunately, technology has provided us with tensile members much better than the natural fiber ropes of antiquity. They may be made of metal or of polymers (UHMW polyethylene, aramids) with far superior strength-to-mass ratios. The limitation of very slender tensile members is that they cannot bear compression loads without buckling.

(U) Conservation of momentum requires that to avoid net acceleration, a tensile force be opposed by a compressive force, and *vice versa*. In order to apply a force to correct a reflecting surface, somewhere else a force of the opposite sign and magnitude must be applied. This produces a moment; to avoid angular acceleration, an opposite moment must be applied elsewhere. Familiar examples are three- and four-point bending.

(U) Correcting the figure of a mirror requires application of force at points across it. Because the weight of the mirror is not available in space to oppose the force, the simplest possible configuration is sketched in Fig. 7 (a). At each surface point, one member is in tension and the other is slack, exerting no force. The disadvantage of this geometry is that the light illuminating the reflector is scattered by the tensile members. This may not be a problem at radio frequencies if the tensile members are thin and made of insulating polymer, but it is prohibitive for visible or infrared light. The same method may be used to correct a flat, as shown in Fig. 7 (b).

(U) The geometry of Fig. 8 (a) solves the problem of tensile members scattering incident radiation by balancing tensile forces with a compression member on the "back" (un-illuminated) side of the reflector. However, the combination of compressive and tensile forces applies bending moments to the reflector, which must be mechanically stiff, as discussed in Sec. 4.3.1.

(U) If the reflector were stiff enough, had a coefficient of thermal expansion small enough, and were made accurately enough, then correction would not be necessary. This is shown in Fig. 8(b)(that does not show the connections

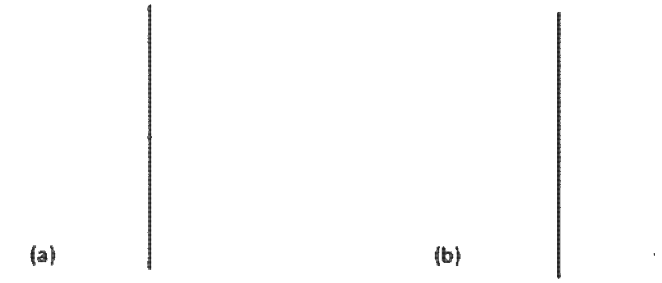

Figure 7: (U) (a) Two-sided active figuring. Forces at each point of the reflector may be applied in either direction, one tensile member in tension and the other slack. The vertical member, thick enough (in practice, a truss) to prevent buckling, takes the corresponding compressive load. (b)Two-sided active figuring applied to a flat.

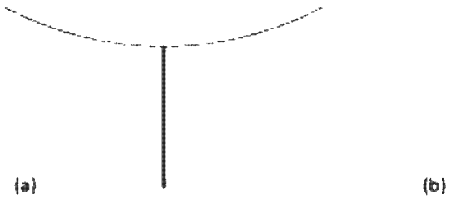

Figure 8: (U) (a)Mechanically correcting a reflector, using a combination of tensile and compressive members that do not scatter radiation in its aperture. Forces and moments are balanced. The reflector must be stiff to smooth the tensile correcting forces applied at points, as discussed in Sec. 4.3.1, (b) The ideal case of a stiff and accurately figured reflector with small coefficient of thermal expansion that does not require correction. These conditions are probably not realistic. Connections necessary to steer and slew it are not shown.

necessary to steer the telescope) However, these conditions are not likely to be met.

4.6 (U) Smoothing of Corrections

(U) Even when employing actuators to make local corrections of the mirror surface, it is necessary that the correcting displacements vary smoothly across the surface on the scale over which the necessary corrections vary. This is true for both optical and radio-frequency apertures. Actuators may apply forces at (ideally) single points of contact or over narrow regions. Smoothness can be achieved in either of two ways: 1) by spacing the actuators closer than the scale over which the required corrections vary; 2) by making the corrected surface sufficiently stiff to flexure that displacements vary smoothly across it.

(U) In terrestrial optical astronomy the isoplanatic [7] patches of seeing that must be corrected are small and the first method is used, with reflecting elements sufficiently flexible that correction can vary with the spatial dependence required. In a segmented reflector subject only to distortions that vary gradually with position, such as those induced by temperature inhomogeneity, the reflector segments can individually be stiff, and each (mechanically uncoupled) segment corrected independently.

4.6.1 (U) Flexible membranes

(U) Here we consider reflectors with negligble flexural stiffness, such as a metallized balloon reflector for radio frequencies.

(U) Applying an inward (tensile on the inside of the curvature or compressive on the outside) point force to a thin shell with negligible bending stiffness, such as a balloon, produces a singular deformation. The balloon's pressure acts to minimize the reduction in volume produced by the inward

[7](U) patches having the same planarity

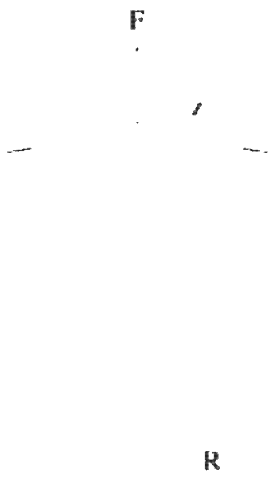

Figure 9: (U) A force applied at a point pulling outward on a completely flexible sphere.

force, narrowing the indentation to a singularity. The sheet will form a corrugated half-cone with the applied force at its apex in the limit of no resistance to crumpling or flexure. The shape and depth of deformation are singular; indenting the shell exacts no energy price if there is no reduction in gas volume. Such a singular deformation is not desired when the purpose is to correct the figure over a finite area.

(U) Another singularity may occur when an outward force is applied to a point on the surface of a balloon of fabric that does not resist flexure. This problem is not symmetric in the direction of the force because gas pressure acts to expand the volume of any distortion of the surface. An approximate geometry is suggested in Fig. 9. The deformed surface is tangent to the undeformed sphere (or local spherical approximation) because there is no bending stiffness to support a bending moment where they join.

(U) If the balloon fabric is stiff to extension, a good approximation for the materials we consider (but not for rubber balloons), its area and the circumferences of its sections (such as those in the plane of the Figure) cannot grow. These constraints enforce a reduction in volume from its initial, maximum volume, spherical shape, doing work on the inflating gas. There will be some crumpling in the conical section shown in the Figure, maximized at its apex. It is possible to calculate the distorted profile as a function of the applied force, but this was beyond the capability of a short study. However, as indicated in Fig. 9, the distorted shape will not be smooth, and applying point forces will not correct a balloon reflector to a desired optical (radio-frequency) figure.

4.6.2 (U) Shells with stiffness

(U) A metallized glass reflector for visible and infrared light has significant flexural stiffness, which removes the singularities that result when point forces are applied to completely flexible membranes. Stiffness may be further increased by supporting this comparatively thin (cm or tens of cm) glass shell on a deep truss. A radio reflector may similarly be stiffened by supporting it on a truss. The geometry (without a supporting truss) is shown in Fig. 8 (a). Flexural stiffness smooths the deformation produced by a point force over a width

$$d \sim \sqrt{hR} \tag{4-19}$$

from the point at which the force is applied (or a displacement is enforced) [41] and falls off rapidly at larger distances. The relation between the deflection w at the point of application and the force F is

$$w = \frac{\sqrt{3(1-\nu^2)}}{4}\frac{FR}{Eh^2}, \tag{4-20}$$

where ν is the Poisson ratio [78].

(U) To control a surface of radius R requires $N = \mathcal{O}(R/h)$ actuators. If accurate control is required (to a small fraction of the actuators' displace-

ment) there is a coefficient (depending on that fraction) $\gg 1$ multiplying that order-of-magnitude estimate. For a spherical reflector of low f-number (a rough approximation) the radius of curvature

$$R = 2\text{Focal Length} = 2f\text{Diameter} \sim 2f\,\text{km} \tag{4-21}$$

for a nominal [redacted] aperture. Combining this with Eq. 4-19 yields the approximate number of actuators required to achieve a smooth contour. (b)(3)

4.6.3 (U) Balloons

(U) Taking $f = 1.25$ and $h = 1$ mil, appropriate for a mylar or similar balloon, yields a requirement for a minimum of $N \sim 10^8$ actuators. No precision of dimensional compensation has been assumed. There is an additional weak dependence of the ratio of that precision to the magnitude of distortion (thermal, manufacturing imprecision in both dimension and stiffness, Solar radiation pressure and Solar wind, *etc.*) that must be compensated, that likely introduces at least another factor of ten.

4.6.4 (U) Optical reflectors

(U) Optical reflectors consist of much thicker and stiffer structures than balloons. As a result, they require many fewer actuators. If the diameter is 30 m and the thickness 2.5 cm, as has been suggested for honeycomb optical elements (the presence of voids within the honeycomb slightly relaxes the requirement because material is concentrated on the surfaces where strain is maximized), the result for $f = 1.25$ is a few thousand actuators. Even allowing another order of magnitude for the gradual fall-off of displacement beyond a distance d from the point of activation, the resulting estimate of $N \sim 3 \times 10^4$ actuators may be daunting, but is not prohibitive in the context of a visionary space system. The task of these actuators is much eased by the fact that they need only respond to slowly varying (on time scales of minutes or hours) transients, rather than the ms atmospheric turbulence transients that ground-based adaptive optics must compensate.

4.6.5 (U) FINDING

(U) It is not feasible to correct a reflectorized balloon for the effects of manufacturing imperfections and other distortions well enough to make it a useful mirror at shorter radio wavelengths.

4.7 (U) Sparse Apertures

(U) The lightweight mirrors discussed in this report are examples of so-called "filled apertures", meaning an aperture filled with reflecting glass, of (usually) circular cross-section with some outer diameter D_{circ} and area $A_{\text{filled}} = \frac{\pi}{4} D_{\text{circ}}^2$. The aperture provides two different parameters of telescope performance: First, the optical power P collected is equal to $I A_{\text{filled}}$, where I is intensity of the incoming light; greater A_{filled} enables greater P and therefore better SNR. Second, the angular resolution of the telescope $\Delta\theta = 1.22\lambda/D_{\text{circ}}$ is better for greater D_{circ}. A "sparse aperture" is an aperture, again of a given outer diameter D_{circ}, which only partly filled with some number of smaller mirror surfaces of total area A and mostly filled with nothing. The fill factor is defined as the ratio of mirror area to available area

$$\alpha \equiv \frac{A}{A_{\text{filled}}} = \frac{4A}{\pi D_{\text{circ}}^2}, \quad (0 < \alpha < 1) \tag{4-22}$$

For example, with N circular mirrors of some smaller diameter D, we have $A = \pi N D^2/4$ and $\alpha = N D^2/D_{\text{circ}}^2$; see Fig. 10. Sparse apertures are also known as "unfilled apertures", or for RF apertures, as "thinned apertures", especially for phased array antennas. The advantage of a sparse aperture is that it offers the same resolution $\Delta\theta = 1.22\lambda/D_{\text{circ}}$ as a filled aperture of the same outer diameter D, the disadvantage is that it collects less power P, and suffers greatly in SNR, as explained below.

(U) In order to provide full resolution, the smaller mirror surfaces must be carefully located and arranged, following certain codes closely related to error-correcting codes in digital communications; Golay codes are often used.[8] See Fig. 11.

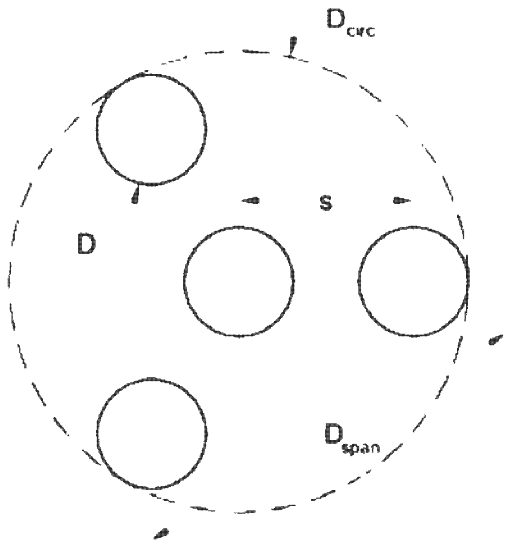

Figure 10: (U) Example of a sparse aperture comprised of 4 smaller mirrors arranged according to a Golay-4 code [54].

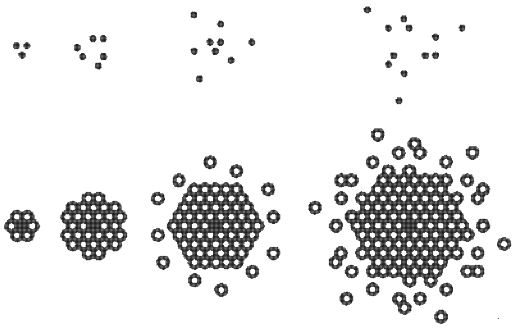

Figure 11: (U) More examples of sparse apertures. Upper subfigures, left to right: Sparse apertures comprised of 3, 6, 9, 12 smaller mirrors (arranged in Golay codes). Lower subfigures: Corresponding autocorrelations; wider means better resolution [54].

[8](U) Technically, the autocorrelation function of the mirrors' surfaces must contain all relevant baselines [54].

(U) Sparse apertures become useful for telescopes that are limited in mass or mirror cost, when one has plenty of power P but wants better resolution $\Delta\theta$, *i.e.*,, greater D_{circ}. A good example is the observation of the daylit Earth from high orbit. Small satellites carrying sparse apertures have already been considered in detail [13]. Therefore we turn to space assemblies to implement large, sparse optical apertures. A concept well worth pursuing is a space assembly, say a planar truss of circular cross-section, carrying a system of smaller mirrors.

(U) However, important trade-offs in image quality remain. Filled-aperture telescopes immediately produce useful images, because the telescope's Point-Spread Function (PSF) is narrowly peaked with width $\sim \Delta\theta$; such images might then be improved further by digital post-processing. But sparse-aperture telescopes produce messy images because the PSR shows broad wings carrying most of the power P from a point source [54]; see Fig. 12. Therefore image restoration by digital post-processing is essential to produce useful images, and signal-to-noise ratio (SNR) inevitably suffers, Fig. 13.

(U) Even for sparse apertures constructed using the best codes, SNR suffers greatly. A useful figure-of-merit is the *stare time*, t_{stare} needed to collect an image of given scene at a given desired SNR. Since power $P \propto A \propto \alpha$ (for fixed D), one might naively guess that $t_{\text{stare}} \propto \alpha^{-1}$. But the truth is much worse; due to the messy PSF and need for digital restoration, it can be shown that $t_{\text{stare}} \propto \alpha^{-3}$ for Golay-coded apertures and in fact for any fixed code.

(U) But a surprising result emerges. A different kind of sparse aperture can be created by rotating a slit-like mirror of length D and smaller width W, so with $\alpha = \frac{4}{\pi}W/D$. While at any one instant, only some of the image's baselines are captured, over half a rotation, all relevant baselines in all directions are captured [64]. For such a rotating sparse aperture, it can be shown that $t_{\text{stare}} \propto \alpha^{-2}$ [64]. Thus, for given D and given A, a rotating sparse aperture has better SNR performance than any fixed coded aperture.

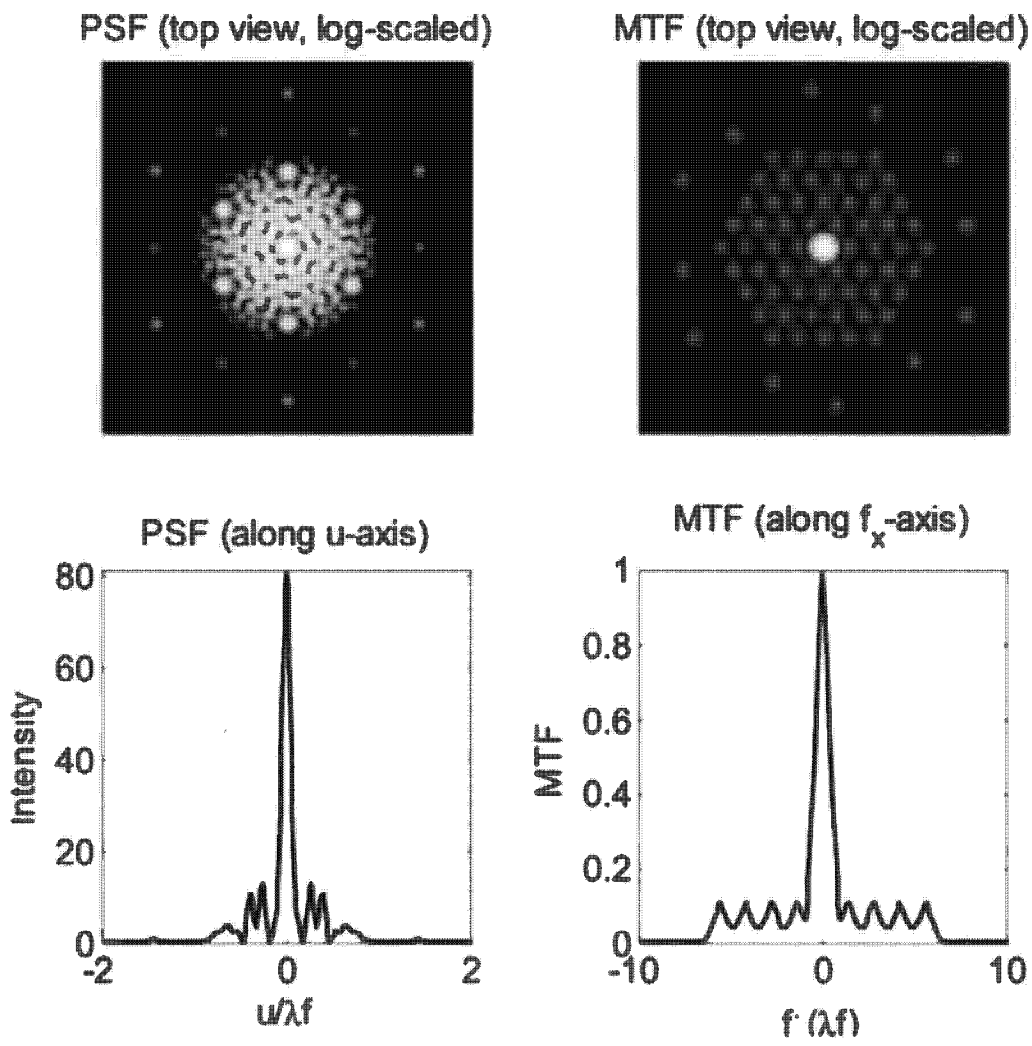

Figure 12: (U) Point-spread function (PSF) of a certain sparse aperture (Golay-9). The modulation-transfer function (MTF) is the corresponding quantity in Fourier-transform image space [54].

(U) What this means for space assembly is that a rotating assembly, shaped like a long, narrow rectangle rotating around the radial axis from Earth, is a promising concept, in addition to the concept of a fixed circular assembly.

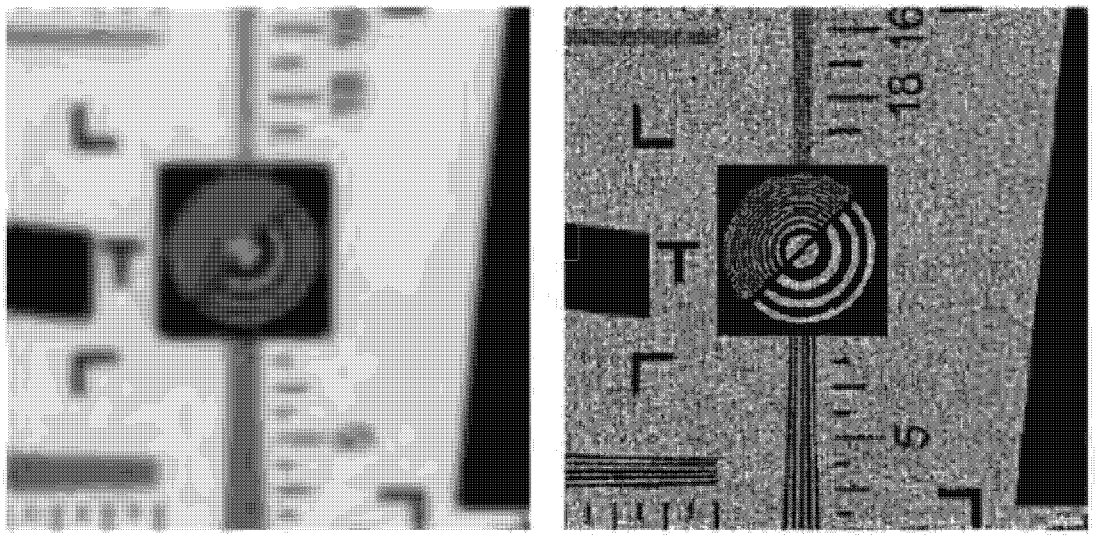

Figure 13: (U) (Left-hand side) a raw Golay-9 "sparse" image, and (right-hand side) the restoration of the image through post-processing of the image using a filter [54].

4.7.1 (U) FINDING

(U) Sparse apertures are useful for telescopes that are limited in mass or mirror cost, and may mitigate constraints for space-assembled mirrors. A rotating sparse aperture can have a better SNR than fixed, coded apertures and is a promising concept to explore.

This Page Intentionally Left Blank

5 (U) TECHNOLOGICAL CONSIDERATIONS

5.1 (U) Thermal Issues

(U) Variation of temperature across a structure distorts its shape. Thermal expansion of one part in 2×10^9 would be significant for a 40 meter optical reflector required to be accurate to $\lambda/20$. In principle, thermal distortions can be corrected, but it is desirable to minimize their amplitude and to make them homologous in order to reduce demands on the adaptive correction system. High wave-number (in the optical surface) correction requires large numbers of actuators, and large amplitudes of correction place demands on their range of motion. Some of these demands can be mitigated by correcting a secondary or tertiary reflector rather than the large primary mirror, but reducing thermal distortions produced by temperature gradients is always desirable.

5.1.1 (U) Coefficient of thermal expansion

(U) Essentially all materials have non-zero coefficients of thermal expansion. Even if nominally zero at some temperature, imperfect manufacture leads to non-zero values in real fabricated objects. In addition, the coefficient of thermal expansion is only the first term in an expansion of dimension as a function of temperature, and for significant temperature excursions the next term (effectively the temperature derivative of the coefficient of thermal expansion) becomes significant. Formally, the dimensionless strain,

$$\epsilon = \alpha|_{T_0}(T - T_0) + \frac{1}{2}\left.\frac{d\alpha}{dT}\right|_{T_0}(T - T_0)^2 + \ldots, \qquad (5\text{-}23)$$

where α is the coefficient of thermal expansion. Near room temperature, $\alpha \approx 10^{-5}$/K for titanium, $\alpha \approx 2 \times 10^{-5}$/K for aluminum and $\alpha \approx 3 \times 10^{-6}$/K for borosilicate glass. The ultra-low expansion glass Zerodur has α nominally as small as 0.7×10^{-8}/K, but with inhomogeneities as much as a few times

greater, so we adopt a value of 10^{-8}/K [71]. Furthermore, glasses such as Zerodur can lock into non-equilibrium configurations such that the time-history of heating becomes important. For example, samples of Zerodur examined with respect to application in the Extremely Large Telescope and Thirty Meter Telescope exhibited hysteresis over a 0.4°C temperature range having a fractional deviation in length of 0.3×10^{-8} [35], a magnitude that is comparable to the anticipated total expansion for a 0.4°C change in temperature. Prediction of mirror deformation would, therefore, require a time-transient model of the heating and cooling of the structure.

(U) In non-metals, such as glass and carbon-carbon materials, coefficients of thermal expansion generally decrease rapidly with decreasing temperature, in proportion to the specific heat, which is $\propto T^3$ below the Debye temperature (far above room temperature for stiff low density materials). This minimizes thermal expansion in a cooled structure. In metals the specific heat varies only $\propto T$, so α declines more slowly with decreasing temperature. For Zerodur, however, expansion coefficients have been found to be smallest in the range between 300-100°K, and then increasing until about 40°K [36], possibly because of the blend not having been optimized for cold conditions. Although such low temperatures are not anticipated, instabilities have been reported for Zerodur at 30°K when cooling and 20°K when heating with fractional lengths of 0.6×10^{-6} [10]. Radiation will also cause compaction, and in Zerodur this behavior can be difficult to predict [11]. Such complex behavior of materials indicates the utility of first undertaking testing at modest scales in space.

5.1.2 (U) Temperature equalization

(U) The demands on active correction of thermally distorted optics are relaxed if temperature gradients can be minimized and the structure's temperature equalized. Heat conducts slowly across large structures, but flows rapidly in heat pipes. These need not be actual pipes, but can consist of an enclosure of any shape containing a condensible vapor and a wick to

carry it from colder regions, where it condenses, to warmer regions, where it evaporates. For example, the back of a primary mirror in a Gregorian or Cassegrain reflector could be enclosed in an annular bag filled with a suitable vapor with a wick across the back of the primary reflecting surface. This bag would be protected against micrometorite perforation by the reflector itself on one side, and by the thermal shields on the other. Use of a mixture of fluids with a range of vapor pressures can enable a heat pipe to function across a wide range of temperature.

(U) Because differential heat loads across a properly shielded reflector are small, a low density gas would be sufficient. Many fluorocarbons and chlorofluorocarbons exist (or can be synthesized) with a wide range of vapor pressures, and one or a mixture suitable to almost any temperature range can be found.

5.1.3 (U) Shielding

(U) Optical space telescopes are shielded from direct Solar illumination by Sun shields, putting them in shadow. This is necessary because scattering of direct Solar illumination would produce so much scattered light, even from a tiny dust particle, as to preclude optical observations. It has the additional benefit of reducing Solar heating.

(U) The operating temperature can be significantly less than the grey-body equilibrium temperature (about 265 K) because the entire structure would be in the shadow of the sunshield. An optical system pointing away from the Earth would only be heated by the fraction of Solar heating reradiated in the infrared by the dark side of the sunshield. This provides passive cooling, and may achieve temperatures far below 265 K, depending on the spacecraft environment (LEO, MEO, GEO or deep space). Passive shielding of external surfaces to as cold as 200 K and internal surfaces to 100 K has been demonstrated [50], with residual heating coming from the infrared radiation emitted by the back side of a sun shield. See [28] for a review of

passive shielding. In deep-space temperatures as low as < 20 K have been predicted [85]. Only the differential heating across the reflector or supporting structure would need to be equalized by heat flow, and this is likely to be a small fraction of the mean heating.

5.1.3.1 (U) Considerations at LEO. (U) Heating by the Earth's thermal radiation and the fraction (the albedo, about 30%) of Solar radiation scattered by the Earth must also be considered. For a reflector in LEO these are comparable to Solar heating, and an Earth shield must be provided. If the reflector is downward-facing, the aperture cannot be shielded, but any truss behind it can be. Reflectorized surfaces absorb only a few tenths of a percent of incident visible and NIR radiation, but trusses of carbon-fiber material are black.

(U) The truss that supports the secondary reflector and the secondary itself are in front of the primary mirror. In a downward-facing telescope they can be shielded from most (but not all) terrestrial thermal and scattered Solar radiation by a wide conical shield enclosing the primary and a narrower shield around the truss. These cannot be complete shields because they must not limit the field of view. These limitations do not arise for upward-facing reflectors; their entire back surfaces (and heat transfer bags) may be shielded.

5.1.3.2 (U) Considerations at GEO. (U) For reflectors in GEO the intensity of terrestrial infrared and scattered Solar radiation is $\approx R_E^2/(4R_{GEO}^2) \approx 0.006$ of that in LEO. An Earth shield may not be necessary, but an effective sun shield would still be required.

5.2 (U) Heat-Pipe Technology

(U) Heat pipes are in common use in industrial and consumer equipment. In brief, they are passive components or subsystems that allow the flexible (literally in some cases) and effective transfer of heat over long distances

with little investment of weight or space. Heat pipes are commonly used to transfer waste heat from the microprocessor in personal computers to a cooling fan or passive radiator.

5.2.1 (U) Introduction

(U) There are many scholarly articles about heat pipes, but Korn (2008) provides a practical, easy-to-read article about general heat pipe design. A heat pipe is a largely or entirely passive device that boils a fluid at its hot end, with the vapor flowing along the internal space of the pipe or plate to the cold end, where it condenses. The vapor flow is driven by a pressure drop while the condensate is transported back to the hot end by a "wick" attached to the internal wall or surface of the heat pipe. The wick need not be in good contact with the wall for most of its length, and is sometimes made of sintered or textured metal that is "wet" by the working fluid, which is often water or ethanol. Note that the heat pipe or heat plate is otherwise evacuated, so that vapor flow is not impeded by non-condensible gas.

(U) Holding one end of a meter-long flexible tube (the hot leg of a heat pipe) while immersing the other in a pot of boiling water will result in a rude shock, because that end will instantly become hot: this is non-intuitive behavior. Furthermore, if you place a cold surface above the tube, the steam will condense there and the water can drip onto a wick or tube that carries it back to the boiling water pot, the cold leg of this very simple heat pipe system.

(U) A recent paper by a group at Nagoya implements heat-pipe technology on a 3.9-kg 3U CubeSat to demonstrate the transfer and radiation of 100W of solar heat input to a phase-change thermal regulator, and to a high-connectivity flexible graphite radiator [79]. Figure 14 shows the device during its development.

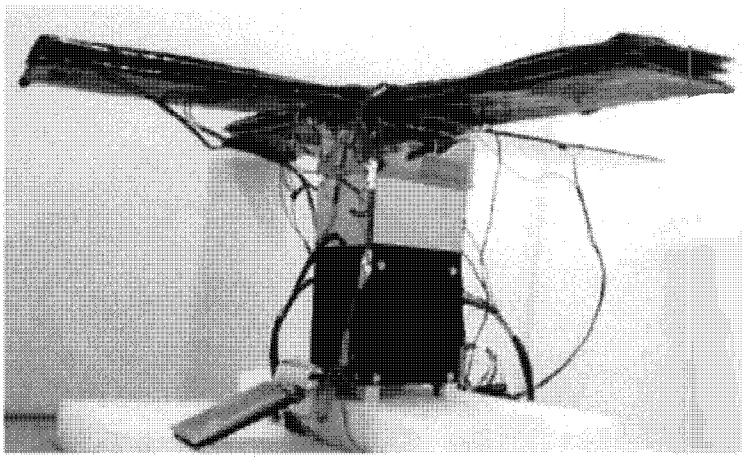

Figure 14: (U) 3U thermal-vacuum test model for 100W heatpipe system. From [79].

(U) Heat-pipe technology can be used to maintain constant temperature of structural elements or metering rods for on-orbit systems, for efficient cooling of payload elements, including passive cooling of elements of the focal plane, and as proposed here, for maintaining large optical elements at uniform temperature so as to enable the use of potentially lightweight, low-cost optics made of borosilicate glass (Ohara E6, similar to Pyrex).

(U) JASON received information that JPL has considered using heat pipes in conjunction with carbon-fiber struts in order to ensure that the strut is at constant temperature. Of course, it is important that the heat pipe itself not contribute rigidity to the strut, because it has a large and uncontrolled coefficient of thermal expansion (CTE). Heat pipes should be the first option for cooling, making transport of heat almost as simple as carrying electricity along wires. Zero-g facilitates the use of heat pipes because there is no significant "gravity" to impede capillary flow even for large structures. The sections below describe approaches to the natural incorporation of heat pipes into the support trusses of the mirrors.

5.2.2 (U) Trusses as heat pipes

(U) An effective way to manage thermal issues and accommodate thermal distortions is to seek means of integrating heat management within the structures itself. For example, in Section 6.3, *A Version of the 40 m Extremely Large Telescope in Space*, the suggestion is made that its structure be a large truss composed of carbon fiber reinforced plastic (CRP) tubes, each 2 m long, 5 cm in diameter, with walls 1 mm thick. These could be heat pipes, filled with a suitable vapor that operates at ambient temperatures and lined with a wick consisting of a fine mesh or bundle of fibers that are wettable by the condensed vapor. Heat pipes are discussed by [62], among many other sources.

(U) Further, it is possible to reduce the thermal expansion of a truss member by the use of a *gridiron structure*, involving anti-parallel expansion of two materials with different coefficients of thermal expansion (both positive). This method is used to minimize the temperature coefficient of pendulum clocks (`https://en.wikipedia.org/wiki/Gridiron_pendulum`). It would add complication that would be unnecessary if active compensation is effective, but could reduce the required range of active compensation by a large factor.

(U) Heat pipes have extremely low thermal impedance if filled with a fluid of suitable vapor pressure, so that the vapor has sufficient density at the working temperature to carry a heat flux sufficient to bring the two ends into equilibrium at a modest (very subsonic) flow speed. The difference between vapor pressures at the two ends drives the flow between them, and the heat flow is the mass flow times the specific enthalpy of evaporation. The wick must also effectively transport the liquid from the cold to the hot end, to avoid "dry-out", a condition in which no liquid reaches the hot end and its temperature rises. These are easy criteria to satisfy by choice of an appropriate working fluid, and with modest power loads (as would be found in

this application) the temperature drop is very small. Including a mixture of fluids with a range of vapor pressures enables operation over a wide temperature range.

(U) The capillary pressure of a convex surface is greater by an amount inversely proportional to its radius of curvature (and analogously for a concave surface but with the opposite sign) so that by grading its mesh the wick can actively drive the return flow of liquid. If the surfaces are convex (requiring a volume of liquid greater than the pore space of the mesh) then a finer mesh at the cold end will tend to drive the liquid to the hot end, as desired. With an ungraded wick accumulation of liquid at the cold end forces it to bulge through the mesh with a radius of curvature that decreases as the liquid accumulates and that drives the return flow.

(U) If each tube were a separate heat pipe, because heat pipes have such low thermal impedance the overall thermal impedance of the truss system would be in conductive contacts between tubes. Assuming the thermal contacts would have area of 1 cm^2 each, fitted to the tube's curvature and extending through its 1 mm thick wall for contact with the heat pipe in the interior, the thermal impedance at each 2 mm contact would be about 0.08 K/W for Al, and about 0.05 K/W for Cu. The thermal impedance of the heat pipe itself is likely less. Because of the branching nature of the truss, its overall thermal impedance is not much greater than the thermal impedance of a single tube or junction (just as the resistance of a large cube of conductor is less than the resistance of a smaller cube).

(U) For a rough estimate of the asymmetric heating, consider a truss in GEO, well-shadowed from the Sun. It is still heated by sunlight scattered from the Earth as well as Earth's thermal radiation. Over long times their sum must be constant, but on short times they are not, and their sum also varies across the face of the Earth. The structure behind the primary mirror may be shielded by the mirror itself, if the telescope is pointed to the Earth. An earthshield rigidly attached to the structure could shade every part of the structure except the optical aperture.

(U) Consider a single tube in the truss, one end of which is shielded from the Earth's radiation and the other not. At GEO this is about 0.006 of the Solar flux at Earth, or about 0.8 mW/cm^2. The heat load on 1 m of tube is then about 0.8 W, implying a temperature drop from one tube to another (the heat pipe keeps each individual pipe closely isothermal) of $\Delta T \approx 0.06$ K for Al contacts. For CFRP (carbon fiber reinforced laminates) the coefficients of thermal expansion are in the range $\alpha = 1\ \ 10 \times 10^{-6}$/K, depending on orientation and layup, indicating strains of $\alpha\Delta T \approx 0.6\ \ 6 \times 10^{-7}$ [19]. This is quite significant, and will require active, though likely slow, compensation.

(U) A linear thermal expansion coefficient of 10^{-6}/K, near the lower end of the range for carbon fiber reinforced plastic near room temperature but likely obtainable by control of fiber orientation, implies a thermal strain of $\sim 10^{-7}$ in GEO and $\sim 10^{-5}$ in LEO. In a 30 m structure, this corresponds to displacements of $\sim 3\,\mu$ in GEO and $\sim 500\,\mu$ in LEO. For a visible light telescope these must be compared to the required figure accuracy of $0.02\,\mu$. At radio frequencies the requirements are relaxed by about four orders of magnitude, inversely proportional to the frequency. Adaptive optics may compensate for these, fortunately slowly varying, thermal distortions, but in Sec. 4.3 we discuss another approach to minimizing them.

(U) Potentially more threatening could be temperature gradients *across* individual tubes because they could cause displacements of tube ends of $\sim \alpha\Delta T L^2/r$, where L is the tube length and r its radius. This is analogous to the thermal roll-up of a flat sheet, in which a temperature drop ΔT across a sheet of thickness h rolls it into a cylinder of radius $\sim h/(\alpha\Delta T)$ (Landau, L. D. and Lifshitz, E. M. "Theory of Elasticity" 3rd ed. Elsevier, Amsterdam [1986] §7). This is a general problem with ("developable") structures with zero Gaussian curvature, in which the only resistance to thermally-induced strain is resistance to bending, which is very small ($\propto h^3$) for a thin sheet. Surfaces with non-zero Gaussian curvature ("shells") are much more resistant to bending, because it requires stretching (Sec. 4.3.1).

(U) This problem can be mitigated by ensuring that the entire interior tube surface is contacted by the heat pipe mesh, to ensure that it effectively transport heat around the tube circumference, minimizing any transverse temperature differences.

(U) The overall thermal impedance of the truss could be much less if the interior voids of the tubes were connected at their joints to form a single multi-branched heat pipe, bypassing any conductive path. However, this would make the entire heat pipe structure vulnerable to a single meteoritic puncture or a leak introduced in assembly or manufacture. With thousands of tubes making up the truss, such is almost inevitable, and would lead to loss of all the heat pipe vapor and complete loss of heat pipe function.

5.2.3 (U) FINDING

(U) Heat-pipe technologies can be effective in controlling temperatures of space structures, particularly when integrated into the structural elements themselves (e.g. mirror and truss modules).

5.3 (U) Lessons from the International Space Station

The International Space Station (ISS) has been continuously operated without major incident since November 2000. With a pressurized module length of 73 meters, truss length of 109 meters, and solar array length of 73 meters, the longterm structural performance of the ISS potentially provides useful lessons for consideration in the construction and operation of other large structures in space.

(U) The ISS is subject to loads associated with microgravity variations, thermal expansion and contraction, venting water, docking, maneuvering, and reboosting. The complexity and size of the ISS allows for resonances at a wide range of modes. In order to minimize fatiguing components that are loaded under particular resonances, attitude control of the ISS, which is

routinely needed to prepare for docking, is achieved through thrusters that are fired at aperiodic intervals chosen not to excite major resonance modes. Periodic loading associated with variations in solar heating associated with the 16 orbits that the ISS makes per day are more difficult to control, though no major damage or stress has been identified.

(U) The instrumentation available to NASA for monitoring loads are principally accelerometers. In addition, cameras are mounted that allow for observations of, for example, solar panels and interior spaces. No direct measurements of stress or deformation are made, however, such that loading models must be calibrated and tested using only accelerometer data. In a phone conference, David York of Boeing indicated that greater instrumentation of the ISS would have been beneficial in order to ensure appropriate operation and to identify and analyse unanticipated events. For example, a semi-routine incident is that periodic loading arises near a 0.1 Hz resonance of the ISS, prompting mission control to call up to the ISS to ask if anything abnormal is occurring, after which the loading ceases. Such a scenario could arise from an astronaut engaging in unauthorized exercise routines.

(U) A potentially serious incident occurred durring an ISS reboosting operation on GMT14 in 2009. A Russian rocket was to boost the ISS into a higher orbit. Thrust vector control automatically attempts to properly orient the ISS during reboosting. The flexural response of the ISS needs to be filtered out for thrust vectoring to correctly operate upon the rigid structural response, but the filter was improperly applied and the flexural response was instead amplified. Thrust vector control gimbaled from hard stop to hard stop, and the effect are apparent from video of an interior cabin showing the 2.5 Hz variations that ensued (Fig. 15).

(U) Analysis of microelectromechanical systems (MEMS) accelerometer data provided by NASA provides more quantitative detail (data accessed at `https://pims.grc.nasa.gov/archive/pad` on October 5th, 2019). Reboosting is intended to accelerate along the orbital trajectory, but ISS accelerations in the plane perpendicular to the trajectory were $\pm 1000\mu$g during

GMT14 2009 reboost. By way of comparison, during a nominal reboosting event on GMT24 2010, perpendicular accelerations were an order-of-magnitude smaller. In both cases, acceleration in the intended direction along the orbital trajectory were approximately 2000 μg. It is estimate that engineering load tolerances were exceeded in certain areas of the ISS during the GMT14 2009 event but, on account of safety factors in these tolerances, the ISS remained certified for operation. Examination of the acceleration environment prior to and after the GMT14 reboosting event that we undertook indicated no systematic change in the flexural rigidity of the ISS.

(U) One other lesson learned involves the integration of the various subsystems constituting the ISS. Shortly before launch it was realized that thrusting to point the ISS could cause exhaust to impinge upon and possibly damage the solar array. By feathering the solar panels, however, it has proven possible to avoid this.

5.4 (U) Mirrors

5.4.1 (U) Lightweight, segmented mirrors

(U) Formation of high-quality telescope mirrors is a long-undertaken and continually-evolving art. The historical approach in forming optical elements, such as lenses or reflectors, has been to shape a three-dimensional material structure where the complex index of refraction and the geometry of the structure will determine optical focus, reflective efficiency, etc. The process should enable high photon collection capability for a given mirror diameter and concomitant highest spatial resolution, requiring control of surface features to better than a tenth of the wavelength of the relevant light used for the imaging. Mirror-making processes require tight control of the component materials and processes.

(U) JASON was briefed by Professor Roger Angel at the University of Arizona's Mirror Laboratory. He described the formation of 8.4 m mirror seg-

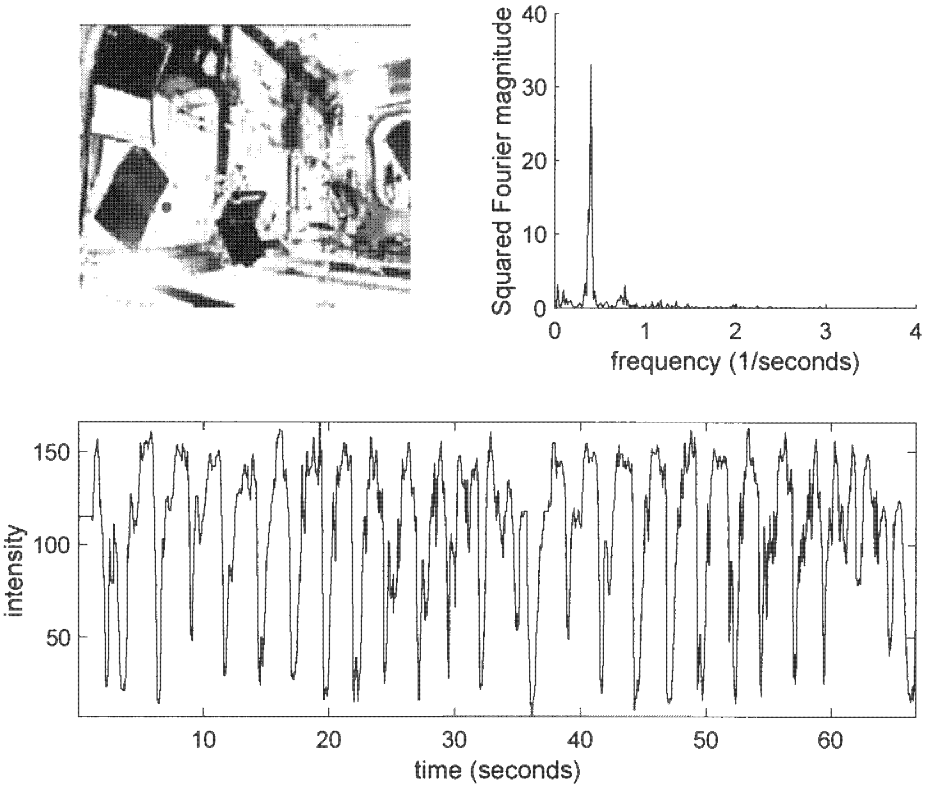

Figure 15: **top left** (U) A grayscale image of an interior cabin extracted from a movie of the GMT14 2009 reboosting event. **bottom** Time-series of image intensity obtained at the point indicated by a red-dot at top left. **top right** Periodogram of the grayscale intensity indicating that most the variability occurs at structural mode near $1/0.4$ s^{-1}.

ments for planned Giant Magellan Telescope, using structures molded from a borosilicate glass (BSG). The mirror surface was subsequently subjected to an automated polishing process that begins with 1000 nm rms smoothness to a final goal of 20 nm rms ($\lambda/20$) over a period of 6 months [68]. The process requires 4 days of polishing per square meter of mirror surface. The components of these segmented mirrors are subsequently actively aligned using actuators forming parts of a computer-controlled active optics system.

(U) The BSG ensures short thermal equilibrium times (30 minutes); near-isothermal performance is achieved by circulating ambient air through apertures in the backplate of the primary mirror made of BSG cells with uniform

faceplates and backplates. Internal air circulation ensures that when the mirror is exposed to the night air, it comes to ambient temperature uniformly within tens of minutes, thus avoiding the impairment of seeing quality otherwise imposed by air rising from the warmer mirror surface. To enable space applications of high-performance BSG optics, one approach would be to seal and evacuate the primary mirror structure after lining it with an appropriate wick material, and provide enough water, ethanol or other working fluid to wet the wick. The mirror cell structure can then serve as a heat pipe at the desired temperature of the primary, which could be arranged (by heat pipe to a radiator viewing deep space, see Section 5.2) to be far below "ambient" temperature; the temperature must be uniform if not a specified temperature. Figure 16 depicts the BSG large primary mirror with rigid cellular structure between faceplate and backing, provided with a heater in each cell to achieve on-orbit figure correction by use of the thermal expansion of E6 BSG glass.

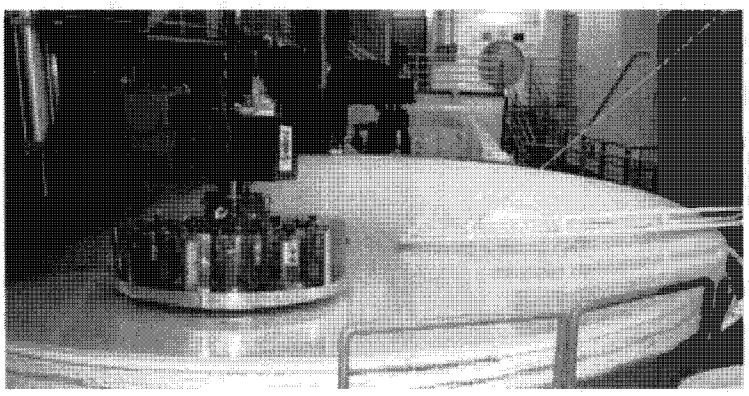

Figure 16: (U) View of the automated polishing tool used to form the mirrors for the GMT [48].

(U) In a 2010 paper with Lockheed, the Arizona group detailed another approach to diffraction-limited BSG mirrors in space by real-time measurement of the surface figure and correction by means of thermal expansion of the BSG front plate in response to heaters in the honeycomb internal pockets of the BSG primary mirror [82]. Thus, this approach uses the relatively high

Coefficient of Thermal Expansion (CTE) of E6 borosilicate glass advantageously by placing a radiative heat panel in each mirror cell with a control system designed to remove shape errors in the mirror figure. Initial analyses proved promising, with mirror surface figure variation less than 6.0 nm rms after input of surface perturbation: this is achieved without the use of additional mechanical actuators [83].

(U) The JASON-proposed alternative to this approach is for the mirror pockets to be lined with material that will provide capillary flow channels for returning a liquid heat transfer fluid to the hotter regions, wherever they may be, where it can evaporate and carry off the excess heat.

(U) As discussed in Section 5.5, each of the seven circular primary mirror segments for the Giant Magellan Telescope is 8.4 m in diameter and has 165 *force actuators.* These not only support the mirror in a properly distributed fashion, but also (as an "active mirror") can compensate low-order errors in fabrication, countering both initial imperfections and aging, as well as the shift of weight that occurs for off-zenith observation in a terrestrial telescope. A further *adaptive optic* component with numerous actuators operating at kHz rates is widely used in terrestrial telescopes which need to image through the inhomogeneous and moving atmosphere at large off-zenith angles, usually on a secondary or tertiary mirror.

(U) For the GMT itself, the 165 force actuators for each 8.4 m diameter segment have a range of command from essentially zero to 1080N, of which +/-50N is allocated for correcting figure errors. This can be carried over to the space application, except that the large forces due to gravity are absent and the actuators need to provide tension as well as compression (averaging to zero force on the primary, of course). A space-based GMT would not need the massive support structure essential on Earth to support and align the optics against gravity and wind; it would be assembled on orbit from packaged mirrors, for which the launch loads would be carried not by the actuators but by special snubbers or other packaging provisions for the system.

5.4.2 (U) Flat lenses

(U) Recently, there has been exciting progress in the design, formation and applications of planar *metasurface* wavefront-shaping structures. The components of the metasurfaces are thin, sub-wavelength (whatever the wavelength of interest, be it mm-wave or optical wavelength) arrays of scatterers such as shown in Figure 17(b), that can introduce controlled phase shifts, amplitude modulation or polarization control. The sub-wavelength size of the components allows the wavefront "shaping" without revealing the discrete nature of the composite elements. Metasurfaces allow the formation of optical components that can perform multiple operations according to the incident wavelength or polarization. For example, a broadband achromatic metalens has been designed with spatially-dependent group delays so that wavepackets of different wavelengths and from different locations simultaneously arrive at a common focal point.

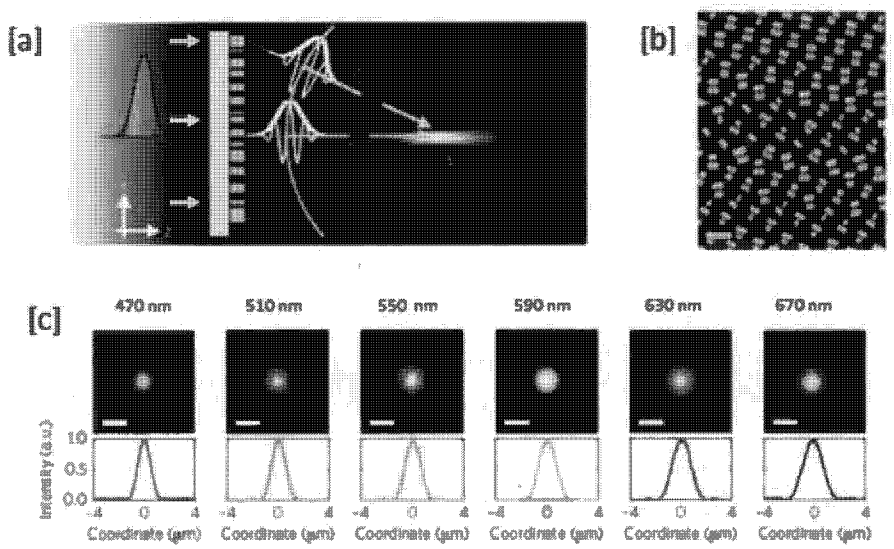

Figure 17: (U) [a] Schematic of an achromatic metalens, [b] scanning electron micrograph of a region of a fabricated metalens. The scalebar corresponds to 500 nm, and [c] normalized intensity profiles for the achromatic metalenses at the various wavelengths indicated. The scalebar corresponds to 2 μm, from [12].

(U) Figure 17(a) is a schematic of the lens, illuminated by a white light source (super-continuum laser with tunable center wavelength and bandwidth). Figure 17(c) shows the experimentally-measured focal spot profiles at different wavelengths, indicated at the top of the different profiles. The scale bar is 20 microns. Figure 17(b) is a scanning electron micrograph (SEM) of a region of the metalens. The scale bar corresponds to 500 nm. The structures in the SEM are TiO_2-clad "nanofin" structures approximately 600 nm in height [12].

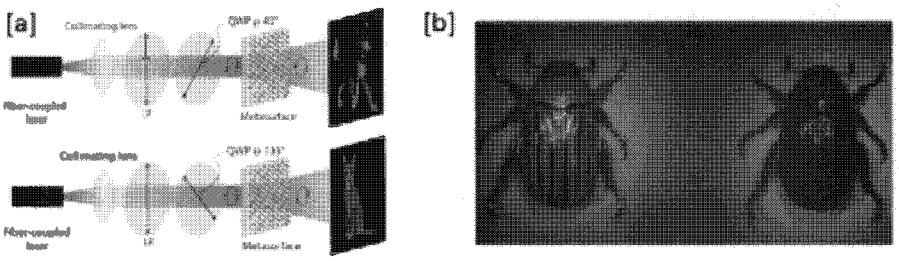

Figure 18: (U) Elements of polarization-sensitive metalenses. [a] A single metasurface encodes two independent holograpm profiles for each circular polarization at $\lambda = 532$ nm. When illuminated with RCP (LCP) light, the metasurface projects an image of a cartoon dog (cat) to the far-field, [b] Polarization-differentiated images of the beetle, *Chrysina gloriosa*. The left image relates to left circularly polarized light reflected from the beetle, while the right image relates to right-circularly polarized light. The illumination is provided by green LEDs paired with a 10 nm bandpass filter centered at 532 nm, [38].

(U) Figure 18(a) illustrates "chiral holograms" where a single metasurface encodes two independent hologram profiles for each circular polarization (right- or left-circularly polarized light, RCP, LCP) at $\lambda = 532$ nm. When illuminated with RCP (LCP), the metasurface projects a cartoon image of a dog (cat) to the far field. The metasurface encoding these images is 350 microns by 300 microns in size, comprised of 420,000 TiO_2 elements [55]. In a similar fashion, Figure 18(b) illustrates a polarization-sensitive metalens, formed on a glass substrate, that creates two spatially-separated images of the beetle, *Chrysina gloriosa*, displaying its natural dichroic behavior [38].

(U) Currently, the use of the flat metalens approach for large space-based assembly may appear far from promising. Although plans are underway for chip-scale (several mm dimension) and perhaps wafer-scale fabrication [72], the areas are still smaller than would be used for modular mirror segments. Metalens elements for optical imaging are 100 nm features: in space additive manufacturing techniques are not able to address that degree of spatial resolution. However, flat metalenses may in the future offer advantages of ease of fabrication of lower-mass structures, particular at longer than optical wavelengths. It is also worth considering the metalens approach of wavefront-control through by patterning surfaces with thin phase-shifting elements as a means of in-space fine-tuning, and adjustments of mirror structures.

5.4.3 (U) FINDING

There have been substantial advances in the formation of light-weight, segmented mirrors for large-area telescopes, with promising approaches for temperature control that will preserve surface features to ensure high resolution imaging. Recent advances in flat lenses may afford dramatic new capabilities in the control of imaging surfaces assembled and repaired in space.

5.5 (U) Laser Metrology for Large Structures, Optics and Antennas in Space

(U) Many publications from the University of Arizona group provide valuable insight and details into the fabrication of their large terrestrial mirrors for leading-edge astronomy. The discussion below draws on that work.

(U) Early in the mirror fabrication process, initial metrology is carried out using a commercial laser tracker, mounted above the mirror. Figure 19 shows a schematic of that system. The components of such laser-based metrology systems are available commercially: the components are compact, have high precision and are often integrated with easy-to-use probes that

helps to map out the dimensions of a structure. (For example, refer to `https://knowledge.faro.com/Hardware/Laser_Tracker/Tracker`.

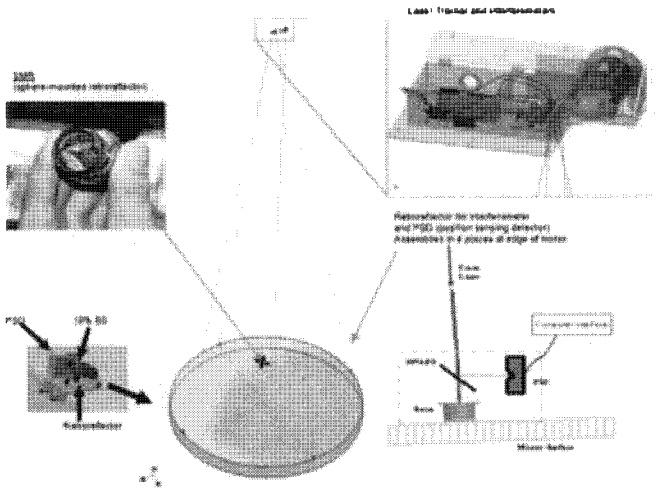

Figure 19: (U) Configuration of the laser tracker set up for measuring the mirror surface, showing the components of the laser tracking system. The laser tracker is a three-dimensional coordinate measurement system that directs a laser beam toward a sphere-mounted retroreflector (SMR). It uses the gimbal angles from encorders and radial distance from distance-measuring interferometry to determine the position of the SMR. The SMR in turn is moved across the suface of the mirror [9].

(U) Because of the greater ease and precision of measuring distance in comparison with angle: multi-lateration rather than triangulation , JASON judges that there is a better path forward that relies heavily on distance measurements (wavelength counting and interpolation). Just as rigid structures can be produced with sticks of known length (aside from thermal expansion and response to forces), so can all the parameters be established by distance-only measurements. This creates a (model of a) rigid body that can then be oriented in order to perform its role as an astronomical telescope in orbit or a space probe, or an Earth-observing system from space.

(U) The multi-lateration approach to adjusting and maintaining large space optics depends on the use of small retroreflectors attached to mirror segments and to other optical elements, with redundant chord measurement,

for instance by the Etalon Multiline technology:`https://www.etalon-gmbh.com/en/products/absolute-multiline-technology/`. This system can handle 124 chords, as is described in the following:

> A single Absolute Multiline System can drive up to 124 measurement channels, depending on the system configuration. The channels are extremely compact: Each sensor consists of a commercial robust fiber and a miniature optical element without any electronic components. It can momentarily measure motions and vibrations of an object with a resolution of over several MHz during one measurement interval. As the distance between the sensors and the system electronics can be several kilometers, it is possible to conduct measurements under extremely rough environmental conditions, far away from the evaluation electronics. The sensor signals are not affected by electromagnetically noisy environments; therefore the placing of sensors in e.g. energy chains is possible without degradation of performance.

(U) In fact, Etalon has been working with the Large Binocular Telescope (LBT) since August, 2017 to prototype GMT "laser truss" technology on the LBT, `https://www.etalon-gmbh.com/wp-content/uploads/pdf/Prototyping_GMT_Telescope_Metrology_on_LBT-SPIE2018-public.pdf` .

(U) JASON was convinced that such a system should be the basis of modern telescopes, terrestrial or space-based, and is happy to find that the technology has developed to a reasonable TRL.

5.6 (U) Guidance, Navigation and Control

(U) As with any spacecraft, a space assembly will need sensors for measuring its state vactor and attitude, and a control system for their management. In addition a space assembly must be stable and controllable through all

stages of its assembly process as well as in its final configuration. Moreover, a space assembly will not not act as a rigid body, but will flex. Historically, nonrigid spacecraft appendages such as solar panels, antennas, or booms have sometimes caused trouble because of unusual and long-period structural modes. One can view a space assembly as a spacecraft that is mostly or entirely appendage, and therefore trouble should be proactively anticipated.

(U) No satellite experiences exactly zero gravity. Forces on a satellite include tidal forces, centrifugal forces if spinning, and Coriolis forces accompanying any motion measurd in a rotating frame. [9] Gravity gradients (tidal accelerations) create forces on any assembly; accelerations are of order

$$a_{\text{tidal}} \sim \frac{GML}{R^3} \sim 3 \cdot 10^{-5} g \left(\frac{R}{R_\oplus}\right)^{-2} \left(\frac{L}{100\,\text{m}}\right) \tag{5-24}$$

where R is orbital radius (assumed circular), $R_\oplus$ is Earth's radius, and L is the size of the assembly. The stable orientation is with long dynamical axis aligned with the direction to Earth; if this orientation is consistent with the mission, gravity gradient offers a "poor man's" attitude control. If other orientations are desired the assembly's attidude must be actively controlled by other means.

(U) Forces on a satellite may also include electrodynamic forces due to the Earth's magnetic field, solar radiation pressure, and (for low orbit) atmospheric drag. All forces create torques affecting the assembly's attitude.

(U) Other feasible means of attitude control include spin stabilization or full 3-axis active control. Combinations are also feasible. A spinning assembly will be stable only if the spin axis is parallel to the axis of greatest moment of inertia. For instance, a thin disk is stable when spinning about its axis of symmetry (like a Frisbee in flight). A dynamically prolate body (such as a long rocket body) spinning about its long axis is unstable against tumbling, caused by excitation of, and dissipation in, structural modes, which

[9](U) Coriolis forces occur in the often-used "Earth-following" frame of reference in which z-axis always points radially away from the Earth.

must be actively controlled. Three-axis control must be effected by momentum wheels, control-moment gyros, or jets (the latter requiring consumable fuel). Magnetic torquing is unlikely to be effective in a large assembly. In any case, jets will be needed for occasional "momentum dumps" to compensate for external tidal torques or radiation-pressure torques, as well as for orbital tweaks.

(U) Gravity-gradient and centrifugal forces offer opportunities as well as possible trouble. A space assembly might be composed, at least in part, of a truss of thin structural members which must carry forces of compression and tension. Members under compression must be stiff and stable against buckling, and therefore must have sufficent width. Members which are always under tension can be replaced with thin flexible tethers to save mass. A spinning lattice may put many[10] of its structural members under tension due to centrifugal force and gravity gradients, so that tethers can be employed instead of stiff members.

5.7 (U) Additive Manufacturing

(U) Additive Manufacturing (AM), or more commonly termed *3D Printing*, has had a profound impact on prototyping and creating structures for purposes ranging from classroom instruction, research innovation to lower-cost manufacture of components. 3D printing has some natural advantages for applications in space and for iSAM:

1. It obviates the need for special molds or machine tools.
2. It can reduce welds and produce components with complicated geometries.
3. It can produce porous, hence light weight materials.

[10](U) or even all

(U) There have already been examples of 3D-printed components utilized in satellites. The JUNO spacecraft , a probe of Jupiter's atmosphere, employed eight 3D-printed titanium brackets to attach the rectangular waveguides that conduct RF signals between spacecraft components (24). A 3D-printed antenna tower was incorporated into SKY Perfect JSAT's JCSAT-110A satellite launched in December 2016 (25)

(U) More recently, the company *Made in Space* launched a 3D printer to the ISS as a technology demonstration project. However promising the prospect of 3D Printing for iSAM, considerable technological development will have to take place before it can be proven as a critically enabling technology. As the IDA report noted [8], it will be necessary to:

1. Expand the range of feedstock materials that can be used.
2. Characterize the material properties of structures manufactured in orbit.
3. Understand the issues of temperature, ambient conditions on the formation and integrity of the additively-manufactured components.

5.7.1 (U) FINDING

(U) Additive Manufacturing approaches such as 3D Printing are currently being explored for space-compatible and in-space-manufactured components. However, considerable more technological development and evaluation of the AM-formed structures will have to take place before this can be a core iSAM technology.

5.8 (U) Autonomous Assembly of a Reconfigurable Space Telescope (AAReST)

(U) The Autonomous Assembly Reconfigurable Space Telescope (ARReST) [80] exemplifies a developing iSAM technology that leverages recent advances

in small satellites. AAReST aims to demonstrate the concept for a large, segmented primary mirror to be constructed out of autonomously assembled small independent spacecraft, each with an identically shaped mirror that can be adjusted on assembly. AAReST consists of three satellites totaling 30 kg, a central 9U "CoreSat" satellite with two smaller 3U satellites "MirrorSats" launched in an attached configuration. Each MirrorSat is capable of autonomous undocking and redocking, utilizing the Surrey developed electromagnetic docking system and near infra-red lidar/machine-vision based relative navigation sensors [80]. Each MirrorSat has an adaptive mirror while the CoreSat has two fixed mirrors and a boom-deployed camera.

(U) The AAReST goal is to demonstrate autonomous maneuvering and docking in different configurations, and at the same time imaging with a larger sparse synthetic aperture. AAReST is a collaboration amongst three institutions, each responsible for one of the satellites (the California Institute of Technology (Caltech), the University of Surrey Surrey Space Centre (SSC), and the Indian Institute of Space Science and Technology). AAReST is planned for launch in early 2020.

(U) Cubesat Proximity Operations Demonstration (CPOD) is a second CubeSat demonstration under development, also with the goal to demonstrate spacecraft working in coordination for observations and as in-space building blocks for more sophisticated systems [7]. CPOD consists of two identical 3U CubeSats that will deploy conjoined then separate. One CubeSat will go into a "walking safety ellipse" of 200x400x200 m as it approaches the second CubeSat in a series of transfer and hold transfers for redocking. The main challenge has been in developing small, low-cost, low-power components that are not COTS available. Each 3U 5 kg satellite uses two visible and two infrared cameras, star trackers, a GPS receiver, and a range-capable intersatellite link (ISL) as primary navigation sensors, and reaction wheels and cold gas thrusters for control [7]. The CPOD project is led by Tyvak Nano-Satellite Systems partnered with Applied Defense Solutions and the California Polytechnic State University of San Luis Obispo, sponsored

by NASA Ames Research Center via the Office of the Chief Technologist. Launch expected in 2020 [7].

5.8.1 (U) FINDING

(U) Approaches to iSAM such as AAReST leverage technological advances in small satellites and may offer a promising pathway to low-cost, flexible iSAM.

This Page Intentionally Left Blank

6 (U) POINT DESIGNS FOR A LARGE APERTURE AT GEO

(U) The following sections describe a set of *Point Designs* for large apertures at GEO that may provide both template and incentive for actual implementation. Sections 6.1 and 6.2 describe designs for [redacted] RF apertures, using quite different approaches. Section 6.3 uses the terrestrial-based 40 m Extremely Large Telescope (ELT) as a possible template for a space-based version. (b)(3)

(U) Besides serving as templates, the point-designs each serve as distinctive illustratrations. Section 6.1 underscores the possibility and current constraints of using Commerical Off-The-Shelf (COTS) components that could be fold-fitted into existing payload fairings. Section 6.2 describes an approach that could be used for flexible RF sensing in either a *"fly's eye mode"* allowing observations with high sensitivity and high spatial and temporal resolution, over a wide field of view. Alternatively, the same system can be reconfigured to allow a *"high resolution mode"*, producing higher sensitivity, spatial and temporal resolution, over a more limited field of view. Finally, Section 6.3 discusses the space-based assembly of a large-scale optical aperture, with initial considerations for the highest-quality optical components for astronomical observations, but which can serve as the basis for a broader set of high-resolution imaging and surveillance applications.

6.1 (U) [redacted] RF Aperture at GEO

(U) We describe a notional design for a [redacted] phased array antenna in geosynchronous orbit. An ideal [redacted] aperture at GEO has a path loss of 102 dB to 103 dB from an isotropic emitter on the surface of the earth visible to the antenna. This is a relatively modest path loss by RF standards. For example, the GSM cellular specification requires phones that can transmit (b)(3)

at +30 to +33 dBm, and receive signals as weak as -102 dBm, for a link margin of 132 dB. In many (perhaps most) cases, the signal received by a [redacted] aperture in GEO would be stronger than the signal power at the intended receiver. (However, we expect that individual antenna elements in the phased array will operate with path loss many orders of magnitude higher, and in general the signal power from an individual antenna will be significantly below the noise power in that antenna). (b)(3)

(U) The design goal for the array is a usable frequency range from 100 MHz to 10 GHz, with ten frequency bands totaling at most 1 GHz observed at any given time. In those ten bands a total of one million separate beams are available.

(U) The architecture consists of a 3D space frame to provide rough alignment of ten thousand sensor tiles on a planar front surface. Each sensor tile consists of one hundred square meters of antenna area and a network hub which also serves as a digital beam aggregator. Tiles are connected via optical fiber. Tiles are made with COTS electronics, and are designed to be replaced on a regular basis by service robots. With a mean time between failure for a tile of ten years we expect an average of three tiles to be replaced per day.

(U) The tile geometry is inspired by SpaceX's Starlink satellites. Starlink v0.9 consists of a flat bus with a 12 panel folded solar panel. It appears that the bus and panels are roughly 4 m^2 each, and fold into a stackable rectangular solid for launch. The total panel area is then roughly 50 m^2. If SpaceX is successful with their plans to launch 12,000 of these satellites, they will have a combined solar panel area of roughly half of a square kilometer.

(U) SpaceX launched 60 v0.9 satellites in May of 2019. According to company PR, they have lost communication with three, intentionally deorbited two, and the remaining 55 have successfully raised their orbits by firing their krypton thrusters, presumably implying that their solar panels have all unfolded successfully.

(U) For our design, we chose a 3x3 m^2 hub so that a folded tile stack would fit inside the Falcon 9 payload fairing, much like the stack of 60 Starlink satellites launched this year. Each of the 12 fold out panels contains an array of antenna elements, for a total antenna area of roughly 100 m^2 per tile, as shown in Figure 20. Each antenna element consists of a fixed phased array of printed PCB antennas design so that the main lobe of the antenna covers the earth. With $\frac{\lambda}{D} = \frac{12{,}700km}{42{,}164km}$, the array is roughly three wavelengths across, or perhaps a 7x7 antennas on half wavelength centers. Multiple co-located antenna arrays on each tile can be used to cover several decades of frequency, from well under 100 MHz to 10 GHz.

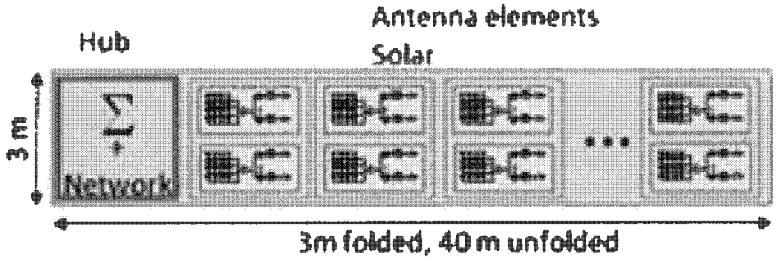

Figure 20: (U) Notional schematic of a "sensor tile" that can be folded in one direction. Each tile contains an array of antenna elements, with a total antenna area of roughly 100m^2 per tile.

(U) Each analog array is sent to a commercial broadband Low Noise Amplifier, followed by multiple tunable bandpass filters, mixers, and ADCs. Each amplifier/mixer/ADC chain with 100 MHz of bandwidth and 16 bit 100 MS/s ADC will burn less than a Watt with off-the-shelf electronics and 3 dB noise figure. At low GHz frequencies, this means a few tens of Watts and a few hundred dollars per square meter. Tens of Watts per square meter can be supplied by dedicating five to ten percent of the panel area to solar cells on front and back of the panel. For example, the end panel on each tile could track the sun throughout the orbit and supply power for the whole tile with power.

(U) At X-band however a single 3x3 m^2 panel will have roughly 1000 antenna elements, and 100 MHz sample rate may not be acceptable. At 1 W per antenna element COTS electronics will give 8 bits/sample at 1 GS/s, and the power dissipation would be 1 kW/m^2. This is possible for brief periods of time if there is power storage on the array, but the incident solar power on the array is of course never more than 1.4 kW/m^2.

(U) Local oscillators across the array will need to operate in phase (or at least with known phase). LO phase synchronization may be maintained via PLL on each panel locked to a 60 GHz broadcast tone, or via a signal carried on optical fiber.

(U) Thermal management of the arrays will be passive. The power dissipated in the electronics is small compared to the incident solar radiation. Using the solar panels on the ends of the tiles to maintain power will also maintain temperature.

(U) The antennas in the array do not need to be maintained on a single plane, or even a constant shape, as long as the positions of all of the antennas are known to better than $\lambda/20$. At X-band this means roughly millimeter position accuracy, centimeter at typical cellular frequencies. The "laser truss" technology in use on the Giant Magellan Telescope is capable of sub-millimeter position measurement accuracy at 500 kHz on 800 points with 30 m of free-space distance at the end of several kilometers of fiber. Similar technology could be used to provide real-time information of antenna panel positions to the phase calculation engines in the tile hub.

(U) Digital data streams from the antenna panels will be sent to the networking hub of the tile. Here the quadrature channels from each of the multiple frequency bands from each of the antenna arrays will be combined into a individual phased array beams.

6.2 (U) RF at GEO

6.2.1 (U) Objectives and introduction: flexible RF sensing using dual mode observations

(U) The objective of this section is to describe a spacecraft cluster concept that could be used for flexible RF sensing in two principal modes. A **'fly's eye' mode** features simultaneous observations with high sensitivity and high temporal and spatial resolution over a wide field of view (FOV). A **'high resolution' mode** features higher sensitivity and higher spatial and temporal resolution, but over a limited FOV. Both modes would have wide bandwidths dictated by the receiving system electronics, probably 300 MHz or better. The concept is described in terms of an RF system, but might find application at shorter wavelengths.

(U) This satellite cluster concept is based on the extension of the Earth based, Australian Square Kilometer Aperture Pathfinder or ASKAP [70] and an update at `https://www.atnf.csiro.au/projects/askap/smart_feeds.html`) to a space based receiver system. An additional feature could be added by the use of spherical apertures that may have advantages in a spacecraft cluster in terms of a large field of regard without reorienting the reflector aperture.

(U) Figure 21 shows the operational ASKAP 36 parabolic dish array with irregular spacing. Each antenna with novel phased array feeds (Hay, et al., 2007) can produce multiple beams, 36 for the ASKAP, that can be individually pointed over a region of sky that is about 30 degrees squared for the system operating in the 700 to 1400 MHz range. The 36 parabolic dishes in the array can be operated independently for a very large field of view, or in an aperture synthesis mode for increased spatial resolution but over a smaller field of view.

(U) The just-commissioned ASKAP array has been decades in the making [47] and other developments with similar goals exist in the Netherlands and

elsewhere. In particular, a new phased-array-feed system is being developed for use at the Arecibo observatory in Puerto Rico (see references in [70]). The use of PAFs has very heavy data transport and computer processing requirements that typically mean some design compromises, depending on objectives. For the ASKAP the objective is astronomy and astrophysics. The financial and observational constraints for ASKAP have meant a very careful development process with changes as technology, e.g. computation and fiber optic data transmission, improves.

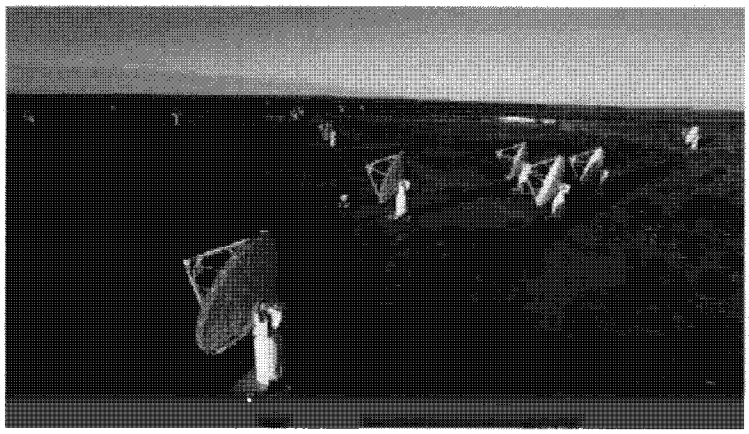

Figure 21: (U) The Australian Square Kilometre Array Pathfinder (ASKAP) is the world's fastest survey radio telescope, consisting of 36 parabolic dish antennas, spread over a 6 km diameter region (after `www.atnf.csiro.au/projects/askap/index.html`).

6.2.2 (U) Combination of features in a spacecraft cluster for flexible observations

(U) The objective in this concept has similarities with the broad objectives of the ASKAP array discussed above. It is a middle way between a single very large reflector aperture and a large phased array. The objective is to have the sensitivity (collecting area) and spatial and temporal resolution of a large reflector while retaining the ability to do simultaneous observations in different directions over a large FOV, the advantages of a phased array. The cluster of spacecraft receivers is designed to operate in both a very

high spatial resolution (aperture synthesis) mode as well as a fly's eye mode for simultaneous observations over a wide FOV. We will show examples of observations of both modes below.

(U) The cluster of spacecraft receivers is shown schematically in Figure 22 operating in fly's eye (pink) and high-resolution (blue) modes. The spacecraft are the same in both modes, but are oriented and perhaps deployed differently.

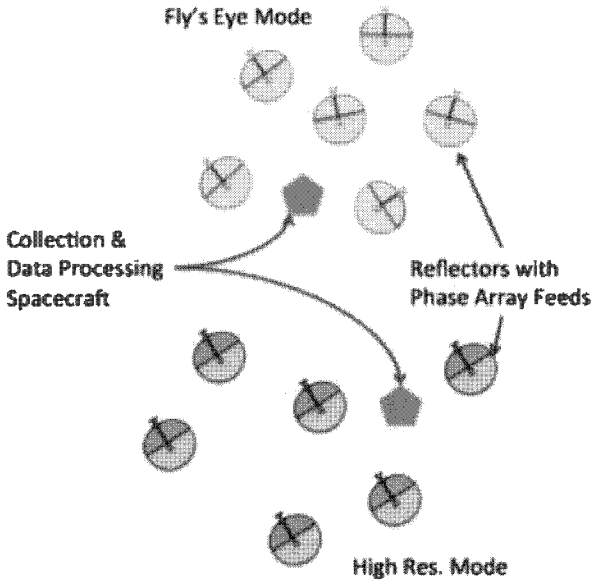

Figure 22: (U) A cluster of very similar observational spacecraft and a data collection and processing spacecraft. The idea is not to have two clusters, but one flexible cluster with two modes. The spacecraft diagram shows spherical apertures, but that is not necessarily the best choice. In fly's eye mode, the apertures point in different directions and their signal are not combined, while in high resolution mode they are combined coherently.

6.2.3 (U) Spherical or parabolic reflectors?

(U) Two straightforward choices emerge for the reflector structure: spherical and parabolic reflectors. The ASKAP and many others use parabolic reflectors and Arecibo and FAST (Five-hundred-meter Aperture Spherical Telescope, in China) radio telescopes use spherical reflectors, as discussed

below. Here we assume that one can construct either reflector geometry with surface accuracy sufficient to provide the required performance at the highest frequency of interest (see also Section 4.6). The observational advantage of the spherical reflector is that it can cover a much wider FOV without reorienting the structure than can the parabolic reflector. The parabolic reflectors at ASKAP can cover about a 30 deg^2 FOV, but the spherical reflector at Arecibo can cover more than 1000 square degrees (albeit by moving the feed structure somewhat and the FAST spherical reflector even more, as discussed below). If the reorientation of the cluster spacecraft and settling of the structure after reorientation are important issues, then the use of spherical apertures is an option to consider seriously, subject to the issues of fabricating such structures in orbit (Section 4.6).

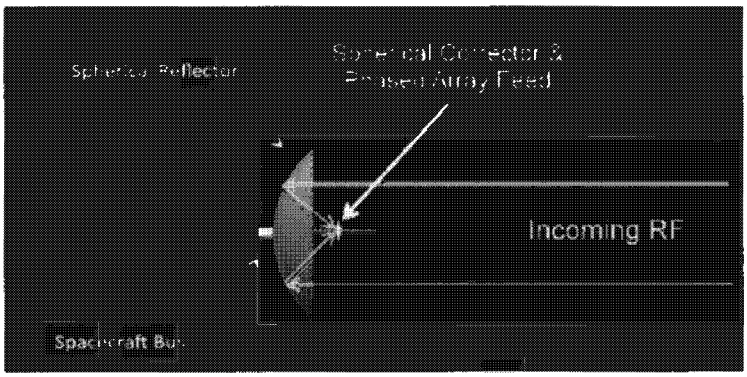

Figure 23: (U) Spherical reflecting aperture concept.

6.2.4 (U) Phased array feeds

(U) A phased array feed (PAF) is simply a small phased array antenna placed at the feed point (focus) of a reflector antenna aperture as shown in Figure 24. PAFs offer advantages, compared to more conventional arrays of feed horns. The choice of appropriate beamformer element weights allows separate maximization of efficiency, sensitivity or beam quality in the beams formed in the sky.

(U) The PAF structure chose for the ASKAP is a dual-polarized connected "chequerboard" array having 94 ports [29]. This PAF operates over 0.7 GHz to 1.8 GHz, enabling each 12 m ASKAP dish to observe a 30 deg^2 field of view with 36 beams, surveying this FOV simultaneously and continuously with ms time resolution. We discuss the PAF for the Arecibo observatory below.

(U) As shown in Figure 25 signals from the 188 sources on the PAF chequerboard are routed through a series of filtering, digitizing and beamforming steps to arrive at a correlator that combines the PAF receivers to form beams using complex weighted sums for the 36 beams. Since beamforming is best done in relatively narrow bandwidths and the beam weighting is frequency dependent ASKAP PAF beams are formed independently in 1 MHz channels over 300 MHz bands in the operating 700 to 1800 MHz operating range. How are the beam weights determined? One method is the *conjugate field method* in which the element weights are determined so as to conjugately match the focal plane field distribution over the entire aperture face of the PAF (the green chequerboard in Figure 24). This method is described by [81]. An alternative technique is *maximum sensitivity beamforming* per [5]. Figure 26 displays the amplitude and phase for a beam profile where the PAF components have been weighted to achieve maximum sensitivity [34].

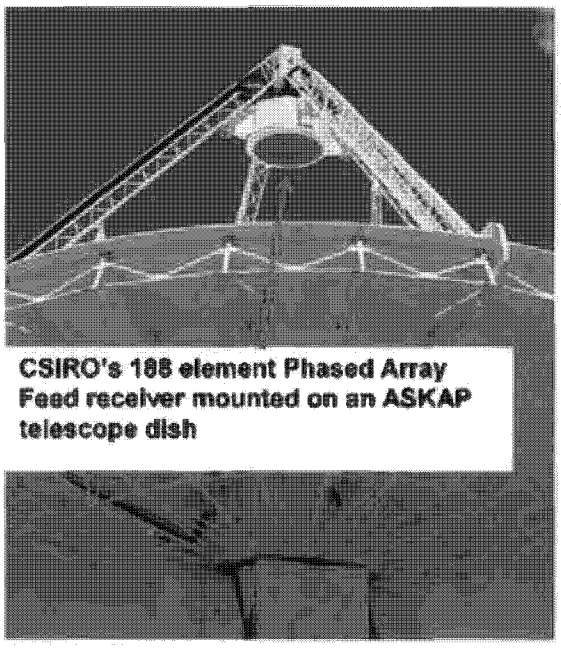

Figure 24: (U) Commonwealth Scientific and Industrial Research Organization (CSIRO) 188 element Phased Array Feed (PAF) receiver mounted on an ASKAP telescope dish (after `www.atnf.csiro.au/projects/askap/index.html`).

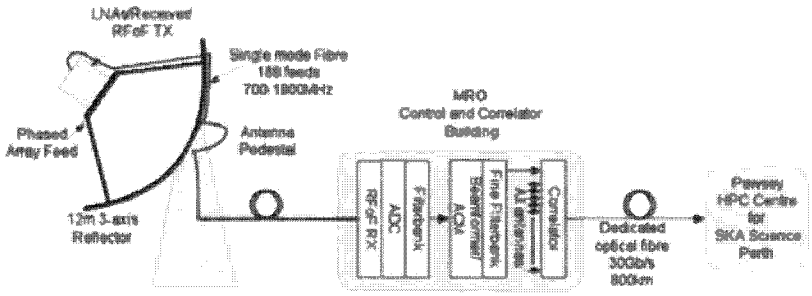

Figure 25: (U) Simplified System diagram of data flow for ASKAP using a Mark II PAF. Note the many signal paths with multi-Gb/s data flow rates (after [70]).

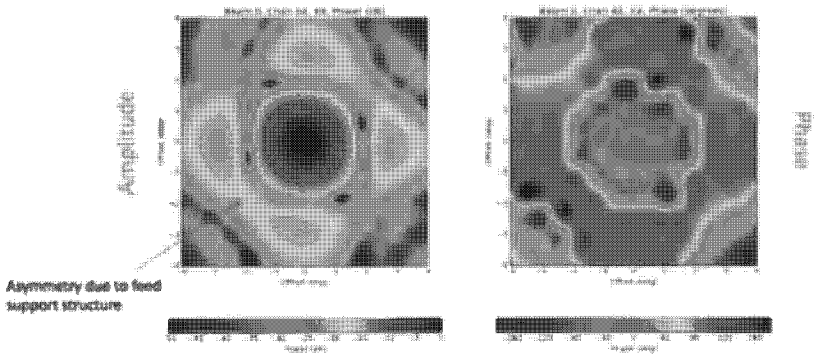

Figure 26: (U) Beam pattern for a single beam from a typical ASKAP PAF. Note the symmetry and low side lobe levels when optimal sensitivity weighting is used in the processing (after [34]).

(U) The beam patterns above emphasize pointing a high gain antenna beam in a desired direction. The PAF also gives one the ability to tailor the beam to reduce interference by placing an antenna null on a known source of interference in a particular direction – Section 6.2.5 gives an example.

(U) Data processing requirements for use of PAF are significant and the data flow rates require the use of optical fibers. This is discussed in Section 6.2.7, below.

6.2.5 (U) Inspiration from astronomy and the Arecibo spherical dish

(U) The ASKAP that has been highlighted here is an excellent example of the methodical approach to developing and implementing a long-term vision to move astronomy forward. It provides excellent guidance on how to develop and implement the dual mode concept in a spacecraft cluster. Schinkel (2012) and Garrett (2013) [70, 26] review the progressive development that led to the first large-area survey with ASKAP's full 36-dish antenna array in August 2019.

(U) Similarly the large spherical reflector at Arecibo Puerto Rico has been a long-term effort in making full use of a zenith looking 1000 ft. spherical aperture. PAF is now being readied for deployment [15]. This PAF, called the Advanced L-band Phased Array Camera (ALPACA) will allow an array of 40 dual polarized beams to be pointed independently over a flexible cone of directions around the primary pointing direction. ALPACA will have four times the number of elements of an initial prototype that was successfully designed and deployed in 2011 and tested for two years.

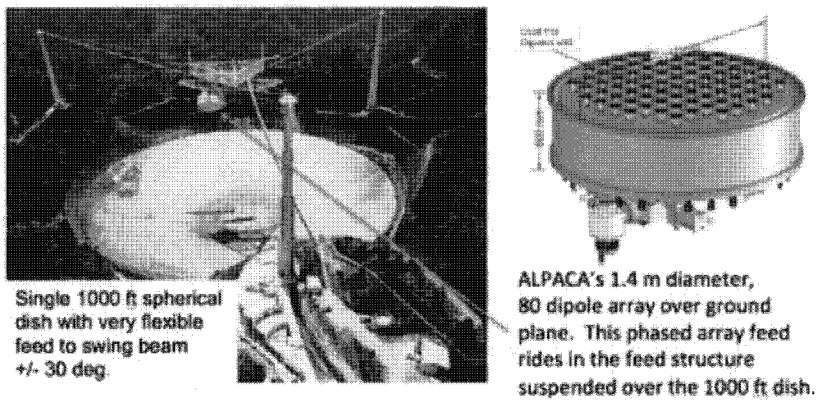

Figure 27: (U) Arecibo observatory's 1000 ft. spherical dish with the next generation phased array feed (ALPACA, after [15]).

(U) When ALPACA is installed at Arecibo the telescope's PAF will have 80 dual polarized elements that will enable some 40 beams in a flexible array, such as shown in Figure 28. The beam widths are 3 arc min at 1500 MHz with spacing 2 arc min. The frequency coverage is 1280 to 1720 MHz with 312 MHz per channel. ALPACA will be the first cryogenically cooled phased array feed, with a goal of 30 K. NSF awarded $5.8 million in new funding in 2018. In Figure 28 we also show the Gregorian corrector assembly that brings the rays from the spherical reflector to a focal plane where the PAF receivers interface with the electromagnetic field in space.

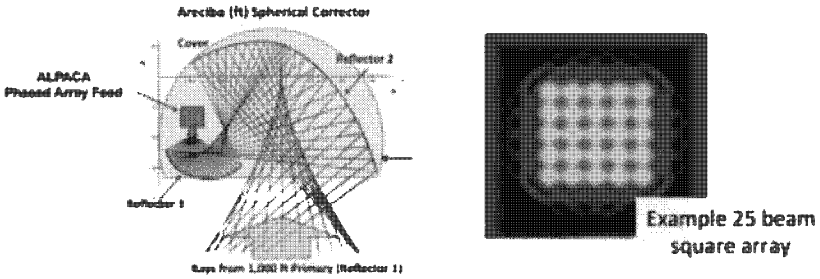

Figure 28: (U) Gregorian corrector (left panel) to bring the rays from a spherical reflector to a focal plane and an example beam pattern (right panel) from the ALPACA PAF in Figure 27.

(U) The Arecibo concept promotes a very large, but stationary receiving aperture. While the aperture can't move, the antenna beam can be steered about ± 20 degrees from the primary direction by steering the feed away nadir region of the spherical reflector and illuminating a region of the reflector that receives incoming radio waves from areas away from the zenith direction, as illustrated in Figure 29 for a similar, but larger spherical radio telescope in China, called FAST. One could use this feature with a spherical reflector in space to avoid reorienting the whole reflector and only moving the rotating feed structure. From a satellite at geocentric distances greater than about 9,000 km (above LEO, but well below GEO orbits) one could view the whole Earth without reorienting the spherical reflector structure.

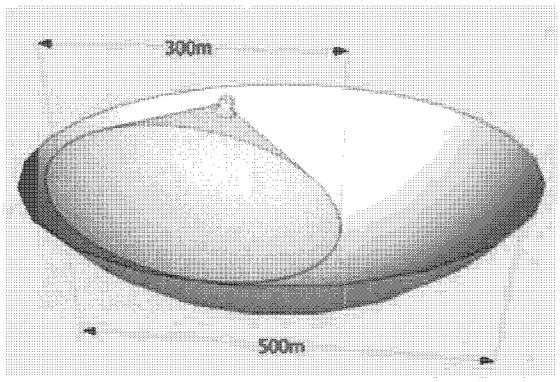

Figure 29: (U) Diagram of the FAST feed cabin moved off the zenith axis by a cable robot using winch servomechanisms on six support towers. At FAST one can shift the antenna look direction within about 60 degrees of the zenith direction.

(U) We use Arecibo as an example here, but we note the construction of the similar, but larger FAST reflector in China. FAST is 500 m in diameter and so is the largest reflector aperture in the world. The reflector surface was completed in 2019 (`https://en.wikipedia.org/wiki/Five-hundred-meter_Aperture_Spherical_Telescope`) and is in the process of commissioning and testing. It operates over the 75 to 3000 MHz band. An improvement in FAST is the ability of moving the feed to illuminate more of the reflector surface than at Arecibo (see Figure 29)) so that a wider range of directions can be observed (60 degrees from zenith of FAST and 20 degrees for Arecibo).

6.2.6 (U) Example observations

(U) In this section we give some example observations for the two modes we have discussed – fly's eye and hi resolution. The fly's eye examples come from the use of ASKAP to search for short duration, fast radio burst (FRB) sources and from a example of radio frequency interference rejection using the capabilities of PAFs. The high-resolution mode example comes from ASKAP observations of the Spector galaxy. Probably the most impressive

use of aperture synthesis was the imaging of the event horizon region of the supermassive black hole in the M87 galaxy [2].

(U) ASKAP has observed 28 FRB (Fast Radio Burst) sources that only lasted a few milliseconds. This was made possible by the ability of ASKAP to survey significant regions of the sky (160 deg^2 in the fly's eye mode) simultaneously with high time (millisecond) and space (10 arc min) resolution, as well as useful sensitivity (12 m aperture).

(U) The 36 beams from a single antenna are arranged in a 6 x 6 square pattern with a separation of 0.9 deg. Each antenna covers about 30 deg^2 and they use some overlap between beams of the 8 antennas, as shown in Figure 30. Because the FRB is very strong (fluence $\approx$60 Jy ms) multiple beams respond to the burst as shown in Figure 30 and the source can be localized to about 8 x 8 arc min using a Bayesian approach, sampling the *posterior distribution* which is the product of a likelihood function and prior probability. The FRB shows a high frequency cutoff at about 1400 MHz with duration of several ms (see Figure 30). This frequency cutoff could be due to either scintillation or an intrinsic feature of the burst.

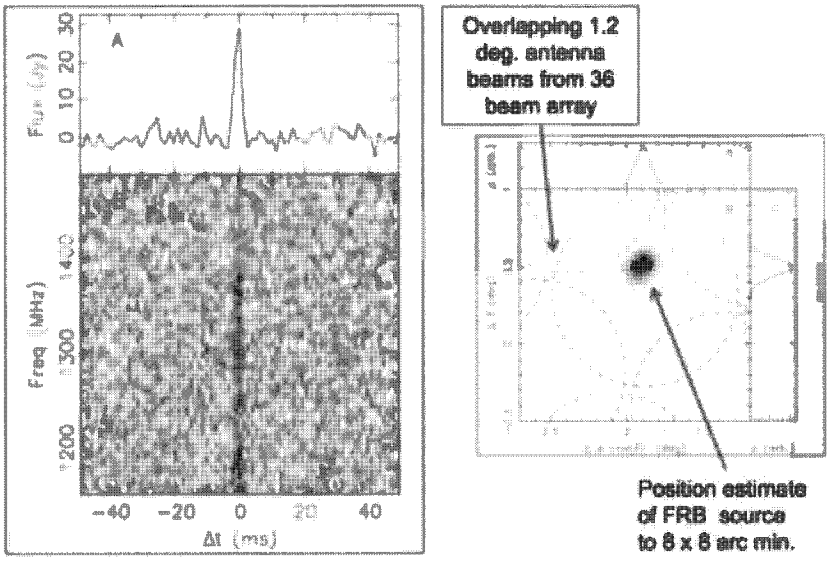

Figure 30: (U) Left panel: Time and frequency characteristics of FRB observed by ASKAP on Jan. 27 2017. Right panel: Localization of the source of the FRB. The highly dense region in the panel shows the region of significant *posterior probability density* (after [6]).

(U) Applebaum (1976) [5] developed and simulated a method of weighting phased array antenna elements to form a beam optimized in terms of signal to noise ratio. Such algorithms are the basis for the weights using to form the beam in Figure 26. In Figure 31 we show and example of using a 21 element, linear array with $\frac{\lambda}{2}$ spacing. In the left panel of Figure 31 we show the antenna pattern for quiescent conditions with no interference and 20 dB sidelobe level. The element weights were determined using Applebaum's control law, but neglecting servo error. In the right panel eight interference sources are introduced and the control loop acts to suppress antenna response at these source locations. We see the resulting antenna pattern nulls placed on the directions associated with the interference.

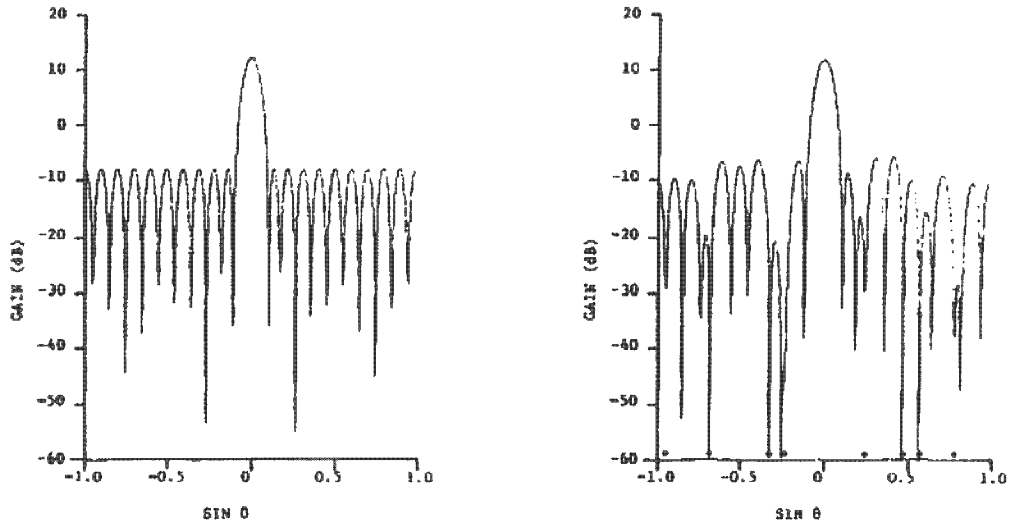

Figure 31: (U) Left Panel: Quiescent antenna pattern with weighting for optimized SNR and -20 dB sidelobes. Θ is the angle in radians from the antenna boresight center. Right Panel: Antenna pattern adapted to presence of 8 randomly located interference sources. Adaptive weighting places nulls at location angles of interference sources (after [5]).

(U) In Figure 32 we show an example taken from Fisher (2010) using a 19 element single polarized PAF and front end box mounted on the Green Bank 20-Meter Telescope. In the left panel of Figure 32 we see an image in the W3(OH) line in an unspecified location in the galaxy. RF interference (RFI) was then introduced by injecting an FM-modulated RFI source that overlapped the W3(OH) spectral line at 1665 MHz in the far sidelobes of the telescope. The RFI was then mostly removed using the subspace projection algorithm of Leshem et al. (2000) [46] as shown in the right panel of Figure 32. Some corruption due to residual RFI remains after adaptive processing, but the very large improvement is evident comparing the center and right panels of Figure 32. A half dozen results demonstrating feasibility of PAF-based interference mitigation in radio astronomy are mentioned in Fisher et al. (2010) [22]. Leshem et al. show an example of the removal of GSM cell phone interference in spectral line observations with the Westerbork Synthesis Radio Telescope in northeastern Netherlands.

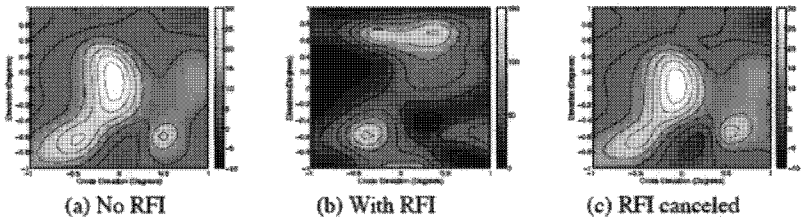

Figure 32: (U) Radio camera image of the W3(OH) hydroxide ion line at 1665 MHz. Left panel: without RFI present, Center panel: image corrupted by RFI and Right panel: image restored by the subspace RFI suppression algorithm of [46] (after [22]).

(U) High angular resolution (high res mode) can be obtained from a distribution of receivers pointing in the same direction and used together as an aperture synthesis instrument, as shown in Figure 22, bottom panel. Aperture synthesis is a type of interferometry that mixes signals (amplitudes and phases) from a collection of antennas, thus synthesizing a very large (and hence high directional resolution) antenna aperture. The interference pattern is related to the source brightness over the sky, T(x,y). The 2D Fourier Transform of T(x,y) results in a complex visibility, V(u,v). This relationship is illustrated in Figure 33, where the left panel denotes the spatial distribution of 30 antennas, and the right panel shows the corresponding coverage in the u-v plane. Those points can be used to to recover the angular map of the incoming radio intensity, using the relationship between V(u.v) and T(x,y).

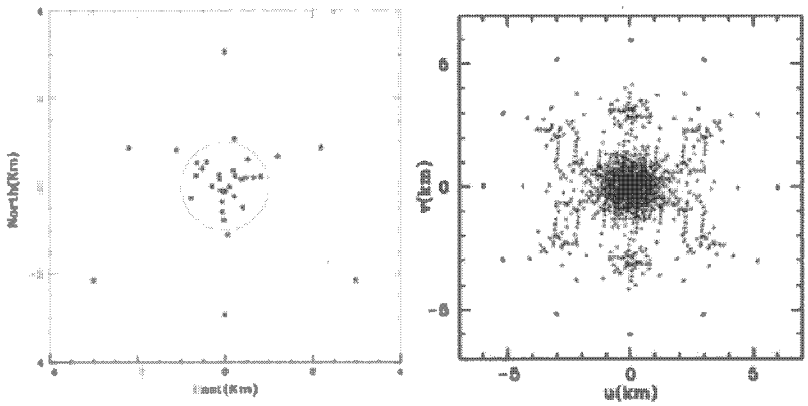

Figure 33: (U) ASKAP antenna configuration design from Schinckel et al. (2012) [70]. Left panel: antenna placement on the ground. Right panel: instantaneous coverage of the (u,v) plane (after [70]).

6.2.7 (U) Data processing for phased array feed systems

(U) An important issue in using PAFs is the data flow and processing. Our best example at present is the ASKAP radio telescope. An overview of the digitizing, data flow and computation is shown in Figure 34. This software system schedules observations, monitors and controls the array during observations, processes observational data into scientifically useful products and archives these products. The first process at left is digitizing the output of the individual (188) PAF elements breaking the 300 MHz bandwidth into 1 MHz segments. These filtered samples are then weighted and summed to form beams as discussed above. The beam samples are then correlated to form an aperture synthesis radio image and the result sent to a central processor for gridding and other processing before being archived. ASKAP will be quite different from previous synthesis radio telescopes in that the enormous data rates require that ASKAP processing and archiving must be performed synchronously with observations. The results are immediately available.

(U) In a spacecraft cluster, the computing load must be reduced to fit the computational sources available. For example, Intel's Teraflops Research

Processor showed 1 teraflop performance with a power requirement of 65 W. Using fewer elements in the PAF and/or fewer antennas allows tailoring the array to the computation chips and power available. The power consumption of the processors is also an issue as power is scarce on a spacecraft and heat dissipation impacts the thermal design of a spacecraft. To give an idea of the processing requirements for a small array of 6 antennas we consider the BETA engineering test array at ASKAP. The hardware requirements estimated for this system [14] are:

1. 3-6 TFlop/s
2. 1-2 TB memory
3. Good memory bandwidth (greater than 15 GB/s per socket)
4. 50 TB persistent storage (1 GB/s I/O rate)
5. Modest network interconnect.

(U) These computational requirements seem achievable on a modest size spacecraft. Communications between spacecraft would need to be in the 100s of Gb/s for a large PAF, but could be reduced with fewer PAF elements. The new starlink satellite communications system is reported to use laser communications between satellites and this would likely be appropriate for a PAF satellite cluster for RF observing.

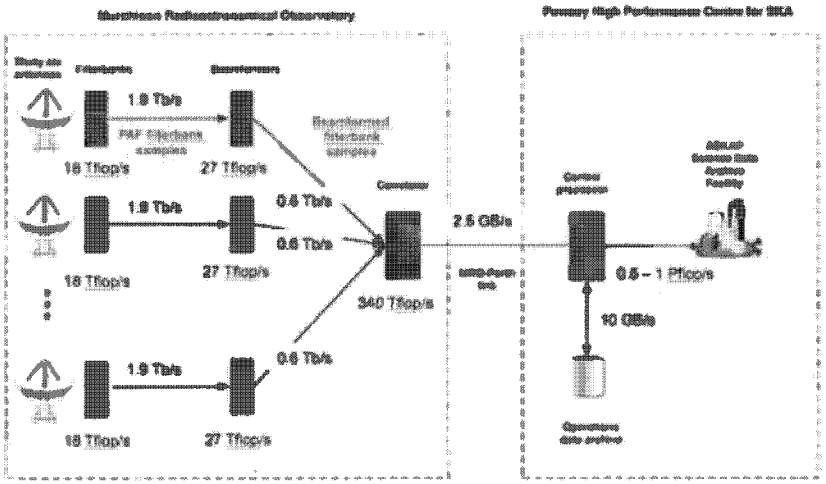

Figure 34: (U) Data flow and processing schematic diagram showing the data rates and computational loads for the various physical elements of the ASKAP telescope. Going from left to right the data flows through the filter banks, beamformers and correlator, through to the central processor, and eventually into the data archive. (Adapted from ASKAP Technologies: Computing `www.atnf.csiro.au/projects/askap/computing.html`).

6.2.8 (U) Applications of a satellite cluster using reflecting apertures & PAFs

(U) We separate applications into two categories: fly's eye (simultaneous survey) and high res (high angular resolution).

(U) In the fly's eye mode one can survey a wide area all at once to observe episodic signals, especially ones that are unscheduled and not confined to a specific frequency, such as follows:

1. Episodic communications uplinks from ground terminals. One example would be a drifting ocean buoy that only communicates intermittent data in real time and jumps in frequency to avoid interference

2. Identification and differentiation of episodic emitters that may change frequency abruptly in unknown locations over a wide FOV .

3. Rejection of Interference or unwanted sources using the capabilities of the PAF array's ability to form very flexible beams and nulls using adaptive weighting.

(U) In high res mode one narrows the FOV, but retains high time and frequency resolution and increases sensitivity and angular resolution. This can be most useful when the source location is known, in such applications as follows:

1. Communications from weak sources in known locations
2. Communications from weak sources with nearby interference, taking advantage of the high sensitivity and the enhanced angular resolution in high res mode as well as RFI rejection by the PAFs
3. Identification and differentiation of episodic emitters that are in known locations and are weak and/or close together and may change frequency abruptly.
4. Very high accuracy geolocation of signals that don't lend themselves to the use of direction finding techniques. From GEO 10 arc sec resolution is about 2 km on the Earth's surface.

(U) While the emphasis in this discussion is on receivers in space, one may use similar techniques with transmit/receive modules for two-way communications. However, the arrays will be more complicated and costly and naturally require significantly more power.

6.2.9 (U) FINDINGS AND RECOMMENDATIONS

1. (U) **FINDING:** The satellite cluster concept of an array of large reflector aperture with phased array feeds (PAFs) has similarities with the broad objectives of the ASKAP array discussed above. It is a middle way between a single very large reflector aperture and a very large

phased array. The objective is to have the sensitivity (collecting area) and spatial and temporal resolution of a large reflector while obtaining the large FOV and ability to do simultaneous observations in different directions of a phased array.

(U) **RECOMMENDATION:** We recommend that PAFs on spacecraft clusters be seriously considered for applications that require a large instantaneous FOV, high sensitivity, high temporal and high directional resolution.

2. (U) **FINDING:** A spacecraft cluster, such as the TechSat21 concept [49], offers the opportunity to use the Australian Square Kilometer Array (ASKAP) as a guide in designing a very cost-effective receiver system in space with the combined advantages of the high sensitivity of large reflecting apertures combined with high sensitivity and high time, angle and frequency resolution over with field of view and frequency band.

   (U) **RECOMMENDATION:** We recommend that such a spacecraft cluster concept, based on ASKAP, be considered in the design space for placing large apertures in space.

3. (U) **FINDING:** The size of the PAFs (number of elements) and number of reflecting apertures in a spacecraft cluster can be tailored to match the power, computing and data transmission capabilities available from the technology of the time that the cluster is manufactured and deployed.

   (U) **RECOMMENDATION:** We recommend that if a spacecraft cluster of large apertures is to be deployed, the step by step approach used in the development of the ASKAP and its successors be studied. Smaller arrays and systems were used to carry the project toward completion, e.g. the 6 aperture, BETA engineering test array as well as

ASKAP itself as a pathfinder.

(U) The concept is described here in terms of an RF system, but might find application at shorter wavelengths.

6.3 (U) 40 m Optical Aperture at GEO

6.3.1 (U) The 40 m extremely large telescope on the ground

(U) The European Southern Observatory (ESO) is constructing the Extremely Large Telescope (ELT) on Cerro Armazones in Chile. It is a three mirror anastigmat (TMA) that consists of a 39.3 m diameter primary mirror, a 4.1 m diameter secondary, a 3.8 m tertiary, and two other mirrors to steer the beam and compensate for atmospheric turbulence. It delivers a beam at f/17.5 to instruments installed at a pair of Nasmyth focal platforms. ESO expects first light in 2025, after 11 years of construction. The cost in 2018 was estimated to be 1.2 billion euros, including the first suite of instruments.

(U) Figure 35 shows the telescope structure.

(U) The primary mirror is a 39.3 m ellipsoid at f/0.93. It comprises 798 hexagonal mirror segments of 1.4 m diameter zerodur with 50 mm thickness, figured to 7.5 nm RMS. The gaps between segments is 4 mm. The weight of just the glass is 200 kg with areal weight 130 kg/m^2. Details about the opto-mechanical design may be found in "E-ELT optomechanics: overview" Proc SPIE, September 2012, DOI:10.1117/12.925175.

(U) The primary mirror figure is maintained with 4608 inductive edge sensors between all mirror segments that are reported to have an accuracy of a few nanometers. Each mirror is supported with a whiffletree and has three actuators to maintain tip, tilt, and piston. These actuators are designed to maintain a 1.7 nm RMS position accuracy with a 900 N load in the presence of vibrations and wind disturbances, while tracking a 15 mm stroke with a velocity up to 1.2 um/s. Each segment also has a quasi-static warping

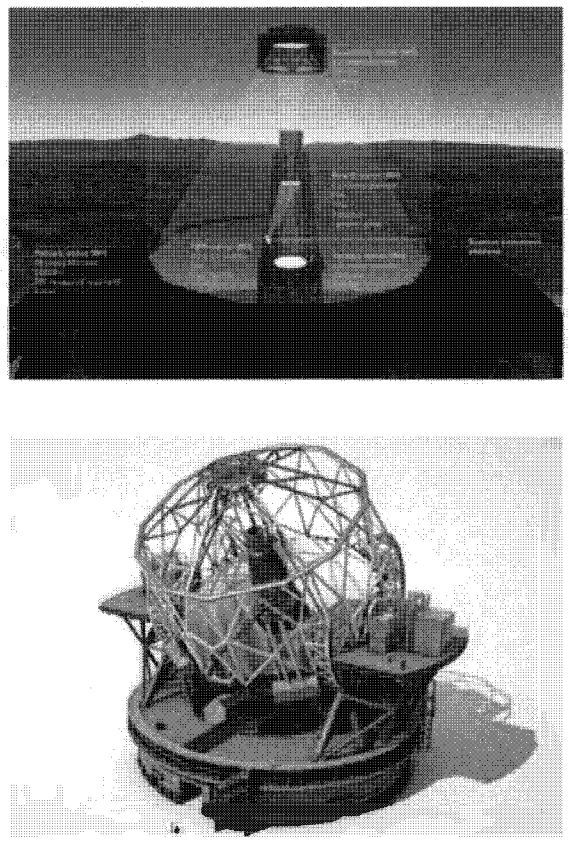

Figure 35: (U) The ESO ELT is a 40 m aperture three-mirror anastigmat (TMA), diffraction limited over a field of view of 10 arcmin (3 mrad).

harness to adjust its low order figure.

(U) The resolution of ELT when adaptive optics are functioning is reported to be 0.005 arcsec (24 nrad), corresponding to a Strehl ratio [11] that approaches the diffraction limit at a wavelength of 1 μm. Diffraction limited performance at shorter wavelengths in the visible part of the spectrum will not be possible without a much finer and faster adaptive optics system to compensate for the more challenging atmospheric wavefront distortions in the visble. This 24 nrad corresponds to a resolution of 10 m on the surface

[11] the Strehl ratio, S is a measure of the quality of optical image formation. S can be defined as the ratio of the peak aberrated image intensity from a point source, compared to the maximum attainable intensity, usingan ideal optical system limited only be diffraction over the system's aperture.

of the moon or 1 m on a geosynchronous satellite.

(U) The diffraction limited field of view is 10 arcmin (3 mrad).

(U) The ELT structure is a truss with sufficient stiffness that the mirror actuators can maintain the mirror figure from zenith to horizon. This is illustrated in Figure 36.

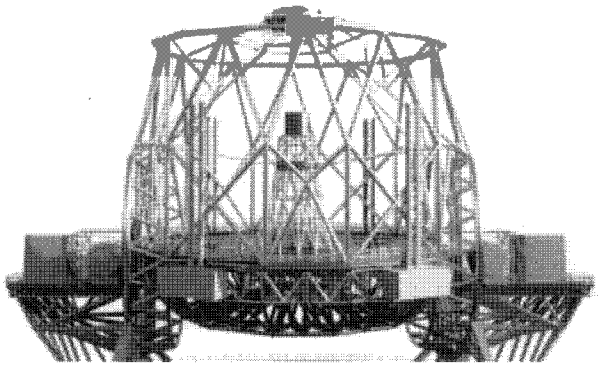

Figure 36: (U) The ESO ELT mirrors are supported by a truss that has a volume of about 12,000 m^3 and another truss that extends up by about 40 m to support the secondary mirror.

(U) The telescope moving mass is estimated to be 3000 tons. The total mass of the mirror segment glass is about 160 tons, and the total mass of the mirror segments including support and actuators is about 200 tons. The primary mirror is about 98% of the total functional mass; the secondary mirror mass is 3.5 tons. The moving mass is therefore about 15× that of the functional, optomechanical elements. This structure is required in order to maintain the optical quality under varying elevation angles and wind loading.

6.3.2 (U) A version of the 40 m ELT in space

(U) The remarkable growth in capability for space manufacturing, launch of heavy payloads in large farings, and robotics creates the opportunity to

build an ELT in geosynchronous orbit (GEO). GEO is really the right spot to place the "Space ELT" (S-ELT) for three reasons: it is not subjected to the ~30 daily thermal shocks of low Earth orbit (LEO), we obtain persistence in surveillance over regions of interest, and it provides a vantage for continuous, high-bandwidth communications downlink to a ground station.

(U) We will assume throughout that launch to GEO costs $15k/kg. SpaceX has recently advertised $90M launch cost for 8 tons to GTO, and we expect that $15k/kg is probably conservative. We will also assume that the ELT opto-mechanical assembly is simply replicated rather than lightweighted as would be possible for a structure is subjected to minimal force. The total mass is therefore overestimated by a substantial factor.

(U) The opto-mechanical mass of the ELT is about 200 tons. The support structure fills a volume of about 12,000 m^3 to provide adequate stiffness. If built with sticks of length 2 m we can anticipate a space truss requiring about 5,000 sticks. If each stick is a cylinder of carbon fiber with length 2m, diameter 5 cm, and wall thickness 1 mm it has a mass of about 1 kg, so the total mass of space truss could be about 5 tons, negligible compared to the opto-mechanical components. We anticipate therefore needing to transport about 200 tons to GEO, about 20× the mass of the Hubble Space Telescope. At $15k/kg, the launch cost is about $3 billion. Replicating the ELT opto-mechanics is evidently about $1 billion. We therefore believe that a JWST-scale budget of $10 billion and 25 years could be easily improved upon.

(U) We anticipate launching a number of packages:

- Two bus units that attach to the sides of the space truss. These provide power, pointing, maneuvering, and communications. Each is similar to a typical communications satellite.
- The solar arrays, rolling out from a long truss that attaches to the back of the space truss.
- General purpose assembly robots.

- The large, monolithic optical elements including secondary and tertiary mirrors.
- A "tinker-toy" kit of sticks and balls that will be assembled into the space truss.
- Approximately 30 launches of "segment robots", each with 25 complete mirror segments that can maneuver and attach themselves to the space truss.
- The (servicable) instrument package.

(U) As designed, the ESO ELT should be capable of providing wavefront errors of about 10 nm RMS across the 40 m aperture. The Strehl ratio is approximately $\exp(-\sigma^2)$, where σ is the RMS wavefront error in radians, so displacement error in mirror spacing of 10 nm RMS corresponds to 20 nm RMS in wavefront error and a Strehl ratio of 0.9 at 400 nm wavelength: diffraction limited to all intents and purposes. We can therefore anticipate a S-ELT point spread function (PSF) of full width half maximum 10 nrad at 400 nm, i.e. 4 m if viewing the moon, 0.4 m if viewing the Earth, 0.01 AU at a distance of 16 light years, and 22 PSFs (500 resolution elements) across the face of Betelgeuse.

(U) Because this 40 m aperture can provide diffraction limited performance from radio frequencies of 1 GHz to optical wavelengths of 300 nm we anticipate a wide variety of instrument packages, and the light from the optical telescope assembly (OTA) should be split to feed many different wavelengths simultaneously. Serious attention must be paid to cost and schedule in weighing the requirements at different wavelengths, however. For example it is probably advisable not to attempt to cool the optics to improve the thermal IR backgrounds beyond the emissivity of warm optics and segment gaps.

(U) We cannot begin to provide serious system engineering advice on how to bring the S-ELT about, but some obvious work packages and concomitant

interfaces might include:

- Universal gripper module: a mechanical interface module available to all subcomponents that provides a tight, accurate mechanical interface as well as power and ethernet. For example it could include an extendable gripper claw that has limited rotation, a pair of pin and socket joints, power through a claw-claw connection, current return where two modules draw each other together, and a free-space laser link across the joint for ethernet.

- Bus package: a pair of spacecraft that attach to the space truss via gripper modules and provide orientation control, maneuverability, power, computation, and communications.

- Solar panel package: suitable solar panels that attach to the space truss and articulate to follow the sun during the daily schedule of pointings.

- The space truss: a truss consisting of sticks and joints that ties all of the components together, along with a suitable robot for assembly.

- Laser metrology: despite the success of edge sensors in ground based telescopes, laser metrology has matured a great deal since the ground ELT's were designed, and this may now be a better way to acquire and maintain phase. All optics could orient themselves to corner cubes on the secondary mirror, for example.

- Mirror segments: 800 autonomous robotic modules. These include mirror, grippers to attach to the space truss, three actuators for positioning, and metrology units to acquire and maintain mirror phase. The edge sensors of ground based ELTs may be more challenging to implement than laser metrology.

- Secondary mirror: this is an autonomous robotic module that can maneuver itself into a position that allows gripper modules to connect it to the space truss. Slow velocities are advised.

- Tertiary mirror: another autonomous robotic module.

- Pointing and fast steering mirror: the field of view of 3 mrad is much larger than a plausible instrument field of view of $\sqrt{N}$ pixels times 5 nrad, so an optical element that can move the field of view without repointing the whole OTA is advisable. It is also likely that using a fast steering mirror to stabilize the image on the instruments at 5 nrad accuracy would be helpful to offload requirements on the OTA pointing and mirror actuator bandwidth.
- Wrap robot: once the truss is complete it should be wrapped in Multi-layer Insulation (MLI) to manage thermal gradients in the space truss.
- Optical instrument package: imagery at various wavelengths, spectroscopy, polarization, etc.
- SWIR instrument package: imagery, spectroscopy, polarization.
- MWIR instrument package: imagery, spectroscopy, polarization.
- LWIR instrument package: imagery, spectroscopy, polarization.
- RF instrument package

(U) NASA is considering construction of the "large ultraviolet, optical, and IR telescope" (LUVOIR), a segmented space telescope with diameter in the range of 8 15 m, intended for L2. Because NASA's design precludes the possibilty of robotic assembly of components the cost and capability are far less than the S-ELT. Given the lien on NASA's resources from JWST, it seems rather unlikely that LUVOIR will exist before 2030, if then. Also, the NASA process of building a consensus science case from all potential stakeholders places many conflicting requirements on the design that drives up the cost enormously, for example the question of whether the optics should be cold.

(U) The Apollo program had a remarkable goal of putting a man on the moon within a decade, but of course its real intent was to rapidly advance

the US state of the art in rocketry, manned space, and other technologies of national interest.

(U) We believe the S-ELT is a similar, visionary organizing principle for bringing space assembly to a degree of functional maturity.

(U) Table 2 lists a set of technical space assembly capabilities whose TRL would benefit from demonstration and risk reduction with a LEO demo program in advance of incorporation into the SELT fabrication project.

Table 2: (U) Key capabilities

#	Task	Perform. Spec.	Pre-reqs.
1	Strut assembly and disassembly, in-line joint	25 um precision	none
2	Three-element strut joint	25 um precision	none
3	Edge alignment mechanism for optical elements	40 nm precision	none
4	Electrical and optical fiber connector plug-unplug	$< 10^{-4}$ failure rate	
5	Macroscopic robotic repositioning/reorienting of system elements	1 mrad and 25 um	none
6	Synthetically rigid structure support w active actuation	fundamental > 10 Hz	none
7	Automated replacement of instrument module	NA	NA
8	Refilling of propellant (hydrazine)	$< 10^{-3}$ failure rate	

This Page Intentionally Left Blank

7 (U) CONCLUSIONS

(U//~~FOUO~~) Numerous studies and partial proofs-of-concept related to iSAM technologies have been carried out. JASON believes that there is great promise for iSAM in helping to realize [redacted] of more effective, agile, resilient and technologically advanced operations in space. However, the key technologies necessary to enable iSAM are at present only partially developed. (b)(3)

(U//~~FOUO~~) JASON's assessment is that full realization of iSAM potential can only be achieved by addressing the systems-level challenges: [redacted] is well-positioned to advance iSAM readiness by spearheading a proof-of-concept deployment that could both benchmark new capabilities and facilitate in-space technological experiments. (b)(3)

(U) A summary of the principal **Findings and Recommendations** can be found in the Executive Summary. This report has discussed a number of technological issues and opportunities, and **Findings** related to some of those issues are integrated within the body of the report.

(U) Rather than repeating the *Findings and Recommendations*, the concluding remarks may benefit from some of the *Lessons Learned* from experience with the *Large Deployable Reflector*, described in Appendix I:

1. A bold, ambitious concept or vision has the capacity to inspire.
2. There are many ways for an over-ambitious vision to fail. These include technological immaturity, underestimation of the difficulty and complexity of the task, and insufficient budgets.
3. Cheaper launch costs, the prospect of autonomous assembly, and improved sensors and communications suggests that the time for in-space assembly of large space telescopes may have finally come.
4. Technology demonstrations are often necessary to build confidence and

gain experience.

5. Technology demonstrations may be the only means to fully understand both systems issues and the pathways to lower cost and higher reliability.

8 (U) APPENDIX I: THE LARGE DEPLOYABLE REFLECTOR (LDR), A SPACE ASSEMBLY CASE STUDY

8.1 (U) Introduction

(U) In briefings provided to JASON, NASA Langley's Bill Doggett discussed"Space Assembly of Persistent Space Assets", giving many examples of challenges that were faced and problems that were solved for in-space assembly of structures. Some of this work was motivated by the Space Station. Another important driver, particularly in the 1980s and 1990s, was the Large Deployable Reflector (LDR) concept. Despite the long history of this work at NASA Langley, the assembly techniques developed have yet to be used in space. It is thus interesting to take a closer look at one of these projects, LDR, to see what lessons we may learn about in-space assembly.

8.2 (U) 1977: The Genesis of LDR

(U) In the introduction to their 1977 paper titled "An Entree for Large Space Antennas", the Jet Propulsion Laboratory's (JPL) Robert Powell and Albert Hibbs[12] wrote:

> "Imagine it is 1987. You are driving through the boondocks of the northwest and you need to be available to your office a thousand miles away. Your proceed on your way with confidence, knowing that you can be reached, far from any urban area, on your mobile communications transceiver. The message alert sounds and you are in contact with the home office, barely perceiving the fraction-of-a-second delay between transmission and response. By now

[12](U) Hibbs [61, 84] was one of Richard Feynman's few graduate students, obtaining his Ph.D. in 1955. He spent most of his career at JPL and played a significant role in setting JPL's course in planetary exploration in the early days of NASA [30]. In 1967 he was selected to be an astronaut for the (cancelled) Apollo 25 mission.

> you have become used to rural mobile communications relayed across the country by an acre-sized antenna in geostationary orbit."

(U) Although their technological forecast now seems amusing given the impending rollout of 5G cellular networks, this quotation reflects the bold imagination prevalent in the first several decades of the space age. Powell and Hibbs had no hesitation in conceiving of a huge antenna, 75 meters in diameter, in geostationary orbit. In fact their paper describes even larger antennas, 100-200 m diameter, serving as a deep-space communications relay in geostationary orbit or as a high-resolution multispectral microwave radiometer in low earth orbit.

(U) One of the more modest concepts described by Powell and Hibbs is illustrated in Figure 37, showing an antenna of only 10 m diameter, but of high precision, springing out of the cargo bay of a space shuttle. The high precision was needed for a space telescope operating at submillimeter wavelengths, a concept that had been discussed at a JPL workshop earlier that year [27]. Although the first orbital flight would not occur until 1981, NASA's name for the shuttle program the Space Transportation System (STS), the only surviving element of a much grander vision developed in 1969 promised a new era of inexpensive access to space for large payloads, and in 1977 NASA's scientists and engineers were busy coming up with ideas for exploiting this anticipated capability.

(U) As described by Powell and Hibbs, the 10 m space antenna shown in Figure 37 was inspired by the work of Robert Leighton at Caltech on the development of high-precision telescopes for millimeter and submillimeter ground-based astronomy. Leighton's work was funded by a 1973 grant from the National Science Foundation; by the late 1970s, his telescopes were being used for millimeter-wave astronomy at the Owens Valley Radio Observatory [45]. A total of seven such telescopes were eventually constructed, six for the millimeter interferometer at Owens Valley Radio Obseratory, and one for the

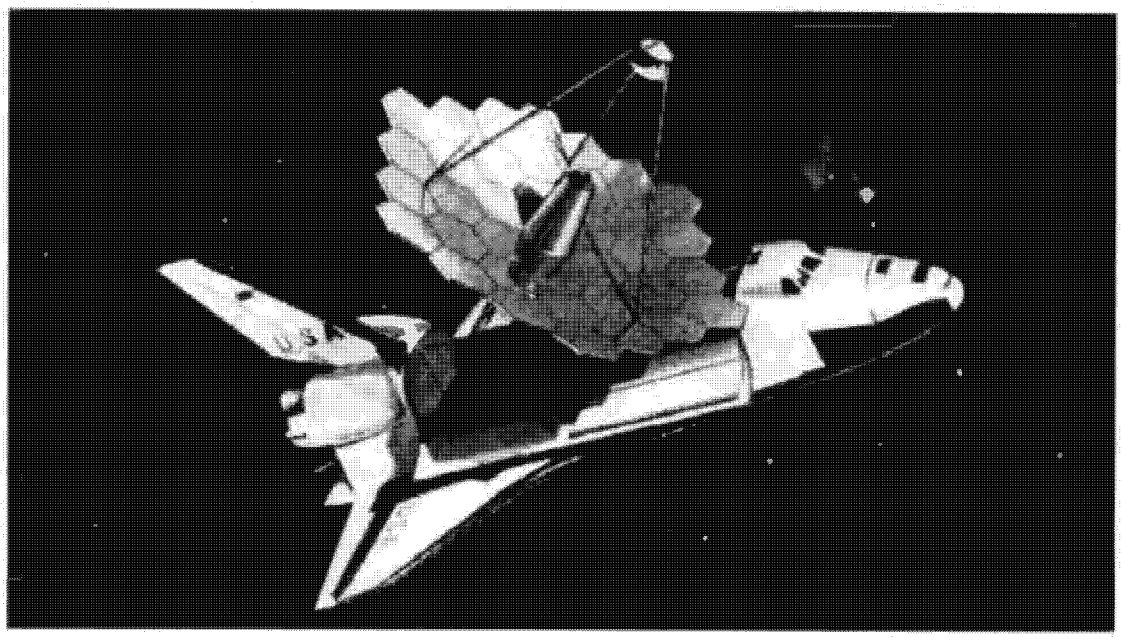

Figure 37: (U) The 10 m space antenna for submillimeter astronomy described by Powell and Hibbs [67], inspired by Leighton's work on ground-based telecopes pictured in Figure 38.

Caltech Submillimeter Observatory on Mauna Kea; a copy was also built in Bangalore by the Raman Research Institute [75].

8.3 (U) 1980: In-Space Assembly for LDR?

(U) By 1980, the concept for the observatory had evolved significantly [57]. NASA's Ames Research Center (ARC) and JPL had joined forces and had contracted Lockheed to perform a study for a large aperture space telescope, or LAT; the stated goal was to start construction by the late 1980s. The LAT represented the union of ARC's interests in infrared astronomy and JPL's interests in submillimeter astronomy – the requirements listed in Figure 39 for LAT specify a very wide wavelength range, from 1000 μm to 2 μm. As shown in Figure 40, the Lockheed's 1980 technology report [3] considered three possible versions of LAT, now renamed as the Large Deployable Reflector (LDR):

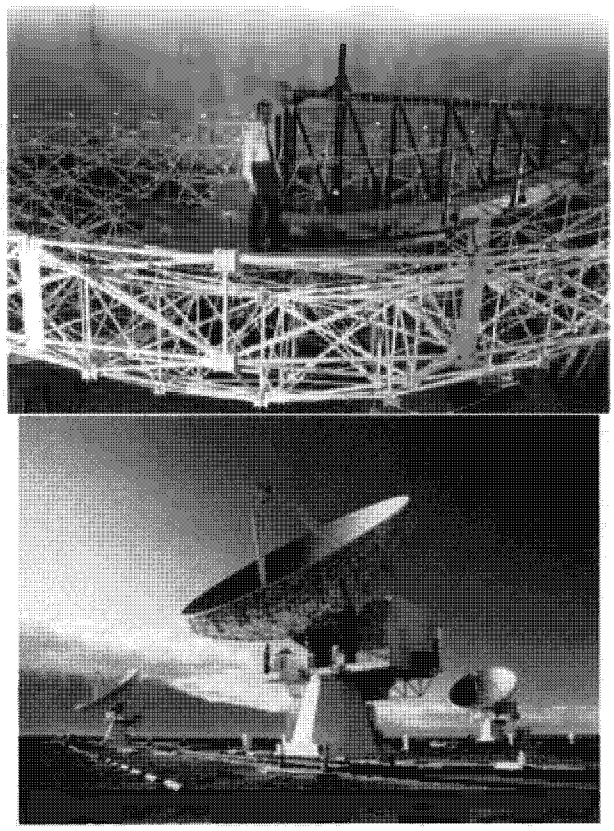

Figure 38: (U) **Left**: Bob Leighton in the process of constructing one of his 10 m telescopes in the mid-1970s. Note the hexagonal reflector panels, similar to those in Figure 37. **Right**: The first three Leighton telescopes had been constructed for the Owens Valley Radio Observatory millimeter interferometer by 1984.

1. A 10 m deployable aperture that was only capable of operating at wavelengths longer than 500 μm, using a completely passive structure and aluminum panels similar to those on Leighton's telescope. This was basically the concept as described by Powell and Hibbs [67].

2. The next step up was again a 10 m deployable aperture, but now with segments made from ultra-low expansion (ULE) glass, and active control of the segment positions. These upgrades allowed diffraction-limited performance to 30 μm.

Table 1. LAT Requirements Summary

Launch/deployment:	Single STS launch to Low Earth Orbit (LEO) semi-automatic deployment (man assisted)
Mission duration:	10 yr; periodic revisits at 2-yr intervals
Time frame:	1987 technology; 1991 launch
Primary collecting aperture, D:	10 m ≤ D ≤ 30 m
Operating wavelength:	1000 μm ≥ λ ≥ 2 μm
Diffraction limited at	λ ≥ 30μm
Field of view:	The greater of 30 sec or 10 × airy disk diameter
Pointing stability:	±0.1 λ_{min}/D for ≥20 min interval
Retargeting slew:	180° in 10 min (5 min desired)
Spatial chopping:	Chopping frequency, 10 Hz; throw = F.O.V.
Stray light rejection:	Stray light from Sun, Earth, and Moon <60° off axis is less than effect of telescope emission (ε = 0.1) and zodiacal light on the detectors.
Primary mirror temperature:	~150–200 K;
Temperature uniformity:	Scan noise of spatial chopping shall not degrade achievable instrument sensitivity
Total telescope emissivity:	ε ≤ 0.1

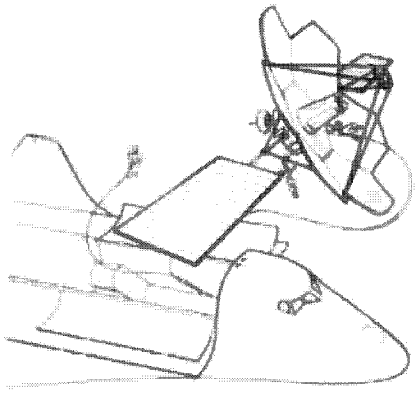

Figure 6. Artists conception of a 10-m LAT.

Figure 39: (U) **Left**: Summary of the basic parameters of the large aperture space telescope (LAT) described by Murphy *et al.* in 1980 [57]. **Right**: The artist's conception of LAT had evolved relative to that shown by Powell and Hibbs (see figure 37): LAT now has solar panels and communication antennas. The deployment scheme is not shown, but interestingly, the illustration features two astronauts performing unspecified EVA activities.

Diameter (m)	10 to 12	10 to 12	15 to 30
f/No.	0.5	0.5	0.5
Deployment	Self-deployed	Self-deployed	Assembled
Passive or active	Passive	Active	Active
Segments (8-m diameter)	Al hexel	ULE	Be (solid), or ULE (light-weight)
Support structure	Gr/Mg	Gr/Mg	Gr/Mg
Segment Alignment	Star (Telescope)	Star, Edge Sensing	Star, Trilateration
Operational λ (μm)	500	30	30
Cost ($M)	250	250	500

Figure 40: (U) The three baseline concepts for the Large Deployable Reflector (LDR) described in the 1980 Lockheed report [3].

3. The most ambitious concept was a 15-30 m aperture that was too large to be deployed, therefore requiring in-space assembly as shown in Figure 41. Segments made from either beryllium or ULE glass would allow operation to 30 μm.

(U) In contrast to the earlier versions of the concept (Figures 37 and 39), all of the Lockheed baseline concepts included a truss structure on which the reflector segments were mounted, similar to the backup structure for Leighton's ground-based telescope illustrated in Figure 38. Although LDR would obviously not be subject to gravitational loads, the Lockheed engineers thought this structure was necessary for thermal stability and for dynamical stability in the presence of vibrations generated by the attitude control system and by the chopping (oscillating) secondary mirror, which at the time was thought to be essential for sensitive infrared observations.

(U) As illustrated in Figure 42, the goal was to launch LDR in a single shuttle launch, which imposed a challenging contraint on the areal density of the primary reflector. Packing density in the shuttle's cargo bay was also a key issue, which forced the switch from deployment to in-space assembly for reflector diameters exceeding 10 m.

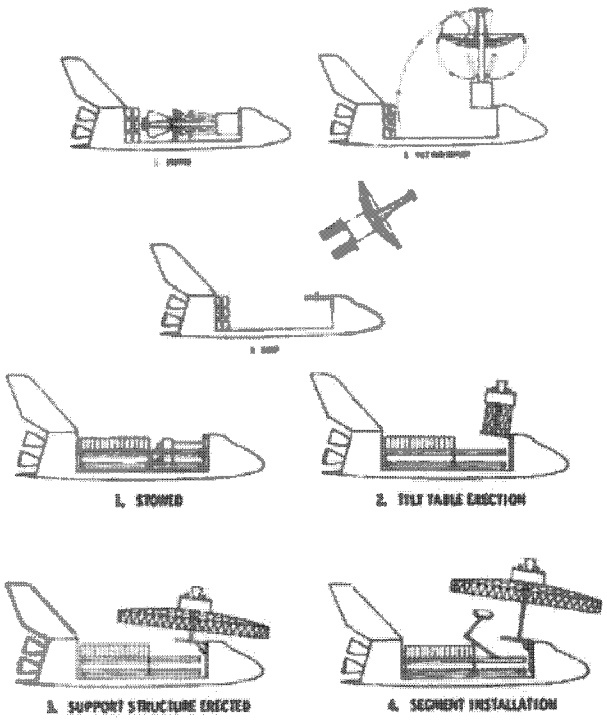

Figure 41: (U) **Left**: Concept for a deployable 10 m telescope described in the 1980 Lockheed LDR report [3]. **Right**: Larger apertures in the 15-30 m range were envisioned to require in-space assembly. This figure appears to show a support structure that unfolds and a robotic arm that installs the reflector segments onto the structure.

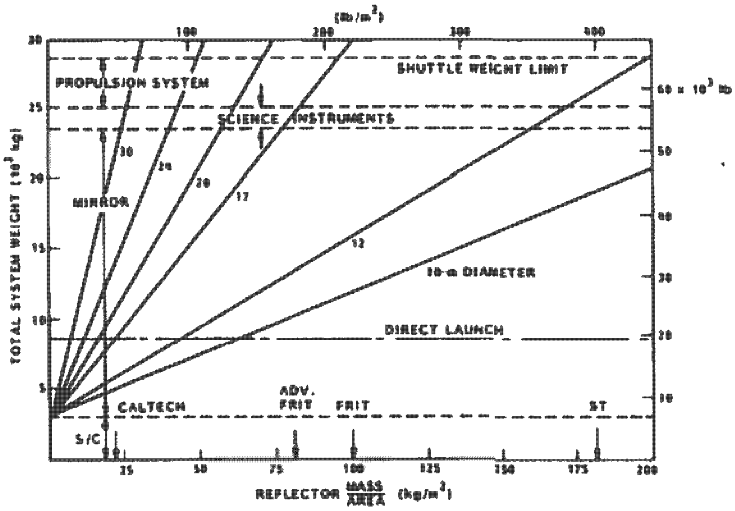

Figure 42: (U) This figure illustrate the areal density of the primary reflector required for LDR to fit within the cargo capacity of a single shuttle launch, for diameters in the 10-30 m range. Arrows labeled "CALTECH" and "ST" indicate the areal densities for Leighton's 10 m telescopes (Figure 38) and by the (Hubble) Space Telescope. Arrows labeled "FRIT" or "ADV. FRIT" show projected values for lightweight bonded-glass reflector panels.

8.4 (U) 1982: The Field Report recommends LDR and ISA

(U) Every decade, the National Academies convenes a panel of scientists to review proposed new projects in astronomy and astrophysics for the coming decade, who then make prioritized recommendations in a report commonly known as the Decadal Survey. In June 1982, the committee led by Harvard's George Field published their report, which contained the following recommendation for a $300M project:

> The Astronomy Survey Committee recommends the construction of a Large Deployable Reflector (LDR) of the 10-m class in space to carry out observations in the far-infrared and submillimeter regions of the spectrum that are inaccessible from the ground. Design studies for such a facility should begin at once.

(U) From today's perspective, the audacity of this recommendation is astounding, and echoes the bold imagination evident in Powell and Hibbs's paper. One cannot imagine the 2020 Decadal Survey panel making such a recommendation today. The technology needed to execute LDR was very immature, whether one considers the reflector segments, deployment or in-space assembly techniques, science instruments and detectors, cryocoolers, etc., yet the 1980 survey panel had confidence that all of these difficulties could be overcome. The boldness of the panel's vision becomes even more apparent in their further recommendation:

> The Astronomy Survey Committee recommends the study and development of the technology required to place a very large telescope in space... By the turn of the century it may be possible to place in orbit a very large telescope perhaps 30 m in diameter – with diffraction-limited performance from the far-infrared to the near ultraviolet regions... Development of technology for the Large Deployable Reflector in space ... should provide a strong

impetus for the further advances needed for this even larger, more powerful instrument.

(U) In essence, the panel made a strong recommendation for development of in-space assembly techniques for large space telescopes, believing that some of the concepts discussed in our report could have been executed two decades ago!

(U) Although the Field report recommended LDR, it was listed as the committee's fourth priority, behind AXAF (an x-ray mission), VLBA (a radio very long baseline array), and NNTT (the optical, ground-based national new technology telescope). The committee stated that the relative immaturity of LDR's technology was the reason that LDR was placed last in this list of recommendations. Notably, AXAF (now Chandra) and VLBA were built, but NNTT [51] and LDR were not.

8.5 (U) 1982-84: The Asilomar LDR Workshop

(U) In late June 1982, immediately after the Field report was published, a workshop was convened to discuss the science and technology of LDR; the conclusions of the workshop were summarized in a 3-volume proceedings published in 1983-84 [43, 33, 44]. The soaring language in Steven Strom's preamble to the science report in Volume 2 again gives a sense of the bold vision of that era:

> "I am compelled to recall President Kennedy's speech nearly 20 years ago at Amherst. He reminded Americans at that time that the measure of a civilization was not to be found in the strength of its armies or its economy - important as they are - but rather in the vigor of its intellectual life as expressed in the visions of its poets and indeed its scientists. I can imagine no more eloquent expression of the best in American civilization than the will to accept the challenge and possibilities of building and launching

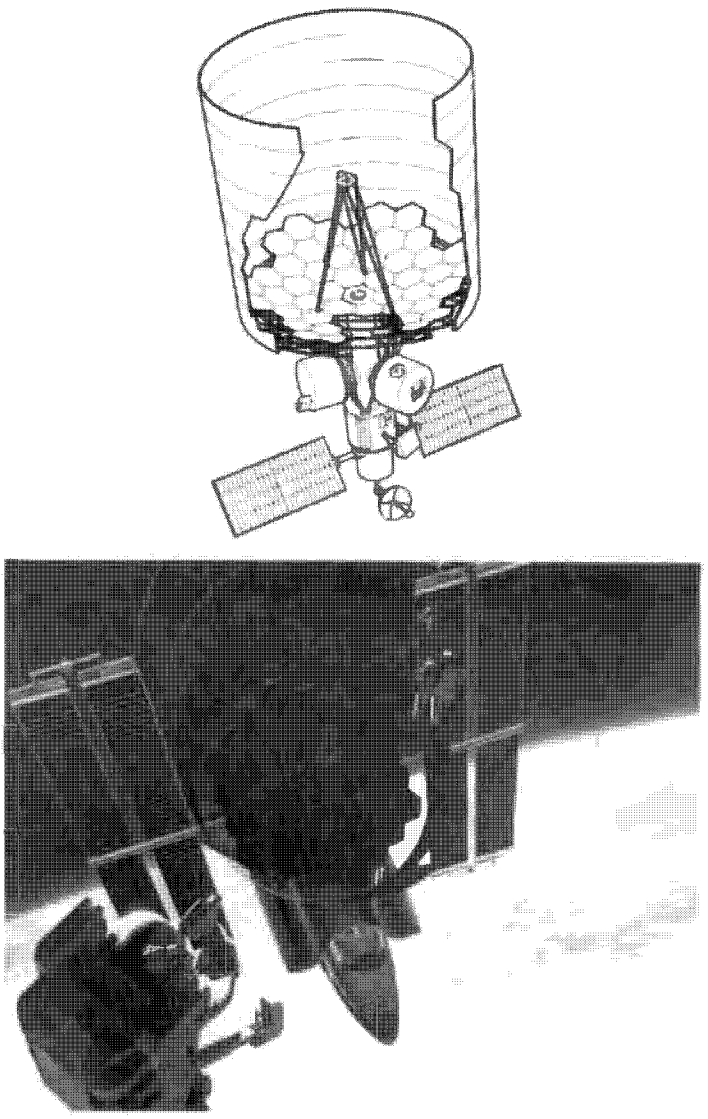

Figure 43: (U) **Top**: By 1982, a large sunshade had been added to the LDR concept, and additional details are shown for the instrument package and spacecraft [43]. **Bottom**: A total of three astronauts are now depicted in this image, with the one furthest in the background apparently busy assembling the sunshade, and the one in the foreground holding what may be a video camera.

> ST, AXAF, and LDR. Indeed, I doubt we could will a grander legacy to succeeding generations of scientists."

Indeed, by 1982, the 10 m LDR recommended in the Field report was no longer considered to be sufficient:

> A telescope diameter of at least 20-m was chosen to produce diffraction-limited spatial resolution of 1 arcsec at 100 μm, a resolution which allows direct comparison with ground-based optical measurements.

(U) However, some realism was also starting to set in as the engineering details for LDR were examined more closely. For example, a sunshade was finally added to the baseline (Figure 43). Furthermore, it was understood that the desire to work in "light bucket" mode at wavelengths beyond the 30 μm diffraction limit and as short as 1 μm imposed significant additional requirements on the reflector segments, and was therefore a major cost driver. Also, as illustrated in Figure 44, the scientific utility of LDR was being compared to a significantly smaller project the Shuttle Infrared Telescope Facility, or SIRTF. At the time, SIRTF was envisioned as a cold 1 m telescope to be periodically carried into orbit by the shuttle for $\sim$ 1 week observing sessions. SIRTF would later evolve to become a free flyer, the Space Infrared Telescope Facility, and was eventually launched in 2003 as the Spitzer Space Telescope.

8.6 (U) 1986: LDR Science Coordinating Group Report

(U) In October 1986, nine months after the STS-51 Challenger accident, the LDR Science Coordination Group published a report that describes the state of the project at that time. The vision is still bold, but is continuing to be tempered by reality. By now it is realized that one shuttle launch will not be sufficient:

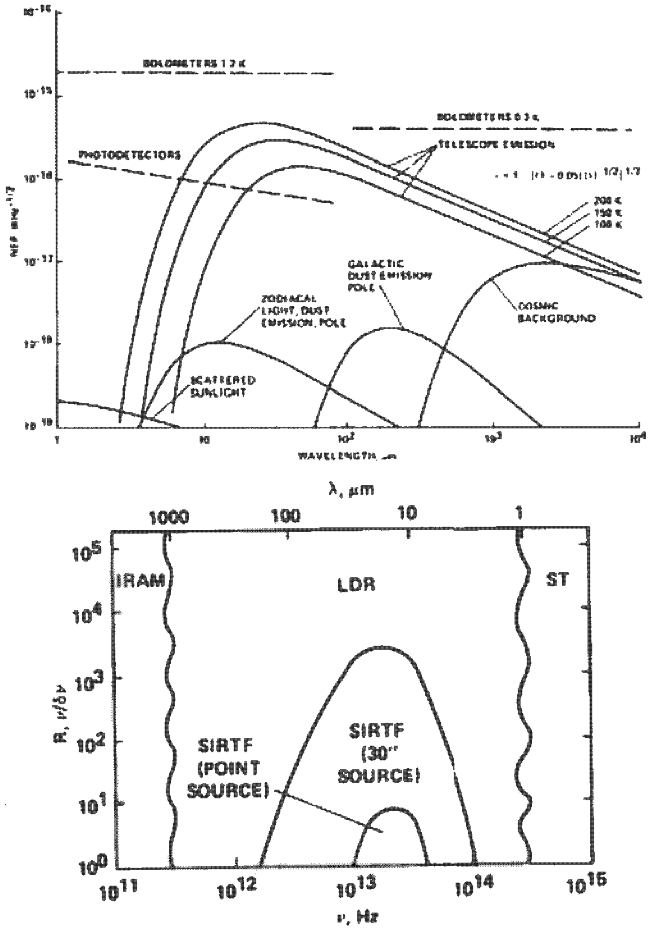

Figure 44: (U) This figure illustrates the scientific competitiveness of LDR vs. SIRTF as understood in 1982. Rapid advances in infrared detectors and arrays throughout the 1980s and 1990s would dramatically shift the balance in favor of SIRTF. **Top**: This plot shows the sensitivity (noise equivalent power, or NEP) as a function of wavelength. Although thermal emission from LDR's warm telescope would greatly exceed the astrophysical backgrounds from zodiacal or galactic dust, the far-infrared bolometers of that era were not sensitive enough to benefit from a colder telescope. **Bottom**: Using a cold 1 m telescope and photodetectors that were much more sensitive than assumed for LDR, SIRTF would have superior sensitivity to LDR at the shorter wavelengths, at low to moderate spectral resolutions.

> "Because of its immense size, the LDR cannot be launched with a single vehicle. Instead, the LDR will be the first astronomical observatory to be erected and assembled in space, a distinction that brings with it major challenges to current technology. At the same time, achieving LDR objectives will provide invaluable experience in the art of constructing high-precision, large space structures. The benefit of bringing this new art into the service of astronomy and mankind's other endeavors cannot be calculated."

Parallel industry studies by Lockheed/Itek and Kodak/McDonnell Douglas are leading to conclusions that

> "...were fairly similar in that both recommended glass mirror primaries of high accuracy, Space Station astronaut-assisted deployment, and more than one Shuttle launch for lifting the LDR total system."

The Science Coordinating Group, chaired by Steven Strom, are not entirely happy with the contractor studies, stating that

> "The general feeling of the SCG was that the contractor systems were somewhat constrained by the choice of glass mirrors and therefore became heavy and bulky, resulting in large costs and Shuttle loads."

A contemporaneous JPL design study [77] offered a potential alternative by eliminating the light bucket mode for $\lambda < 30\,\mu$m which enabled lightweight composite panels to be used; together with an active quaternary mirror for wavefront correction, this brought LDR potentially back into the realm of one shuttle launch. But despite the SCG's misgivings about the contractors growing estimates for the cost and mass of LDR, they continue to find scientific justification for a 20 m aperture:

> "The direct detection of Jupiter-like planets drives the technology requirements of the LDR. The distance to which a 100-K Jupiter-sized planet can be detected in 3-hours' integration time in a broadband observation with a 20-m LDR at 30 μm (the peak of the thermal emission) is approximately 4 pc (and is directly proportional to the telescope diameter). There are 26 stars within 4 pc. Thus, a 20-m LDR is required for a statistically significant search."

(U) In-space assembly of LDR is now envisioned to take place using the Space Station:

> "The LDR will be partially assembled and functionally tested on the ground. It will then be disassembled and packed into containers or holding fixtures for installation in the Shuttle bay. The Shuttle will transport the LDR pieces to the Space Station where they will be temporarily stored for later assembly. The individual pieces need not all be brought up to the Space Station on the same Shuttle. The LDR, after assembly and checkout, will be boosted to its > 700-km orbit by the orbital maneuvering vehicle (OMV)."

As the engineers think more deeply about the project, they realize that

> "A structural flight experiment may be required to validate the high-fidelity modeling necessary to accurately predict the micrometer-level dynamic responses to achieve the desired LDR performance goals. This experiment would determine the overall dynamic structural behavior of the joints, structural members, panels, and damping in the space environment. In addition,this experiment would validate the construction procedures and the overall structure performance capability. This data base would reduce

> the program risks and uncertainties associated with high-fidelity modeling capability."

(U) The SCG are also now confronting the technical challenges of LDR and discussing the wisdom of pursuing a smaller precursor project:

> "The LDR is a most ambitious project; it consists of a 20-m dish that approaches the Hale 5-m telescope in its requirements of surface accuracy expressed in terms of aperture divided by rms tolerance; a structure sufficiently lightweight that it can be launched into space, yet sufficiently stiff and predictable that it can be deployed and aligned virtually automatically; a telescope that must be pointed to subarc seconds of accuracy; a group of focal-plane instruments that push the state of the art in virtually every area; refrigeration requirements that require either thousands of liters of liquid helium annually or coolers that even exist only in the laboratory. Any of these would be tough problems to solve even if the telescope were fixed to the ground. NASA will have to expend considerable effort resolving these and other questions. Space verification may be required in a few cases."

The SCG also understand that a precursor would help build the scientific case for LDR:

> "The possible types of LDR precursor range from a $10 million Spartan to a $100 million Explorer. While each has advantages and disadvantages, it is essential to develop a broad base of support among the astronomical community for the precursor and for the LDR itself. For if the LDR is to be built, it will be because all astronomers, not just the submillimeter community, feel it is crucial to the continued progress of the science."

Indeed, in 1986, Tom Phillips at Caltech led a proposal to NASA for a

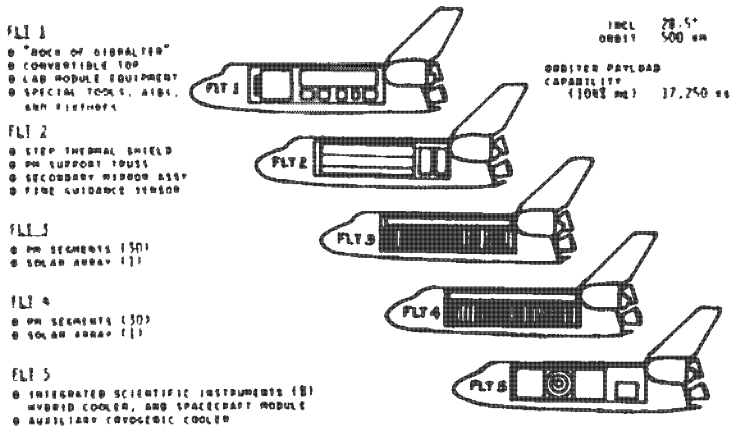

Figure 45: (U) Five shuttle launches required for LDR as described in the 1989 Kodak/McDonnell Douglas report [1].

"Submillimeter Explorer", the first of several precursor mission concepts that were considered in the late 1980s and early 1990s.

8.7 (U) 1988: LDR Asilomar III Workshop

(U) A third LDR Asilomar workshop was held in September 1987. At that time, the development of LDR science instruments was envisioned to start in 1994, with a \$250M budget, while the full project was notionally to enter implementation (phase C/D) by 1997 with a \$1B budget. Compared to the Field report recommendation for a \$300M project starting in the late 1980s, this represented a 3.4× increase in cost (accounting for inflation) and a decade delay. The workshop report focused on the need to develop lightweight segments (panels) using composite materials; this was the thrust of a new NASA-funded Precision Segmented Reflector (PSR) program at JPL and NASA/Langley [53].

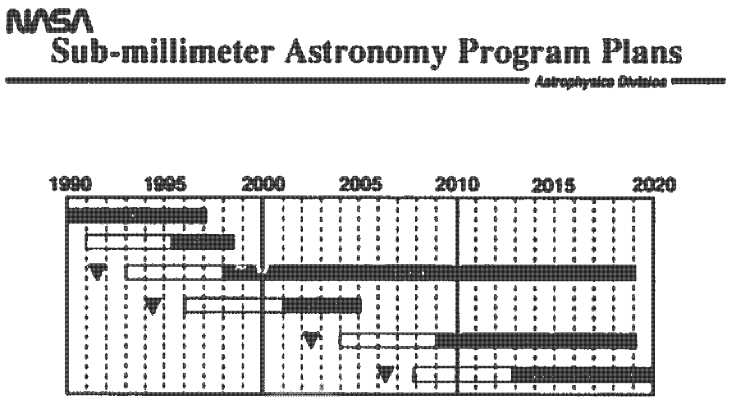

Figure 46: (U) NASA's submillimeter program plan as presented by Mike Kaplan at JPL on February 26, 1991, showing an LDR launch in the late 2000s.

8.8 (U) 1989: Space Station Requirements for LDR

(U) Kodak/McDonnell Douglas, one of the contractor teams studying LDR for NASA, produced a report in April 1989 [1] examining the implications of assembling LDR on the space station in more detail. In addition to revisiting the issue of the number of shuttle launches required (see Figure 45) this report estimated the amount of astronaut EVA (extravehicular activity) and IVA (in-vehicle activity) time that would be required. The estimates provided in the report were quite daunting:

> "It may take as many as five STS flights, over a 9 to 12 month period, to bring the entire LDR Observatory to the Space Station. Assembly is expected to take about 250 hours of IVA and 400 hours of EVA over about 100 operational days. Checkout, on the Station, will take another 144 hours of EVA and 108 hours of IVA. Final alignment and checkout, with LDR orbiting in close proximity to the Space Station, will take about 50 hours of IVA. These estimates assume maximum use will be made of teleoperation and robotics techniques and automatic test equipment."

8.9 (U) 1991: The Bahcall Report

(U) A decade had now passed, and any potential launch date for LDR seemed to be receding. Indeed, NASA's planning documents showed a potential precursor mission the Submillimeter Moderate Mission or SMMM potentially launching in the early 2000s, with LDR following in the late 2000s (Figure 46). Some astronomers openly referred to the concept as the "Large Deplorable Reflector". But it was now time for the Decadal Survey to weigh in again. The report, chaired by John Bahcall, listed SIRTF as its top priority, at a budget level of $1.3B. The Bahcall report did not match the bold if perhaps unrealistic vision laid out in the Field report. Rather than a 30 m telescope in space, the Bahcall report offered:

> One example of a next-generation space observatory is a large space telescope, a 6-m telescope that would combine the light-gathering power of a large ground-based telescope with the excellent image quality, ultraviolet capability, and low-infrared background that are achievable in space.

which we might recognize as being similar to the James Webb telescope. The Bahcall report continues with:

> "Other possible missions with great scientific potential include a large x-ray telescope equipped with detectors capable of simultaneous imaging and spectroscopy; a submillimeter observatory consisting of a deployable 10-m telescope or an orbiting array of smaller telescopes operating as an interferometer..."

Thus, with LDR relegated to a grab-bag of potentially interesting concepts, there was no future for the mission recommended by the Field report in 1982.

8.10 (U) 1997: ESA and NASA collaborate

(U) With the demise of LDR, US scientists decided to join forces with their European counterparts in pursuing a submillimeter/far-infared space mission. The effort in Europe was started in 1982 with a proposal to ESA for a Far Infrared Submillimetre Space Telescope, or FIRST [73, 24]; perhaps this name was chosen to contrast with the US concept, then known as the large-aperture space telescope or LAST [57]. By 1997, NASA and ESA had entered into a collaboration on FIRST, which was launched in 2009 as the 3.5 m Herschel Space Observatory [63].

8.11 (U) LDR in Retrospect

(U) What lessons can we draw from the LDR example? Some highlights are listed below

1. A bold, ambitious concept or vision has the capacity to inspire.
2. There are many ways for an over-ambitious vision to fail. In the case of LDR, one can point to technological immaturity, underestimation of the difficulty and complexity, insufficient budgets to overcome technical hurdles, etc. The requirement for in-space assembly was not necessarily the primary reason for failure.
3. A successful project has to be ambitious enough to inspire, but not overly ambitous so that it fails. Jerry Nelson's success with the 10-meter segmented telescope concept provides a good example of threading this needle.
4. Technology demonstrations are often necessary to build confidence and gain experience.
5. A concept or project does not exist in isolation but is part of an evolving landscape. The advances in infrared detector arrays in the 1980s and

1990s greatly boosted SIRTF relative to LDR (Figure 44). It helps to be able to predict the future.

6. Reliance on the space shuttle as the launch vehicle was a serious weak point. The actual shuttle cargo capacity ended up being lower than predicted, and the launch costs were far higher. The Challenger accident created a 3-year gap and considerable uncertainty.

7. Reliance on astronauts as assembly agents was another serious weak point.

8. The concept of using in-space assembly for large space telescopes has a long history. Perhaps its time has finally come. Space launch costs are dropping, and enabling technologies such as robotics, autonomy, sensors, and communications have advanced greatly. We no longer need to rely on the shuttle or on astronauts.

9 (U) APPENDIX II: ACRONYMS/ABBREVIATIONS

DOF	Degree of Freedom
GEO	Geostationary Orbit
GNC	Guidance, Navigation and Control
ISL	Inter-Satellite Link
LEO	Low Earth Orbit
LIDAR	Light Detection And Rangin g
SDR	Software Defined Radio
TRL	Technology Readiness Levelr

This Page Intentionally Left Blank

References

[1] D. L. Agnew, V. F. Vinkey, and F. C. Runge. Large deployable reflector (LDR) system concept and technology definition study. analysis of space station requirements for LDR. NASA Contractor Report NASA-CR-177414, 1989.

[2] Kazunori Akiyama, Antxon Alberdi, Walter Alef, Keiichi Asada, Rebecca Azulay, Anne-Kathrin Baczko, David Ball, Mislav Baloković, John Barrett, Dan Bintley, et al. First m87 event horizon telescope results. iv. imaging the central supermassive black hole. *The Astrophysical Journal Letters*, 875(1):L4, 2019.

[3] W. H. Alff, L. W. Bandermann, M. K. Bartosewcz, and R. H. Pohle. Large Deployable Reflector (LDR). NASA Contractor Report NASA-CR-152402, 1980.

[4] Pedro Alvarez, Jose Miguel Rodriguez-Espinosa, and Felix R Kabana. Gtc project: present and future. In *Telescope Structures, Enclosures, Controls, Assembly/Integration/Validation, and Commissioning*, volume 4004, pages 26 35. International Society for Optics and Photonics, 2000.

[5] Sidney Applebaum. Adaptive arrays. *IEEE Transactions on Antennas and Propagation*, 24(5):585 598, 1976.

[6] Keith W Bannister, RM Shannon, J-P Macquart, Chris Flynn, PG Edwards, Morgan O'Neill, Stefan Osłowski, Matthew Bailes, Barak Zackay, Nathan Clarke, et al. The detection of an extremely bright fast radio burst in a phased array feed survey. *The Astrophysical Journal Letters*, 841(1):L12, 2017.

[7] John Bowen, Al Tsuda, John Abel, and Marco Villa. Cubesat proximity operations demonstration (cpod) mission update. In *2015 IEEE Aerospace Conference*, pages 1 8. IEEE, 2015.

[8] ID Boyd, RS Buenconsejo, D Piskorz, B Lal, KW Crane, and E De La Rosa Blanco. On-orbit manufacturing and assembly of spacecraft. *IDA Science & Technology Institute, IDA Paper P-8335,(January 2017)*, 2017.

[9] James H Burge, W Davison, HM Martin, and C Zhao. Development of surface metrology for the giant magellan telescope primary mirror. In *Advanced Optical and Mechanical Technologies in Telescopes and Instrumentation*, volume 7018, page 701814. International Society for Optics and Photonics, 2008.

[10] James H Burge, T Peper, and SF Jacobs. Thermal expansion of borosilicate glass, zerodur, zerodur m, and uncer amized zerodur at low temperatures. *Applied optics*, 38(34):7161 7162, 1999.

[11] Antoine Carré, Thomas Westerhoff, Tony Hull, and D Doyle. Review of space radiation interaction with zerodur. In *Astronomical Optics: Design, Manufacture, and Test of Space and Ground Systems*, volume 10401, page 104010M. International Society for Optics and Photonics, 2017.

[12] Wei Ting Chen, Alexander Y Zhu, Vyshakh Sanjeev, Mohammadreza Khorasaninejad, Zhujun Shi, Eric Lee, and Federico Capasso. A broadband achromatic metalens for focusing and imaging in the visible. *Nature nanotechnology*, 13(3):220, 2018.

[13] Soon-Jo Chung, David W Miller, and Olivier L de Weck. Design and implementation of sparse-aperture imaging systems. In *Highly Innovative Space Telescope Concepts*, volume 4849, pages 181 192. International Society for Optics and Photonics, 2002.

[14] Cornwell, T. and Humphreys, B. Parallel and distributed processing for askap, csiro presentation. `https://safe.nrao.edu/wiki/pub/Software/CalIm09Program/Cornwell_CalIm2009.pdf`, 2009.

[15] German Cortes-Medellin, Stephen Parshley, Donald B Campbell, Karl F Warnick, Brian D Jeffs, and Rajagopalan Ganesh. Concept design of

an 80-dual polarization element cryogenic phased array camera for the arecibo radio telescope. In *Ground-based and Airborne Instrumentation for Astronomy VI*, volume 9908, page 99085F. International Society for Optics and Photonics, 2016.

[16] Julianne Dalcanton, Sara Seager, Suzanne Aigrain, Steve Battel, Niel Brandt, Charlie Conroy, Lee Feinberg, Suvi Gezari, Olivier Guyon, Walt Harris, et al. From cosmic birth to living earths: the future of uvoir space astronomy. *arXiv preprint arXiv:1507.04779*, 2015.

[17] Philippe Dierickx, Enzo T Brunetto, F Comeron, Roberto Gilmozzi, Frédéric YJ Gonté, Franz Koch, Miska le Louarn, Guy J Monnet, Jason Spyromilio, Isabelle Surdej, et al. Owl phase a status report. In *Ground-based Telescopes*, volume 5489, pages 391 406. International Society for Optics and Photonics, 2004.

[18] Jeanette L Domber, Paul D Atcheson, and Jeff Kommers. Moire: ground test bed results for a large membrane telescope. In *Spacecraft Structures Conference*, page 1510, 2014.

[19] Chengzhi Dong, Kai Li, Yuxi Jiang, Dwayne Arola, and Dongsheng Zhang. Evaluation of thermal expansion coefficient of carbon fiber reinforced composites using electronic speckle interferometry. *Optics express*, 26(1):531 543, 2018.

[20] Gilles Durand, Marc Sauvage, Aymeric Bonnet, Louis Rodriguez, Samuel Ronayette, Pierre Chanial, Loris Scola, Vincent Révéret, Hervé Aussel, Michael Carty, et al. Talc: a new deployable concept for a 20m far-infrared space telescope. In *Space Telescopes and Instrumentation 2014: Optical, Infrared, and Millimeter Wave*, volume 9143, page 91431A. International Society for Optics and Photonics, 2014.

[21] R. Mukherjee et al. When is it worth assembling observatories in space? *ASTRO 2020 APC White Paper*, 2019.

[22] J. R. Fisher, K. F. Warnick, B. D. Jeffs, G. Gortes-Medellin, R. D. Norrod, F. J. Lockman, J. M. Cordes, and R. Geovanelli. Phased array feeds. *Astro2010 Technology Development White Paper*, 2010.

[23] W. et al. Freedman. Final results from the hubble space telescope key project to measure the hubble constant. *The Astrophysical Journal*, 553(47), 2001.

[24] U. O. Frisk. FIRST Far Infrared and Submillimetre Space Telescope. In *International Astronomical Union Colloquium*, volume 123, pages 223 230. Cambridge University Press, 1990.

[25] Jonathan P Gardner, John C Mather, Mark Clampin, Rene Doyon, Matthew A Greenhouse, Heidi B Hammel, John B Hutchings, Peter Jakobsen, Simon J Lilly, Knox S Long, et al. The james webb space telescope. *Space Science Reviews*, 123(4):485 606, 2006.

[26] Michael A Garrett. Radio astronomy transformed: Aperture arrays past, present and future. In *2013 Africon*, pages 1 5. IEEE, 2013.

[27] S. Gulkis, T. B. H. Kuiper, and P. N. Swanson, editors. *Submillimeter Wavelength Astronomy from Space*, volume Rep. 740 -3 (internal document). Jet Propulsion Laboratory, Pasadena, California, 1977.

[28] TG Hawarden, RO Cummings, CM Telesco, and HA Thronson. Optimised radiative cooling of infrared space telescopes and applications to possible missions. In *Next Generation Infrared Space Observatory*, pages 113 144. Springer, 1992.

[29] SG Hay and JD O'sullivan. Analysis of common-mode effects in a dual-polarized planar connected-array antenna. *Radio Science*, 43(6), 2008.

[30] A.R. Hibbs. The national program for lunar and planetary exploration. *Journal of Geophysical Research*, 66(7):2003 2012, 1961.

[31] John M Hill. The large binocular telescope. *Applied optics*, 49(16):D115 D122, 2010.

[32] Kristina Hogstrom. *Robotically Assembled Space Telescopes with Deployable Modules: Concepts and Design Methodologies*. PhD thesis, California Institute of Technology, 2017.

[33] D. Hollenbach. Large Deployable Reflector Science and Technology Workshop. Volume 2: Scientific Rationale and Technology Requirements. NASA Conference Publication NASA-CP-2275-VOL-2, 1983. Workshop held at Asilomar Conference Center, Pacific Grove, CA, June 21-25, 1982.

[34] A. Hotan. Phased array feeds: a new technology for multi-beam radio astronomy. `https://www.atnf.csiro.au/research/conferences/2015/radio-school/Phased_Array_Feeds_-_Aidan_Hotan.pdf`, 2015. 2015 Radio School, CSIRO Astronomy and Space Science.

[35] Ralf Jedamzik, Thoralf Johansson, and Thomas Westerhoff. Modeling of the thermal expansion behaviour of zerodur at arbitrary temperature profiles. In *Modern Technologies in Space-and Ground-based Telescopes and Instrumentation*, volume 7739, page 77390I. International Society for Optics and Photonics, 2010.

[36] Ralf Jedamzik and Thomas Westerhoff. Zerodur tailored for cryogenic application. In *Advances in Optical and Mechanical Technologies for Telescopes and Instrumentation*, volume 9151, page 91512P. International Society for Optics and Photonics, 2014.

[37] Matt Johns, Patrick McCarthy, Keith Raybould, Antonin Bouchez, Arash Farahani, Jose Filgueira, George Jacoby, Steve Shectman, and Michael Sheehan. Giant magellan telescope: overview. In *Ground-based and Airborne Telescopes IV*, volume 8444, page 84441H. International Society for Optics and Photonics, 2012.

[38] M Khorasaninejad, WT Chen, AY Zhu, J Oh, RC Devlin, D Rousso, and F Capasso. Multispectral chiral imaging with a metalens. *Nano letters*, 16(7):4595 4600, 2016.

[39] Fabian Korn. Heat pipes and its applications. *Heat and Mass Transport, Project Report*, 2008.

[40] Victor L Krabbendam, Thomas A Sebring, Frank B Ray, and James R Fowler. Development and performance of hobby-eberly telescope 11-m segmented mirror. In *Advanced Technology Optical/IR Telescopes*

VI, volume 3352, pages 436 445. International Society for Optics and Photonics, 1998.

[41] L. D. Landau and E. M. Lifshitz. *Theory of Elasticity.* Elsevier, Amsterdam, 3 edition, 1986.

[42] Nicolas N Lee, Joel W Burdick, Paul Backes, Sergio Pellegrino, Kristina Hogstrom, Christine Fuller, Brett Kennedy, Junggon Kim, Rudranarayan Mukherjee, Carl Seubert, et al. Architecture for in-space robotic assembly of a modular space telescope. *Journal of Astronomical Telescopes, Instruments, and Systems*, 2(4):041207, 2016.

[43] C.A. Leidich and R.B. Pittman. Large Deployable Reflector Science and Technology Workshop. Volume 1: Executive Summary. NASA Conference Publication NASA-CP-2275-VOL-1, 1984. Workshop held at Asilomar Conference Center, Pacific Grove, CA, June 21-25, 1982.

[44] C.A. Leidich and R.B. Pittman. Large Deployable Reflector Science and Technology Workshop. Volume 3: Systems and Technology Assessment. NASA Conference Publication NASA-CP-2275-VOL-3 , 1984. Workshop held at Asilomar Conference Center, Pacific Grove, CA, June 21-25, 1982.

[45] Robert B Leighton. A 10-meter telescope for millimeter and submillimeter astronomy. Final report to the National Science Foundation, 1977.

[46] Amir Leshem, Alle-Jan van der Veen, and Albert-Jan Boonstra. Multichannel interference mitigation techniques in radio astronomy. *The Astrophysical Journal Supplement Series*, 131(1):355, 2000.

[47] Colin J Lonsdale, Roger J Cappallo, Miguel F Morales, Frank H Briggs, Leonid Benkevitch, Judd D Bowman, John D Bunton, Steven Burns, Brian E Corey, Ludi DeSouza, et al. The murchison widefield array: Design overview. *Proceedings of the IEEE*, 97(8):1497 1506, 2009.

[48] HM Martin, J Roger P Angel, James H Burge, B Cuerden, WB Davison, M Johns, Jeffrey S Kingsley, LB Kot, RD Lutz, SM Miller, et al. Design

and manufacture of 8.4 m primary mirror segments and supports for the gmt. In *Optomechanical Technologies for Astronomy*, volume 6273, page 62730E. International Society for Optics and Photonics, 2006.

[49] Maurice Martin and Michael Stallard. Distributed satellite missions and technologies-the techsat 21 program. In *Space Technology Conference and Exposition*, page 4479, 1999.

[50] PV Mason. Long-term performance of the passive thermal control systems of the iras spacecraft. *Cryogenics*, 28(2):137 141, 1988.

[51] W. P. McCray. What makes a failure?: Designing a New National Telescope, 1975-1984. *Technology and Culture*, 42(2):265 291, 2001.

[52] Alistair McPherson, Jason Spyromilio, Markus Kissler-Patig, Suzanne Ramsay, Enzo Brunetto, Philippe Dierickx, and Mark Cassali. E-elt update of project and effect of change to 39m design. In *Ground-based and Airborne Telescopes IV*, volume 8444, page 84441F. International Society for Optics and Photonics, 2012.

[53] Martin M Mikulas Jr, Timothy J Collins, and John M Hedgepeth. Preliminary design approach for large high precision segmented reflectors. 1990.

[54] Nicholas J Miller, Matthew P Dierking, and Bradley D Duncan. Optical sparse aperture imaging. *Applied optics*, 46(23):5933 5943, 2007.

[55] JP Balthasar Mueller, Noah A Rubin, Robert C Devlin, Benedikt Groever, and Federico Capasso. Metasurface polarization optics: independent phase control of arbitrary orthogonal states of polarization. *Physical Review Letters*, 118(11):113901, 2017.

[56] Rudranarayan Mukherjee, Nicholas Siegler, Harley Thronson, Matthew Greenhouse, Bradley Peterson, John Grunsfeld, Lynn Bowman, Ronald Polidon, and Howard MacEwen. In space assembled telescope (isat) study preliminary findings. 2019.

[57] J. P. Murphy, M. K. Kiya, M. Werner, P. N. Swanson, T. B. H. Kuiper, and P. D. Batelaan. A large-aperture space telescope for infrared and submillimeter astronomy. *Proc. SPIE*, 228:117 127, 1980.

[58] N. Siegler, R. Mukherjee, H. Thronson. Nasa-chartered in-space assembled telescope study: Final report. slides, July 2019.

[59] Jerry Nelson and Gary H Sanders. Tmt status report. In *Ground-based and Airborne Telescopes*, volume 6267, page 626728. International Society for Optics and Photonics, 2006.

[60] Jerry E Nelson, Terry S Mast, and Sandra M Faber. The design of the keck observatory and telescope. 1985.

[61] M. Oliver. A. R. Hibbs obituary, Los Angeles Times. `https://www.latimes.com/archives/la-xpm-2003-feb-27-me-hibbs27-story.html`.

[62] George P Peterson. An introduction to heat pipes: modeling, testing, and applications. 1994.

[63] GL Pilbratt, JR Riedinger, T Passvogel, G Crone, D Doyle, U Gageur, AM Heras, C Jewell, L Metcalfe, S Ott, et al. Herschel Space Observatory-An ESA facility for far-infrared and submillimetre astronomy. *Astronomy & Astrophysics*, 518:L1, 2010.

[64] R Polidan and G Raffanelli. A rotating synthetic aperture (rsa) space telescope for future uv/opt/ir astronomical missions (white paper). NGAS Case 15-0366, 2015.

[65] Marc Postman, Thomas M Brown, Kenneth R Sembach, Jason Tumlinson, C Matt Mountain, Rémi Soummer, Mauro Giavalisco, Daniela Calzetti, Wesley Traub, Karl R Stapelfeldt, et al. Advanced technology large-aperture space telescope: science drivers and technology developments. *Optical Engineering*, 51(1):011007, 2012.

[66] Marc Postman, William B Sparks, Fengchuan Liu, Kim Ess, Joseph Green, Kenneth G Carpenter, Harley Thronson, and Renaud Goullioud.

Using the iss as a testbed to prepare for the next generation of space-based telescopes. In *Space Telescopes and Instrumentation 2012: Optical, Infrared, and Millimeter Wave*, volume 8442, page 84421T. International Society for Optics and Photonics, 2012.

[67] Robert V Powell and Albert R Hibbs. An entree for large space antennas. 1977.

[68] R. Angel. Design and manufacture of ground and space telescopes. Presentation to JASON, June 2019.

[69] Justin J Rey, Allan Wirth, Andrew Jankevics, Franklin Landers, David Rohweller, C Bill Chen, and Allen Bronowicki. A deployable, annular, 30m telescope, space-based observatory. In *Space Telescopes and Instrumentation 2014: Optical, Infrared, and Millimeter Wave*, volume 9143, page 914318. International Society for Optics and Photonics, 2014.

[70] Antony E Schinckel, John D Bunton, Tim J Cornwell, Ilana Feain, and Stuart G Hay. The australian ska pathfinder. In *Ground-based and Airborne Telescopes IV*, volume 8444, page 84442A. International Society for Optics and Photonics, 2012.

[71] SCHOTT. `https://www.us.schott.com/advanced_optics/english/products/optical-materials/zerodur-extremely-low-expansion-glass-ceramic/zerodur/index.html`. Accessed: 2019-10-01.

[72] Alan She, Shuyan Zhang, Samuel Shian, David R Clarke, and Federico Capasso. Large area metalenses: design, characterization, and mass manufacturing. *Optics express*, 26(2):1573 1585, 2018.

[73] P. H. Siegel. Terahertz pioneer: Mattheus (Thijs) de Graauw. *IEEE Transactions on Terahertz Science and Technology*, 4(2):138 146, 2014.

[74] N. Siegler. `https://exoplanets.nasa.gov/exep/technology/in-space-assembly/iSAT_study/`. Accessed: 2019-10-01.

[75] T.K. Sridharan. The RRI 10.4 m millimeter-wave telescope. *Bulletin of the Astronomical Society of India*, 1993.

[76] Robert Stobie, Jacobus G Meiring, and David AH Buckley. Design of the southern african large telescope (salt). In *Optical Design, Materials, Fabrication, and Maintenance*, volume 4003, pages 355 362. International Society for Optics and Photonics, 2000.

[77] Paul N Swanson, James B Breckinridge, Alan Diner, Robert E Freeland, William R Irace, Paul M McElroy, Aden B Meinel, and A Fernando Tolivar. System concept for a moderate cost large deployable reflector (LDR). *Optical Engineering*, 25(9):251045, 1986.

[78] Stephen P Timoshenko and Sergius Woinowsky-Krieger. *Theory of plates and shells*. McGraw-hill, 1959.

[79] Ai Ueno, Kohei Yamada, Kikuko Miyata, and Hosei Nagano. Proposal of functional thermal control systems for high-power micro-satellite and its demonstration under thermal vacuum condition. *Journal of Electronics Cooling and Thermal Control*, 8(01):1, 2018.

[80] Craig Underwood, Sergio Pellegrino, Hari Priyadarshan, Harsha Simha, Chris Bridges, Ashish Goel, Thibaud Talon, Antonio Pedivellano, Yuchen Wei, Fabien Royer, et al. AAReST autonomous assembly reconfigurable space telescope flight demonstrator. In *Proceedings of the 69th International Astronautical Congress (IAC)*. International Astronautical Federation (IAF), 2018.

[81] Karl F Warnick, Rob Maaskant, Marianna V Ivashina, David B Davidson, and Brian D Jeffs. *Phased Arrays for Radio Astronomy, Remote Sensing, and Satellite Communications*. Cambridge University Press, 2018.

[82] SC West, SH Bailey, S Bauman, B Cuerden, Z Granger, and BH Olbert. A space imaging concept based on a 4m structured spun-cast borosilicate monolithic primary mirror. In *Space Telescopes and Instrumentation 2010: Optical, Infrared, and Millimeter Wave*, volume 7731, page 77311O. International Society for Optics and Photonics, 2010.

[83] SC West, SH Bailey, S Bauman, B Cuerden, Z Granger, and BH Olbert. A space imaging concept based on a 4m structured spun-cast

borosilicate monolithic primary mirror. In *Space Telescopes and Instrumentation 2010: Optical, Infrared, and Millimeter Wave*, volume 7731, page 77311O. International Society for Optics and Photonics, 2010.

[84] Wikipedia. A. R. Hibbs wikipedia page. `https://en.wikipedia.org/wiki/Albert_Hibbs`.

[85] André Pilan Zanoni, Johannes Burkhardt, Ulrich Johann, Markus Aspelmeyer, Rainer Kaltenbaek, and Gerald Hechenblaikner. Thermal performance of a radiatively cooled system for quantum optomechanical experiments in space. *Applied Thermal Engineering*, 107:689 699, 2016.

UNCLASSIFIED//~~FOR OFFICIAL USE ONLY~~

Approved for Release: 2021/04/27 C05132459